Compositional Stability, Performance, and Safety Certification of Interconnected Systems

by

Christopher Ryan Meissen

A dissertation submitted in partial satisfaction of the

requirements for the degree of

Doctor of Philosophy

in

Engineering - Mechanical Engineering

in the

Graduate Division

of the

University of California, Berkeley

Committee in charge:

Professor Andrew Packard, Chair
Professor Murat Arcak
Professor Roberto Horowitz

Spring 2017

Compositional Stability, Performance, and Safety Certification of Interconnected Systems

Abstract

Compositional Stability, Performance, and Safety Certification of Interconnected Systems

by

Christopher Ryan Meissen

Doctor of Philosophy in Engineering - Mechanical Engineering

University of California, Berkeley

Professor Andrew Packard, Chair

Modern computational tools for stability, performance, and safety certification are not scalable to large nonlinear systems. In this dissertation we propose a compositional analysis approach that takes advantage of the interconnected structure of many modern large-scale systems to solve this problem. Specifically, we pose the certification problem as a distributed optimization that searches over the input-output properties of each subsystem to certify a desired property of the interconnected system. The alternating direction method of multipliers (ADMM), a popular distributed optimization technique, is employed to decompose and solve this problem.

This approach is very general in that it allows us to search over a wide range of input-output properties for each subsystem. We demonstrate the use of dissipativity, equilibrium independent dissipativity (EID), and integral quadratic constraints (IQCs) to characterize the properties of the individual subsystems and the entire interconnection. Multiple examples showing the applicability and scalability of the approach are presented.

Furthermore, we demonstrate how symmetries in the interconnection topology can be exploited to further improve the computational efficiency and scalability of the distributed optimization problem. Unlike other symmetry reduction techniques this approach does not require the subsystems to be identical, but only to share input-output properties. Thus, it can be applied to many real world systems. We demonstrate these reduction techniques on a large-scale nonlinear example and a vehicle platoon example.

Finally, we present a passivity-based formation control strategy for multiple unmanned aerial vehicles (UAVs) cooperatively carrying a suspended load. This strategy is designed such that the input-output properties of the individual UAVs and the interconnection structure guarantee stability of the system under appropriate conditions. Specifically, we show that the system is stable for any configurations where the cables carrying the suspended load are in tension.

Contents

List of Figures

List of Tables

Acknowledgments

I would like to take this opportunity to thank the following people.

First and foremost, I would like to thank my advisors Andy Packard and Murat Arcak for sharing their knowledge and experience with me as well as providing me many interesting ideas and opportunities. Thanks to Roberto Horowitz for serving on my dissertation and qualifying exam committee. I also thank Kameshwar Poolla, Ben Recht, and Michael Christ for serving on my qualifying exam committee. I would like to thank my other coauthors including Laurent Lessard, Ana Rufino Ferreira, Kristian Klausen, and Thor Fossen. Thanks to Laurent El Ghaoui for many interesting discussions on optimization and machine learning. Thanks also to all of the people in the BCCI for their friendship and support.

I would also like to acknowledge organizations that provided financial support throughout my graduate education. Specifically, NSF under grant ECCS 1405413, entitled "A Compositional Approach for Performance Certification of Large-Scale Engineering Systems" (program director Dr. Kishan Baheti), NASA under grant No. NRA NNX12AM55A, entitled "Analytical Validation Tools for Safety Critical Systems Under Loss-of-Control Conditions" (technical monitor Dr. Christine Belcastro), and the Fanuc Corportation through the Fanuc Chair in Mechanical Engineering at UC Berkeley.

Finally, thanks to my parents, Jan and Greg, for their support and encouragement.

Chapter 1

Introduction

In this dissertation we describe a compositional approach to stability, performance, and safety certification that takes advantage of the interconnected structure of many modern large-scale systems. This research is motivated by the fact that modern computational tools are not scalable to large-scale nonlinear systems and many modern systems like robot swarms, power systems, or biological networks have a natural structure that consists of many small interconnected subsystems. Therefore, we consider interconnected systems as shown in Figure 1.1 where the Σ_i blocks are known subsystems mapping $u_i \mapsto y_i$ and M is a static matrix that characterizes the interconnection topology.

The goal of compositional analysis is to establish properties of the interconnected system using only properties of the subsystems and their interconnection. Henceforth, the term *local* is used to refer to properties or analysis of individual subsystems in isolation. Likewise, *global* refers to the entire interconnected system.

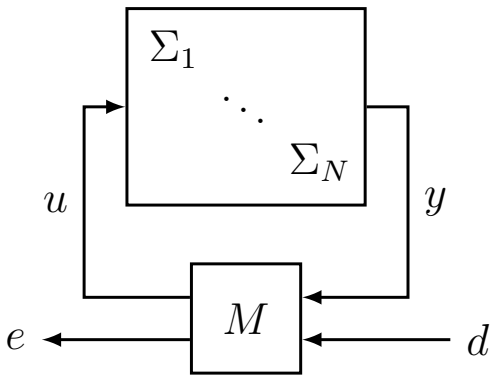

Figure 1.1: Interconnected system with input d and output e.

We formulate the certification problem as a feasibility problem with local constraints that guarantee certain input-output properties of each subsystem and a global constraint that depends on the input-output properties of all the subsystems and the interconnection structure. The alternating direction method of multipliers (ADMM) [1], a popular distributed optimiza-

tion technique, is employed to decompose and solve this problem. The ADMM algorithm iteratively searches over the local input-output properties of each subsystem to certify the desired global properties of the interconnected system.

Local input-output properties and global performance are cast and quantified in the framework of dissipative systems [2], [3]; specifically the case with quadratic supply rates. The global supply rate is specified by the analyst and dictates the system performance that is to be verified. For example, supply rates can be chosen to characterize L_2-gain, passivity, output-strict passivity, etc., for the input-output pair (d,e). A storage function is then sought to certify dissipativity with respect to the desired supply rate. We demonstrate how this framework can also be extended to the more general case when the subsystems are equilibrium independent dissipative (EID) or satisfy integral quadratic constraints (IQCs). Furthermore, we show this framework can be easily modified to also certify safety of the interconnected system under finite energy disturbances.

A conventional approach to compositional analysis, as presented for example in [2]–[7], is to establish individual supply rates (and storage functions) for which each subsystem is dissipative. Then, a storage function certifying dissipativity of the interconnected system is sought as a conic combination of the subsystem storage functions.

The method presented here also searches for a conic combination of subsystem storage functions that certify properties of the interconnected system, but it is less conservative because the local supply rates (and storage functions) are optimized with regards to their particular suitability in certifying global properties. Thus, the local certificates are automatically generated, as opposed to being preselected.

The ADMM algorithm decomposes the certification into parallelizable, local problems for each subsystem and a global problem. The overall problem is then solved by iteratively solving the local and global subproblems in a coordinated fashion until they converge to a solution certifying the desired global properties. At every iteration each local problem receives a proposed supply rate from the global problem and solves an optimization problem certifying dissipativity of the corresponding subsystem with a supply rate close to the proposed one. The global problem, with knowledge of the interconnection M and the updated supply rates, solves an optimization problem to certify dissipativity of the interconnected system and proposes new supply rates.

In order to further improve the computational efficiency and scalability of this problem we also take advantage of symmetries in the interconnection. These symmetries, defined by invariance under specific row and column permutations of the interconnection matrix M, can be exploited to further improve the computational efficiency and scalability of the distributed optimization algorithm. Unlike other symmetry reduction techniques this approach does not require the subsystems to be identical, but only to share input-output properties. Thus, it can be applied to many real world systems.

Finally, a passivity-based formation control strategy for multiple unmanned aerial vehicles (UAVs) cooperatively carrying a suspended load is presented. This application does not explicitly use the compositional analysis framework, but it has many similarities. The strategy uses the input-output properties of the individual UAVs and the interconnection

structure to find a storage function guaranteeing stability of the system under appropriate conditions. Specifically, we prove the system is stable for any configurations where the cables carrying the suspended load are in tension.

The content and contributions of each chapter are briefly described below.

Chapter 2 presents a summary of background material that will be used throughout this work. First, the primary system analysis tools that will be used are described. This includes the concepts of dissipativity, equilibrium independent dissipativity (EID), and integral quadratic constraints (IQCs). We describe how for linear systems these properties can be verified via semidefinite programming and for nonlinear polynomial systems they can be verified using sum-of-squares (SOS) programming. We also briefly discuss how SOS problems are transformed into SDPs. Finally, we discuss the computational complexity of solving SDPs using standard primal-dual interior point algorithms.

Chapter 3 describes a compositional framework for certifying stability or performance of an interconnected system. This is posed as a feasibility problem with local constraints that require each subsystem to be dissipative and a global constraint that involves all the subsystem properties and the interconnection structure. We also prove that for linear systems this approach is equivalent to searching for a separable storage function.

We extend this compositional framework to interconnections of subsystems that are EID or satisfy IQCs. This also allows us to certify properties of the interconnected system that are described by EID or IQCs. Finally, we present an extension of this framework to certify safety of the interconnected system under finite energy disturbances. Similar to the performance certification this is applicable for subsystems that are dissipative, EID, or satisfy IQCs. The material in this chapter is expanded on from [8], [9].

Chapter 4 formulates the compositional certification problems presented in Chapter 3 as an optimization problem. Using distributed optimization techniques, specifically the alternating direction method of multipliers (ADMM), this problem is decomposed into several smaller subproblems that can be solved iteratively. The subproblems consist of N local problems that only involve an individual subsystem and one global problem that depends on the interconnection structure and the properties of the subsystems determined from the local problems. Convergence guarantees of the ADMM algorithm for the performance certification problem are described and a relaxed exit criterion for the algorithm is presented. We demonstrate the ADMM algorithm on a simple example with linear subsystems and compare its performance to other distributed optimization techniques. The material in this chapter is expanded on from [8]–[10].

Chapter 5 presents multiple examples using the ADMM algorithm to certify properties of large interconnected systems. The first example demonstrates the algorithms ability to reliably certify stability for a large-scale linear problem. The second example demonstrates the benefits of characterizing the subsystem properties with IQCs. The next example certifies the performance of a large interconnection of nonlinear systems. In this example we demonstrate that the compositional framework with the ADMM algorithm significantly improves the computational efficiency and scalability of the performance certification compared

to traditional methods. The final example certifies EID and safety properties of a vehicle platoon model. The material in this chapter is expanded on from [8], [9].

Chapter 6 exploits symmetries in the interconnection structure to reduce the number of decision variables and, in some cases, the dimension of the performance certification problem. First, this is presented for interconnections of dissipative and EID subsystems; then extended to the case where the subsystems satisfy IQCs. The reduction methods are demonstrated on the vehicle platoon example presented in Chapter (5) and on a large cyclic interconnection of nonlinear subsystems. The material in this chapter is reported in [9], [11].

Chapter 7 presents a passivity-based control design for multiple UAVs carrying a suspended load. The proposed control strategy regulates the relative position between the UAVs and compensates for the vertical force applied by the suspended load. We prove that the equilibrium points of the system when the cables are in tension are stable and provide simulation results demonstrating the performance of the control strategy. The material in this chapter is reported in [12].

Chapter 2

Properties of Dynamical Systems

In this chapter we introduce the main analysis tools that will be used throughout this dissertation to characterize the properties of dynamical systems. First, we introduce the concept of dissipativity and demonstrate how it can be used to characterize commonly used input-output properties of dynamical systems. Generalizations of dissipativity, including equilibrium independent dissipativity (EID) and integral quadratic constraints (IQCs), are then introduced.

We also describe how these properties can be numerically certified using using sum-of-squares (SOS) and semidefinite programming (SDP). Then, we show how SOS programs can be converted to SDPs and describe the number of decision variables and dimension of the resulting SDP. Finally, we briefly discuss the computational complexity of solving SDPs using standard primal-dual interior point methods.

2.1 Notation

For a vector $w \in \mathbb{R}^n$ we denote the Euclidean norm as $|w|$. The L_2 norm of a signal $v : [0, \infty) \to \mathbb{R}^n$ is

$$\|v\| := \left(\int_0^\infty |v(t)|^2 dt \right)^{\frac{1}{2}}$$

and $v \in L_2$ if $\|v\| < \infty$. The *extended* L_2 space is defined as

$$L_{2e} := \left\{ v : [0, \infty) \to \mathbb{R}^n \;\middle|\; \left(\int_0^T |v(t)|^2 dt \right)^{\frac{1}{2}} < \infty \text{ for all } T \in [0, \infty) \right\}.$$

This is the space of all signals that are square integrable over finite intervals. Therefore, L_2 is a subset of L_{2e}.

2.2 Dissipativity

Dissipativity introduced by Willems [2], [3] allows us to characterize the input-output properties of dynamical systems. By the choice of a scalar-valued function called the supply rate different properties of the system can be characterized. For example dissipativity can certify many commonly used properties such as passivity or finite L_2 gain.

Definition 1. Consider a time-invariant dynamical system

$$\begin{aligned} \dot{x}(t) &= f(x(t), u(t)), \quad f(0,0) = 0 \\ y(t) &= h(x(t), u(t)), \quad h(0,0) = 0 \end{aligned} \tag{2.1}$$

with $x(t) \in \mathbb{R}^n$, $u(t) \in \mathbb{R}^m$, and $y(t) \in \mathbb{R}^p$.

A system of the form (2.1) is *dissipative* with respect to the supply rate $w : \mathbb{R}^m \times \mathbb{R}^p \to \mathbb{R}$ if there exists a nonnegative function $V : \mathbb{R}^n \to \mathbb{R}_+$ such that $V(0) = 0$ and

$$V(x(\tau)) - V(x(0)) \leq \int_0^\tau w(u(t), h(x(t), u(t)))dt \tag{2.2}$$

for all initial conditions $x(0) \in \mathbb{R}^n$, all input signals $u : [0, \tau] \to \mathbb{R}^m$, and all $\tau \geq 0$ in the interval of existence of the solution $x(t)$. Equation (2.2) is referred to as the *dissipation inequality* (DIE) and V as a *storage function.*

Clearly, dissipativity is a generalization of Lyapunov stability. Specifically, if V is positive definite and the supply rate satisfies

$$w(0,0) = 0 \quad \text{and} \quad w(0,y) \leq 0 \quad \text{for all } y \in \mathbb{R}^p \tag{2.3}$$

then (2.2) implies the origin of the system is Lyapunov stable. Furthermore, if V is radially unbounded, that is $V(x) \to \infty$ as $|x| \to \infty$, then the interconnected system is globally stable.

The choice of the supply rate dictates the property that the system satisfies. Some commonly used properties and the corresponding supply rates are described below.

- Finite L_2 gain: $\quad w(u,y) = \gamma^2|u|^2 - |y|^2 \quad \gamma > 0$

  Substituting this supply rate into (2.2) with $x(0) = 0$ gives

  $$V(x(\tau)) \leq \gamma^2 \int_0^\tau |u(t)|^2 dt - \int_0^\tau |y(t)|^2 dt$$

  for all u and $\tau \geq 0$ which implies the L_2 norm of y is less than or equal to $\gamma\|u\|$. Therefore, we refer to γ as an L_2 gain for the system.

- Passivity: $\quad w(u,y) = u^\top y$

  This supply rate substituted into (2.2) with $x(0) = 0$ implies

  $$\int_0^\tau u(t)^\top y(t) dt \geq 0$$

  for all u and $\tau \geq 0$.

- Output Strict Passivity: $w(u,y) = u^\top y - \epsilon|y|^2 \quad \epsilon > 0$

  This supply rate strengthens the passivity supply rate since (2.2) with $x(0) = 0$ implies

  $$\int_0^\tau u(t)^\top y(t)dt \geq \epsilon \int_0^\tau |y(t)|^2.$$

  for all u and $\tau \geq 0$. It can also be shown that this supply rate implies the system has an L_2 gain of $1/\epsilon$.

- L_2 Reachability: $w(u,y) = \|u\|^2$

  This supply rate substituted into (2.2) with $x(0) = 0$ implies

  $$V(x(\tau)) \leq \int_0^\tau |u(t)|^2 dt$$

  for all u and $\tau \geq 0$. Assuming that $\|u\|_2^2 \leq \beta$ this implies that all possible state trajectories are contained in the sublevel set

  $$\mathcal{V}_\beta := \{x \mid V(x) \leq \beta\}.$$

2.3 Numerical Certification of Dissipativity

In general, certifying that (2.2) holds for all possible initial conditions $x(0)$ and input signals u is very difficult. However, if the storage function V is differentiable then (2.2) is equivalent to the algebraic inequality

$$\nabla V(x)^\top f(x,u) - w(u, h(x,u)) \leq 0. \tag{2.4}$$

holding for all $x \in \mathbb{R}^n$ and $u \in \mathbb{R}^m$ [2]. Therefore, we can certify dissipativity by searching for a differentiable storage function V such that $V(x) \geq 0$, $V(0) = 0$, and (2.4) is satisfied for all $x \in \mathbb{R}^n$ and $u \in \mathbb{R}^m$.

A linear system (i.e. f and h are linear in u and x) is dissipative with respect to a quadratic supply rate if and only if there exists a quadratic storage function satisfying (2.4) [3]. Therefore, certifying dissipativity of a linear system can be cast as a linear matrix inequality (LMI) and solved via standard SDP solvers. This is demonstrated in the following example.

Example 2. Consider the linear system

$$\dot{x}(t) = Ax(t) + Bu(t)$$
$$y(t) = Cx(t) + Du(t)$$

with $x(t) \in \mathbb{R}^n$, $u(t) \in \mathbb{R}^m$, $y(t) \in \mathbb{R}^p$, and the quadratic supply rate

$$w(u, y) = \begin{bmatrix} u \\ y \end{bmatrix}^\top X \begin{bmatrix} u \\ y \end{bmatrix} \tag{2.5}$$

where $X \in \mathbb{R}^{(m+p)\times(m+p)}$ is a symmetric matrix characterizing the supply rate. We assume without loss of generality the storage function is a quadratic function of the form $V(x) = x^\top P x$ where $P \in \mathbb{R}^{n\times n}$ is a symmetric positive semidefinite matrix. Substituting the dynamics, supply rate, and storage function into (2.4) gives

$$\frac{1}{2}(Ax + Bu)^\top P x + \frac{1}{2} x^\top P (Ax + Bu) - \begin{bmatrix} u \\ Cx + Du \end{bmatrix}^\top X \begin{bmatrix} u \\ Cx + Du \end{bmatrix} \leq 0$$

for all $x \in \mathbb{R}^n$ and $u \in \mathbb{R}^m$. Therefore, if there exists a symmetric $P \succeq 0$ such that

$$\frac{1}{2}\begin{bmatrix} A^\top P + PA & PB \\ B^\top P & 0 \end{bmatrix} - \begin{bmatrix} 0 & I \\ C & D \end{bmatrix}^\top X \begin{bmatrix} 0 & I \\ C & D \end{bmatrix} \preceq 0$$

then the system is dissipative with respect to the supply rate in (2.5).

When the system dynamics and supply rates are more general polynomials, it is not possible to directly formulate (2.4) as an LMI constraint. However, we can relax the dissipativity certification problem to a SOS program which can be converted to an SDP. SOS programming is reviewed in Section 2.6 and a brief discussion of the computational complexity of SDP solvers is given in Section 2.7.

Let $\mathbb{R}[x]$ be the set of polynomials in the indeterminate x with real coefficients and $\Sigma[x] \subset \mathbb{R}[x]$ be the set of all SOS polynomials. Suppose f and h are polynomials then certification of dissipativity with respect to a polynomial supply rate w can be relaxed to the SOS feasibility program:

$$\begin{aligned} V(x) &\in \Sigma[x] \\ -\nabla V(x)^\top f(x, u) + w(u, y) &\in \Sigma[x, u]. \end{aligned} \tag{2.6}$$

If each element of f is a rational polynomial then this can also be cast as a SOS program. Suppose each element of the dynamics are given by

$$\dot{x}_i = f_i(x, u) = \frac{p_i(x, u)}{q_i(x, u)} \quad \text{for } i = 1, \ldots, n$$

where $p_i \in \mathbb{R}[x, u]$ and $q_i - \epsilon \in \Sigma[x, u]$ for $\epsilon > 0$, then certifying dissipativity of the system with respect to a polynomial supply rate, w, can be relaxed to:

$$\begin{aligned} V(x) &\in \Sigma[x] \\ -\sum_{i=1}^{n} \nabla_{x_i} V(x) p_i(x, u) \prod_{j\neq i} q_j(x, u) + \prod_{i=1}^{n} q_i(x, u) w(u, y) &\in \Sigma[x, u]. \end{aligned} \tag{2.7}$$

2.4 Equilibrium-Independent Dissipativity (EID)

EID is a generalization of the dissipativity framework that allows us to characterize properties of systems whose equilibrium are nonzero and may depend non-trivially on the input of the system [13], [14]. EID guarantees that the system is dissipative with respect to any possible equilibrium point of the system.

Definition 3. Consider a time-invariant dynamical system

$$\begin{aligned} \dot{x}(t) &= f(x(t), u(t)) \\ y(t) &= h(x(t), u(t)) \end{aligned} \tag{2.8}$$

and assume there exists a nonempty set $\mathcal{X}^\star \subseteq \mathbb{R}^n$ such that for each $x^\star \in \mathcal{X}^\star$ there exists a unique $u^\star \in \mathbb{R}^m$ such that $f(x^\star, u^\star) = 0$. The *equilibrium state-input map* is then defined as

$$k_u(x) : \mathbb{R}^n \to \mathbb{R}^m \text{ such that } u^\star = k_u(x^\star).$$

The system (2.8) is *EID* with respect to a supply rate w if there exists a differentiable nonnegative storage function $V : \mathbb{R}^n \times \mathbb{R}^n \to \mathbb{R}_+$ such that $V(x^\star, x^\star) = 0$ and

$$\nabla_x V(x, x^\star)^\top f(x, u) - w(u - u^\star, y - y^\star) \leq 0 \tag{2.9}$$

for all $x^\star \in \mathcal{X}^\star$, $x \in \mathbb{R}^n$, and $u \in \mathbb{R}^m$ where $u^\star = k_u(x^\star)$, $y = h(x, u)$, and $y^\star = h(x^\star, u^\star)$.

This definition ensures dissipativity with respect to any possible equilibrium point rather than a particular point. This is advantageous for the analysis of interconnected systems since the equilibrium may be hard to compute. This property is especially important for compositional analysis, since the goal is to analyze the subsystems in isolation even though the inputs, and consequentially the equilibrium of each subsystem depends on the interconnection.

As presented in [14], certifying polynomial systems are EID can be relaxed to the SOS program:

$$\begin{aligned} V(x, x^\star) &\in \Sigma[x, x^\star] \\ r(x, u, x^\star, u^\star) &\in \mathbb{R}[x, u, x^\star, u^\star] \\ -\nabla_x V(x, x^\star)^\top f(x, u) + w(u - u^\star, y - y^\star) & \\ + r(x, u, x^\star, u^\star) f(x^\star, u^\star) &\in \Sigma[x, u, x^\star, u^\star]. \end{aligned} \tag{2.10}$$

Note that $x^\star$ and $u^\star$ in (2.10) are variables and not assumed to satisfy $f(x^\star, u^\star) = 0$. Instead, the r term ensures that whenever $f(x^\star, u^\star) = 0$ then

$$\begin{aligned} V(x, x^\star) &\in \Sigma[x, x^\star] \\ -\nabla_x V(x, x^\star)^\top f(x, u) + w(u - u^\star, y - y^\star) &\in \Sigma[x, u, x^\star, u^\star] \end{aligned}$$

as desired.

Similarly to the polynomial case, certifying rational polynomial systems are EID can also be formulated as an SOS feasibility program.

2.5 Integral Quadratic Constraints (IQCs)

IQCs are a generalization of the dissipativity framework that capture frequency dependent properties of a system. Originally, IQCs were formulated in the frequency-domain [15], but in this work we will use a time-domain state space formulation. Under certain technical assumptions these formulations can be shown to be equivalent [16], [17].

The time-domain formulation can also be interpreted as dissipativity with respect to a dynamic supply rate. The dynamic supply rate is described by a stable linear system Ψ that filters the input u and output y of a system Σ to be analyzed as shown in Figure 2.1.

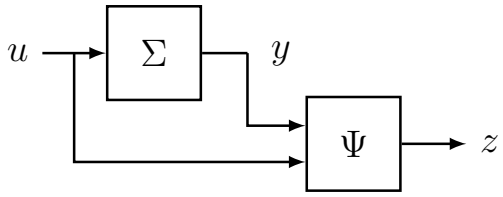

Figure 2.1: The inputs and outputs of the system Σ are filtered through the stable linear system Ψ with output z. The IQC is $\Pi = \Psi^* X \Psi$ where X is a real symmetric matrix.

Definition 4. Let $(\hat{A}, \hat{B}, \hat{C}, \hat{D})$ be the realization of a stable LTI system $\Psi : \mathbb{R}^m \times \mathbb{R}^p \to \mathbb{R}^r$ with state $\eta \in \mathbb{R}^q$ and $X \in \mathbb{R}^{r \times r}$ be a real symmetric matrix. Then (2.1) satisfies the IQC defined by $\Pi = \Psi^* X \Psi$ if there exists a differentiable nonnegative storage function $V : \mathbb{R}^n \times \mathbb{R}^q \to \mathbb{R}_+$ such that $V(0,0) = 0$ and

$$\nabla_x V(x,\eta)^\top f(x,u) + \nabla_\eta V(x,\eta)^\top \left(\hat{A}\eta + \hat{B} \begin{bmatrix} u \\ y \end{bmatrix} \right) \leq z^\top X z \tag{2.11}$$

for all $x \in \mathbb{R}^n$, $\eta \in \mathbb{R}^q$, and $u \in \mathbb{R}^m$ where $z = \hat{C}\eta + \hat{D} \begin{bmatrix} u \\ y \end{bmatrix}$ and $y = h(x,u)$.

Therefore, (2.11) guarantees that the signal $z := \Psi \begin{bmatrix} u \\ y \end{bmatrix}$ satisfies

$$\int_0^\infty z(\tau)^\top X z(\tau) d\tau \geq 0$$

with $x(0) = 0$ and $\eta(0) = 0$. Furthermore, it also implies that for all $u \in L_{2e}$ the signal $z := \Psi \begin{bmatrix} u \\ y \end{bmatrix}$ satisfies

$$\int_0^\tau z(\tau)^\top X z(\tau) d\tau \geq V(x(\tau), \eta(\tau)) \geq 0$$

for all $\tau \geq 0$ with $x(0) = 0$ and $\eta(0) = 0$.

Standard dissipativity with respect to a quadratic supply rate is recovered when $\hat{C} = 0$ (or when the state dimension is 0) and $\hat{D} = I$. Then the output of Ψ is $z = \begin{bmatrix} u \\ y \end{bmatrix}$ and the supply rate is of the form

$$w(u, y) = \begin{bmatrix} u \\ y \end{bmatrix}^\top X \begin{bmatrix} u \\ y \end{bmatrix}.$$

Furthermore, we can generalize IQCs to also be equilibrium independent. Since we assume that the linear system Ψ is stable then the matrix $\hat{A}$ has all nonzero eigenvalues and is invertible. Thus, the equilibrium of Ψ with input $u^\star$ satisfies

$$\begin{aligned} \eta^\star &= -\hat{A}^{-1}\hat{B} \begin{bmatrix} u^\star \\ y^\star \end{bmatrix} \\ z^\star &= \hat{C}\eta^\star + \hat{D} \begin{bmatrix} u^\star \\ y^\star \end{bmatrix} \end{aligned} \tag{2.12}$$

Definition 5. Let $(\hat{A}, \hat{B}, \hat{C}, \hat{D})$ be the realization of a stable LTI system $\Psi : \mathbb{R}^m \times \mathbb{R}^p \to \mathbb{R}^r$ with state $\eta \in \mathbb{R}^q$ and $X \in \mathbb{R}^{r \times r}$ be a real symmetric matrix. Assume there exists a nonempty set $\mathcal{X}^\star \subseteq \mathbb{R}^n$ such that for each $x^\star \in \mathcal{X}^\star$ there exists a unique $u^\star \in \mathbb{R}^m$ such that $f(x^\star, u^\star) = 0$. Then (2.8) satisfies the equilibrium independent IQC defined by $\Pi = \Psi^* X \Psi$ if there exists a differentiable nonnegative storage function $V : \mathbb{R}^n \times \mathbb{R}^q \times \mathbb{R}^n \times \mathbb{R}^q \to \mathbb{R}_+$ such that $V(x^\star, \eta^\star, x^\star, \eta^\star) = 0$ and

$$\begin{aligned} \nabla_x V(x, \eta, x^\star, \eta^\star)^\top f(x, u) + \nabla_\eta V(x, \eta, x^\star, \eta^\star)^\top \left(\hat{A}\eta + \hat{B} \begin{bmatrix} u \\ y \end{bmatrix} \right) \\ \leq (z - z^\star)^\top X (z - z^\star) \end{aligned} \tag{2.13}$$

for all $x \in \mathbb{R}^n$, $x^\star \in \mathcal{X}^\star$, and $u \in \mathbb{R}^m$ where $u^\star = k_u(x^\star)$, $y = h(x, u)$, $y^\star = h(x^\star, u^\star)$, $z = \hat{C}\eta + \hat{D} \begin{bmatrix} u \\ y \end{bmatrix}$, and $(z^\star, \eta^\star)$ satisfy (2.12).

In the case of linear dynamics certifying a system satisfies an IQC or equilibrium independent IQC can be formulated as an LMI. Similarly, certifying a system with polynomial or rational polynomial system satisfies an IQC or equilibrium independent IQC can be formulated as a SOS feasibility program.

2.6 SOS Programming

As shown in the previous sections certifying dissipativity or IQC satisfaction of a system requires finding a storage function such that an algebraic expression holds for all values of the independent variables. For a linear system this can be expressed as an LMI since the inequalities involve quadratic forms in the independent variables.

For polynomial or rational polynomial systems these algebraic expressions are higher order polynomials and checking nonnegativity of polynomials is in general an NP-hard problem [18]. In this section we describe how we can relax this problem of certifying nonnegativity of polynomials to a SOS programming problem. The relaxed SOS program can be formulated as a SDP for which efficient computational solvers exist.

Let $\mathbb{R}[x]$ denote the set of all polynomials in variables $x \in \mathbb{R}^n$ with real coefficients.

Definition 6. A polynomial $p \in \mathbb{R}[x]$ is *sum-of-squares* (SOS) if there exists polynomials $g_1, \ldots, g_N \in \mathbb{R}[x]$ such that $p = \sum_{i=1}^{N} g_i^2$.

Let $\Sigma[x]$ denote the set of all SOS polynomials. Clearly if $p \in \Sigma[x]$, then p is nonnegative for all x, but in general the converse is not true. In fact, the set $\Sigma[x]$ is equal to the set of nonnegative polynomials for only univariate polynomials, quadratic polynomials, and quartic polynomials in two variables [19].

Finding the SOS decomposition of a polynomial or determining that none is possible can be expressed as a SDP [20]. In order to do this the polynomial is expressed as a quadratic form in its monomials. For every polynomial $p \in \mathbb{R}[x]$ with degree less than or equal to $2d$ there is a symmetric matrix Q such that

$$p(x) = z(x)^\top Q z(x)$$

where $z(x)$ is the vector of monomials up to order d. This is called a Gram matrix representation of p and plays a key role in the sum of squares decomposition [20], [21]. The following theorem provides a complete characterization of SOS polynomials.

Theorem 7. *A polynomial $p \in \mathbb{R}[x]$ with degree less than or equal to $2d$ is SOS if and only if there exists a symmetric matrix $Q \succeq 0$ such that*

$$p(x) = z(x)^\top Q z(x) \tag{2.14}$$

for all $x \in \mathbb{R}^n$, where $z(x)$ is the vector of all monomials of degree up to d.

Note for a given polynomial p, the symmetric matrix Q satisfying (2.14) is in general not unique. In fact, we can parametrize all possible symmetric matrices Q satisfying (2.14). Since the elements of $z(x)$ are not algebraically independent there exists unique symmetric matrices $(N_1, \ldots, N_v)$ that form a basis for all matrices N such that $z(x)^\top N z(x) = 0$ for all $x \in \mathbb{R}^n$. Hence, if there exists a symmetric matrix Q_0 such that $p(x) = z(x)^\top Q_0 z(x)$ then

$$p(x) = z(x)^\top \left(Q_0 + \sum_{i=1}^{v} \lambda_i N_i \right) z(x)$$

for all $\lambda \in \mathbb{R}^v$ where λ parameterizes the set of all symmetric matrices Q satisfying $p(x) = z(x)^\top Q z(x)$. Therefore, p is SOS if and only if there exists a $\lambda \in \mathbb{R}^v$ such that $Q_0 + \sum_{i=1}^{v} \lambda_i N_i$ is positive semidefinite.

	2d			
n	4	6	8	10
2	6	10	15	21
6	28	84	210	462
10	66	286	**1001**	**3003**
14	120	**680**	**3060**	**1.2e4**
18	190	**1330**	**7315**	**3.3e4**

(a) Dimension of semidefinite constraint s

	2d			
n	4	6	8	10
2	6	27	75	165
6	196	2646	1.9e4	9.9e4
10	1210	3.3e4	**4.6e5**	**4.3e6**
14	4200	**1.9e5**	**4.4e6**	**6.6e7**
18	1.1e4	**7.5e5**	**2.5e7**	**5.5e8**

(b) Number of decision variables v

Table 2.1: Dimension and number of decision variables for certifying a polynomial in n variables and of degree $2d$ is SOS. Numbers in bold indicate problem sizes where the certification is computationally intractable.

For a polynomial in n variables with degree $2d$ the dimension of the vector of monomials $z(x) \in \mathbb{R}^s$ and the Gram matrix $Q = Q^\top \in \mathbb{R}^{s \times s}$ will be

$$s = \binom{n+d}{d}.$$

The number of unique symmetric matrices $(N_1, \dots N_v)$ that form the basis for all matrices N such that $z(x)^\top N z(x) = 0$ is

$$v = \frac{1}{2}\left[\binom{n+d}{d}^2 + \binom{n+d}{d}\right] - \binom{n+2d}{2d}.$$

This is important because when converted to an SDP s is the dimension of the semidefinite constraint and v is the number of decision variables. In Table 2.1 we report the resulting s and v for certifying polynomials in n variables with degree $2d$ are SOS. The bold numbers indicate problems where the SOS certification becomes computationally intractable. As can be seen this happens for moderately-sized problems and s and v increase dramatically for only slightly larger problems.

Software packages that convert SOS programs to SDPs are available [22]–[24]. These packages call standard SDP solvers and then convert the results back to polynomial form.

2.7 Computational Complexity of SDP Solvers

A semidefinite program (SDP) in *inequality form* consists of a linear objective subject to a linear matrix inequality (LMI) constraint:

$$\begin{aligned} \underset{z \in \mathbb{R}^v}{\text{minimize}} \quad & c^T z \\ \text{subject to} \quad & B + \sum_{i=1}^{v} z_i A_i \succeq 0. \end{aligned} \tag{2.15}$$

The problem data are the vector $c \in \mathbb{R}^v$ and symmetric matrices $B \in \mathbb{R}^{s\times s}$, $A_i \in \mathbb{R}^{s\times s}$.

Standard SDP solvers [25]–[27] use primal-dual interior point algorithms. These algorithms have worst-case polynomial complexity [28] but can become computationally intractable for large problems. The computational complexity depends on the number of decision variables v, the dimension of the semidefinite cone s, and the structure and sparsity of the problem data. As shown in Section 2.6 v and s can become very large for certifying moderately-sized polynomials are SOS.

These algorithms are guaranteed to converge to an ϵ-suboptimal solution in $\mathcal{O}\left(\sqrt{s}\log\left(\frac{1}{\epsilon}\right)\right)$ iterations and for each iteration the computational complexity is

$$\alpha v^2 s^2 + \beta v s^3 + \gamma v^3 + \mathcal{O}(vs^2 + v^2 s + s^3) \tag{2.16}$$

where $\alpha, \beta, \gamma > 0$ are constants that depend on the specific algorithm [29]. Sparsity in the problem allows the first two terms in (2.16) to be reduced [30], but it is still necessary to perform a Cholesky factorization or similar operation with complexity $\mathcal{O}(s^3)$. The third term γv^3 also remains and is the complexity of solving a linear system to compute the step direction.

Therefore, significantly improving the scalability of solving SDPs requires reducing both v and s. This can be accomplished by taking advantage of the structure of the problem. For example, [31] shows that for SDPs with symmetry in the problem data both the dimension and number of decision variables can be reduced. References [32], [33] consider SDPs that have a chordal sparsity pattern in the problem data. This allows the LMI constraint to be reduced to multiple smaller LMIs without adding conservatism. In this work we take advantage of the interconnected structure of our problem to decompose it into many significantly smaller subproblems and by solving them iteratively are able to find a solution to the original problem.

Chapter 3

Compositional Analysis of Interconnected Systems

In this chapter we present a compositional framework for certifying the stability or performance of interconnected systems. In this framework we express the certification problem as a feasibility problem with *local* constraints that only involve individual subsystems and a *global* constraint that depends on the properties of each subsystem and the interconnection structure. The certification problems are written in this fashion because it allows us to easily apply distributed optimization techniques in Chapter 4 that take advantage of the problem structure.

Similar approaches to compositional analysis have been extensively studied [2]–[7]. These approaches establish individual supply rates (and storage functions) for which each subsystem is dissipative. Then, a storage function certifying dissipativity of the interconnected system is sought as a combination of the subsystem storage functions.

The method presented here is less conservative because we take advantage of the fact that most systems are dissipative with respect to a large number of supply rates. Therefore, for each subsystem we search for the supply rate (and storage function) that is optimal in terms of certifying the desired global properties.

Optimizing over the local supply rates (and storage functions) to certify stability of an interconnected system was first introduced in [34], with the individual supply rates constrained to be diagonally-scaled L_2-gains. This perspective, coupled with dual decomposition, gave rise to a distributed optimization algorithm. We generalize this approach in several ways: certifying dissipativity, EID, or IQC satisfaction of the interconnected system; searching over arbitrary quadratic supply rates for the local subsystems; and employing ADMM [1] to decompose and solve the resulting problem.

We also extend this framework to certify safety of the interconnected system under disturbances with bounded energy. A similar safety certification procedure was developed in [35] for disturbances with L_∞ norm bounds rather than L_2 norm bounds. In [36] a direct application of sum of squares techniques to safety verification, without the compositional approach here, is given. An overview of the broader literature on establishing invariant sets

is given in [37].

In this chapter we first present the compositional framework for dissipative systems. We prove that for linear systems this approach is equivalent to searching for a separable storage function for the entire interconnected system. Then, we extend the framework for systems that are EID or satisfy IQCs. Finally, we show how safety certification can also be incorporated into this framework.

3.1 Stability and Performance Certification

Consider the interconnected system in Figure 3.1 where the subsystems $\Sigma_1, \ldots, \Sigma_N$ are known. Each subsystem Σ_i has dynamics

$$\dot{x}_i(t) = f_i(x_i(t), u_i(t)), \quad f_i(0,0) = 0 \tag{3.1}$$
$$y_i(t) = h_i(x_i(t), u_i(t)), \quad h_i(0,0) = 0 \tag{3.2}$$

with $x_i(t) \in \mathbb{R}^{n_i}$, $u_i(t) \in \mathbb{R}^{m_i}$, and $y_i(t) \in \mathbb{R}^{p_i}$. Define $n := n_1 + \cdots + n_N$ as the total state dimension of the interconnected system.

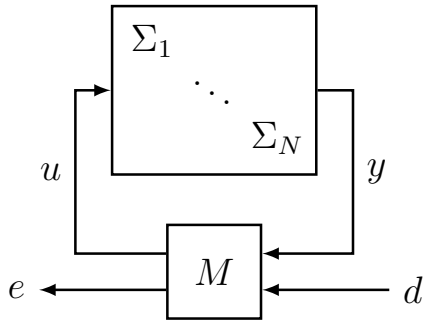

Figure 3.1: Interconnected system with input d and output e.

The static interconnection $M \in \mathbb{R}^{m \times p}$ relates

$$\begin{bmatrix} u \\ e \end{bmatrix} = M \begin{bmatrix} y \\ d \end{bmatrix} \tag{3.3}$$

where $d(t) \in \mathbb{R}^{p_d}$, $e(t) \in \mathbb{R}^{m_e}$, $m = m_1 + \cdots + m_N + m_e$, and $p = p_1 + \cdots + p_N + p_d$. We assume the interconnection is well-posed: for any $d \in L_{2e}$ and initial condition $x(0) \in \mathbb{R}^n$ there exist unique $e, u, y \in L_{2e}$ that causally depend on d.

The global and local supply rates are assumed to be quadratic forms. In particular, the global supply rate, which is specified by the analyst, is

$$\begin{bmatrix} d \\ e \end{bmatrix}^\top W \begin{bmatrix} d \\ e \end{bmatrix} \tag{3.4}$$

where W is a real symmetric matrix. The local supply rates are

$$\begin{bmatrix} u_i \\ y_i \end{bmatrix}^\top X_i \begin{bmatrix} u_i \\ y_i \end{bmatrix} \tag{3.5}$$

where X_i are real symmetric matrices to be determined.

The dissipativity certification problem will be posed as a feasibility problem involving N *local* constraints, one for each subsystem, and one *golobal* constraint. The *local* constraint sets are defined as

$$\mathcal{L}_i := \left\{ X_i \;\middle|\; \Sigma_i \text{ is dissipative w.r.t. } \begin{bmatrix} u_i \\ y_i \end{bmatrix}^\top X_i \begin{bmatrix} u_i \\ y_i \end{bmatrix} \right\} \tag{3.6}$$

and the *global* constraint set as

$$\mathcal{G} := \left\{ X_1, \ldots, X_N \;\middle|\; \begin{bmatrix} M \\ I_p \end{bmatrix}^\top P_\pi^\top Q P_\pi \begin{bmatrix} M \\ I_p \end{bmatrix} \preceq 0 \right\} \tag{3.7}$$

where $Q = \operatorname{diag}(X_1, \ldots, X_N, -W)$ and P_π is a permutation matrix defined by

$$\begin{bmatrix} u_1 \\ y_1 \\ \vdots \\ u_N \\ y_N \\ d \\ e \end{bmatrix} = P_\pi \begin{bmatrix} u \\ e \\ y \\ d \end{bmatrix}. \tag{3.8}$$

The following elementary theorem gives conditions for certifying dissipativity of the interconnected system. This theorem is a direct extension of previous results given in [7], [38].

Theorem 8. *Consider N subsystems interconnected according to* (3.3)*, with a global supply rate of the form* (3.4)*. If there exist $X_1, \ldots, X_N$ satisfying*

$$\begin{aligned} &X_i \in \mathcal{L}_i \quad \text{for } i = 1, \ldots, N \\ &(X_1, \ldots, X_N) \in \mathcal{G} \end{aligned} \tag{3.9}$$

then the interconnected system is dissipative with respect to the global supply rate. A storage function certifying global dissipativity is $V(x_1, \ldots, x_N) := \sum_{i=1}^N V_i(x_i)$ where each V_i is a storage function certifying $X_i \in \mathcal{L}_i$.

Proof. Multiplying the LMI in (3.7) on the left by $\begin{bmatrix} y \\ d \end{bmatrix}^\top$ and on the right by $\begin{bmatrix} y \\ d \end{bmatrix}$ and making use of (3.3), we obtain

$$\sum_{i=1}^{N} \begin{bmatrix} u_i \\ y_i \end{bmatrix}^\top X_i \begin{bmatrix} u_i \\ y_i \end{bmatrix} - \begin{bmatrix} d \\ e \end{bmatrix}^\top W \begin{bmatrix} d \\ e \end{bmatrix} \leq 0. \tag{3.10}$$

Since $X_i \in \mathcal{L}_i$ a storage function V_i exists such that

$$\nabla V_i(x_i)^\top f_i(x_i, u_i) - \begin{bmatrix} u_i \\ y_i \end{bmatrix}^\top X_i \begin{bmatrix} u_i \\ y_i \end{bmatrix} \leq 0 \tag{3.11}$$

for all $x_i \in \mathbb{R}^n$, $u_i \in \mathbb{R}^m$, and $y_i = h_i(x_i, u_i)$. Adding to (3.10) the local dissipativity inequalities (3.11) for each subsystem, we obtain

$$\sum_{i=1}^{N} \nabla V_i(x_i)^\top f_i(x_i, u_i) - \begin{bmatrix} d \\ e \end{bmatrix}^\top W \begin{bmatrix} d \\ e \end{bmatrix} \leq 0 \tag{3.12}$$

which certifies dissipativity with respect to the global supply rate. ∎

Furthermore, if each storage function V_i is positive definite and the global supply rate satisfies (2.3) then Theorem 8 certifies stability of the origin of the interconnected system with the Lyapunov function

$$V(x_1, \ldots, x_N) := \sum_{i=1}^{N} V_i(x_i).$$

The following simple example demonstrates Thereom 8 for a negative feedback interconnection of two passive subsystems. By the passivity theorem [7], [39] this interconnection will be passive, but in the example we certify this via the compositional approach.

Example 9. Consider the subsystems

$$\begin{aligned} \Sigma_1 : \quad & \dot{x}_1 = -x_1^3 + u_1, \quad y_1 = x_1^3 \\ \Sigma_2 : \quad & \dot{x}_2 = -x_2 + u_2, \quad y_2 = x_2 \end{aligned}$$

interconnected by

$$\begin{bmatrix} u_1 \\ u_2 \\ e_1 \\ e_2 \end{bmatrix} = M \begin{bmatrix} y_1 \\ y_2 \\ d_1 \\ d_2 \end{bmatrix} = \begin{bmatrix} 0 & 1 & 1 & 0 \\ -1 & 0 & 0 & 1 \\ 1 & 0 & 0 & 0 \\ 0 & 1 & 0 & 0 \end{bmatrix} \begin{bmatrix} y_1 \\ y_2 \\ d_1 \\ d_2 \end{bmatrix}.$$

We want to certify that the interconnection of these subsystems is passive, i.e. dissipative with respect to the supply rate

$$w(d, e) = \begin{bmatrix} d \\ e \end{bmatrix}^\top W \begin{bmatrix} d \\ e \end{bmatrix} = \begin{bmatrix} d \\ e \end{bmatrix}^\top \begin{bmatrix} 0 & I_2 \\ I_2 & 0 \end{bmatrix} \begin{bmatrix} d \\ e \end{bmatrix}.$$

The storage functions

$$V_1(x_1) = \frac{1}{2}x_1^4 \quad \text{and} \quad V_2(x_2) = x_2^2$$

certify the subsystems are output strictly passive with supply rates parameterized by

$$X_1 = \begin{bmatrix} 0 & 1 \\ 1 & -2 \end{bmatrix} \quad \text{and} \quad X_2 = \begin{bmatrix} 0 & 1 \\ 1 & -2 \end{bmatrix}.$$

The LMI in the global constraint is satisfied when we substitute in W, X_1, X_2, and M. Therefore, the interconnected system is passive.

3.2 Linear Systems with Quadratic Supply Rates

Theorem 8 certifies dissipativity of the interconnected system from the dissipativity properties of the individual subsystems and the interconnection structure M. The following theorem gives evidence that this compositional approach is not overly conservative: for linear systems the existence of a separable quadratic storage function for the interconnection is *equivalent* to the existence of supply rates satisfying (3.9). Related results in [40], [41] show that, under certain assumptions on the interconnection, passivity of an interconnected system is equivalent to passivity of the subsystems. First, we make a mild assumption on the interconnection.

Assumption 10. *The block diagonal elements of M mapping $y_i \to u_i$ are zero and the rows of M mapping $\left[\begin{smallmatrix} y \\ d \end{smallmatrix}\right] \to u_i$ are linearly independent for each i.*

The first part of Assumption 10 implies the subsystems do not have self-feedback loops. The second part implies that no elements of the input u_i for each subsystem are identical for all $\begin{bmatrix} y \\ d \end{bmatrix} \in \mathbb{R}^m$.

Theorem 11. *Consider N linear subsystems*

$$\dot{x}_i = A_i x_i + B_i u_i \tag{3.13a}$$
$$y_i = C_i x_i \tag{3.13b}$$

interconnected according to (3.3) *where M satisfies Assumption 10. Suppose a global supply rate of the form* (3.4) *is given. The following are equivalent:*

(i) There exists a separable quadratic storage function of the form

$$V(x_1, \ldots, x_N) = \sum_{i=1}^{N} x_i^\top P_i x_i$$

certifying dissipativity of the interconnected system.

(ii) Each subsystem is dissipative and the associated supply rate matrices $X_1, \ldots, X_N$ satisfy the global constraint $\mathcal{G}$. Dissipativity of each subsystem can be certified with a storage function of the form

$$V_i(x_i) = x_i^\top P_i x_i$$

for $i = 1, \ldots N$.

Proof. (ii) $\implies$ (i) follows by specializing Theorem 8 to linear subsystems and quadratic storage functions of the form $V_i(x_i) = x_i^\top P_i x_i$. Then, the dissipation inequality (3.12) implies condition (i).

(i) $\implies$ (ii): Condition (i) is equivalent to the existence of $P_i \succeq 0$ for $i = 1, \ldots, N$ such that

$$\sum_{i=1}^{N} \begin{bmatrix} x_i \\ u_i \end{bmatrix}^\top \begin{bmatrix} A_i^\top P_i + P_i A_i & P_i B_i \\ B_i^\top P_i & 0 \end{bmatrix} \begin{bmatrix} x_i \\ u_i \end{bmatrix} \leq \begin{bmatrix} d \\ e \end{bmatrix}^\top W \begin{bmatrix} d \\ e \end{bmatrix} \tag{3.14}$$

for all x and d, where u and e are expressed in terms of x and d using (3.3) and (3.13b).

Defining $V_i(x_i) := x_i^\top P_i x_i$, the i^{th} summand on the left-hand side of (3.14) is

$$\dot{V}(x_i, u_i) := \nabla V_i(x_i)^\top f_i(x_i, u_i).$$

We will prove the V_i are storage functions that certify local dissipativity of the subsystems. We assume without loss of generality that for each subsystem

$$C_i = \begin{bmatrix} 0_{m_i \times (n_i - m_i)} & I_{m_i \times m_i} \end{bmatrix}.$$

This allows each x_i to be partitioned as $x_i = \begin{bmatrix} z_i \\ y_i \end{bmatrix}$ where $z_i \in \mathbb{R}^{n_i - m_i}$ and $y_i \in \mathbb{R}^{m_i}$. Eliminating x_i from (3.14) and rearranging, we obtain

$$\sum_{i=1}^{N} \left(z_i^\top Q_i z_i + 2 z_i^\top R_i \begin{bmatrix} u_i \\ y_i \end{bmatrix} + \begin{bmatrix} u_i \\ y_i \end{bmatrix}^\top S_i \begin{bmatrix} u_i \\ y_i \end{bmatrix} \right) \leq \begin{bmatrix} d \\ e \end{bmatrix}^\top W \begin{bmatrix} d \\ e \end{bmatrix} \quad \text{for all } z, y, d \tag{3.15}$$

and appropriately chosen Q_i, R_i, and S_i. Since (3.15) holds for all z, y, d, it holds in particular when $y = d = 0$. We then have from (3.3) that $u = e = 0$, and we conclude that $Q_i \preceq 0$.

Using a similarity transform, we may assume, again without loss of generality, that z_i can be decomposed as:

$$z_i = \begin{bmatrix} \xi_i \\ \hat{z}_i \end{bmatrix}, \text{ where } z_i^\top Q_i z_i = \hat{z}_i^\top \hat{Q}_i \hat{z}_i \text{ and } \hat{Q}_i \prec 0.$$

The dimensions of $\hat{z}_i$ and $\hat{Q}_i$ correspond to the number of nonzero eigenvalues of Q_i. Rewriting

$$z_i^\top R_i \begin{bmatrix} u_i \\ y_i \end{bmatrix} = \xi_i^\top Y_i y_i + \xi_i^\top U_i u_i + \hat{z}_i^\top \hat{R}_i \begin{bmatrix} u_i \\ y_i \end{bmatrix}$$

where Y_i, U_i, and $\hat{R}_i$ are appropriately defined matrices, the summands in (3.15) take the form

$$\dot{V}_i(\hat{z}_i, \xi_i, y_i, d) = \hat{z}_i^\top \hat{Q}_i \hat{z}_i + 2\xi_i^\top Y_i y_i + 2\xi_i^\top U_i u_i + 2\hat{z}_i^\top \hat{R}_i \begin{bmatrix} u_i \\ y_i \end{bmatrix} + \begin{bmatrix} u_i \\ y_i \end{bmatrix}^\top S_i \begin{bmatrix} u_i \\ y_i \end{bmatrix}. \tag{3.16}$$

Because (3.15) holds for all z, y, d it must also hold if we maximize over $\hat{z}_i$. Performing the maximization,

$$\dot{V}_i(\hat{z}_i^\star, \xi_i, y_i, d) = \begin{bmatrix} u_i \\ y_i \end{bmatrix}^\top (S_i - \hat{R}_i^\top \hat{Q}_i^{-1} \hat{R}_i) \begin{bmatrix} u_i \\ y_i \end{bmatrix} + 2\xi_i^\top Y_i y_i + 2\xi_i^\top U_i u_i \tag{3.17}$$

where $\hat{z}_i^\star := \arg\max_{\hat{z}_i} \dot{V}_i(\hat{z}_i, \xi_i, y_i, d)$. If we further define $X_i := S_i - \hat{R}_i^\top \hat{Q}_i^{-1} \hat{R}_i$, we can write

$$\sum_{i=1}^N \dot{V}_i(\hat{z}_i^\star, \xi_i, y_i, d) = \sum_{i=1}^N \begin{bmatrix} u_i \\ y_i \end{bmatrix}^\top X_i \begin{bmatrix} u_i \\ y_i \end{bmatrix} + 2\xi^\top \bar{Y} y + 2\xi^\top \bar{U} u \tag{3.18}$$

where $\bar{Y} := \mathrm{diag}(Y_1, \ldots, Y_N)$ and $\bar{U}$ is similarly defined. Thus,

$$\sum_{i=1}^N \dot{V}_i(\hat{z}_i, \xi_i, y_i, d) \leq \sum_{i=1}^N \dot{V}_i(\hat{z}_i^\star, \xi_i, y_i, d) \leq \begin{bmatrix} d \\ e \end{bmatrix}^\top W \begin{bmatrix} d \\ e \end{bmatrix} \tag{3.19}$$

for all $\hat{z}, \xi, y, d$ where e, u satisfy (3.3). Note that the the right-hand side of (3.19) does not depend on ξ, yet its lower bound (3.18) is linear in ξ. The only way this inequality can be true for all ξ is if

$$2\xi^\top \bar{Y} y + 2\xi^\top \bar{U} u = 0 \qquad \text{for all } \xi,\ y,\ d.$$

From (3.3), we have $u = M^{11} y + M^{12} d$ and so

$$\bar{Y} + \bar{U} M^{11} = \bar{U} M^{12} = 0. \tag{3.20}$$

By denoting M_{ij}^{11} as the submatrix of M mapping $y_j \to u_i$ and M_j^{12} as the submatrix of M mapping $d \to u_i$, then for each i, (3.20) simplifies to

$$\begin{aligned} Y_i + U_i M_{ii}^{11} &= 0 \\ U_i M_{ij}^{11} &= 0 \quad \text{for } j \neq i \\ U_i M_j^{12} &= 0 \quad \text{for } j \in 1, \ldots, N \end{aligned}$$

Assumption 10 implies that $U_i = Y_i = 0$. Therefore, (3.17) simplifies to

$$\dot{V}_i(x_i, d) \leq \dot{V}_i(\hat{z}_i^\star, \xi_i, y_i, d) = \begin{bmatrix} u_i \\ y_i \end{bmatrix}^\top X_i \begin{bmatrix} u_i \\ y_i \end{bmatrix} \tag{3.21}$$

and hence, the storage function V_i certifies dissipativity of the i^{th} local subsystem with respect to the supply rate matrix X_i. Combining (3.19) and (3.21) gives

$$\sum_{i=1}^{N} \begin{bmatrix} u_i \\ y_i \end{bmatrix}^\top X_i \begin{bmatrix} u_i \\ y_i \end{bmatrix} \leq \begin{bmatrix} d \\ e \end{bmatrix}^\top W \begin{bmatrix} d \\ e \end{bmatrix}. \tag{3.22}$$

It follows from (3.21)–(3.22) that each subsystem is dissipative with respect to the supply rate parameterized by X_i and $X_1, \ldots, X_N$ is contained in the global constraint set (3.7). ∎

We next extend the results of Theorem 8 by using EID or IQCs to characterize the local and global properties.

3.3 Certification of EID Systems

In order to extend this approach to subsystems whose equilibrium is not necessarily at the origin we use EID. Therefore, we assume that for the interconnected system there exists a nonempty set $\mathcal{X}^\star \subseteq \mathbb{R}^n$ such that for each $x^\star \in \mathcal{X}^\star$ there is a unique $d^\star$ such that $f_i(x_i^\star, u_i^\star) = 0$ for $i = 1, \ldots, N$ where $y_i^\star = h_i(x_i^\star, u_i^\star)$ and

$$\begin{bmatrix} u^\star \\ e^\star \end{bmatrix} = M \begin{bmatrix} y^\star \\ d^\star \end{bmatrix}.$$

The global and local supply rates must be modified to depend on $u^\star$, $y^\star$, $d^\star$, and $e^\star$. Specifically, the global supply rate becomes

$$\begin{bmatrix} d - d^\star \\ e - e^\star \end{bmatrix}^\top W \begin{bmatrix} d - d^\star \\ e - e^\star \end{bmatrix} \tag{3.23}$$

and the local supply rates are

$$\begin{bmatrix} u_i - u_i^\star \\ y_i - y_i^\star \end{bmatrix}^\top X_i \begin{bmatrix} u_i - u_i^\star \\ y_i - y_i^\star \end{bmatrix} \tag{3.24}$$

where W and X_i are real symmetric matrices.

For each subsystem we must determine a supply rate X_i such that the subsystem is EID. Therefore, the local constraints sets are defined as

$$\mathcal{L}_i^{EID} := \left\{ X_i \;\middle|\; \Sigma_i \text{ is EID w.r.t. } \begin{bmatrix} u_i - u_i^\star \\ y_i - y_i^\star \end{bmatrix}^\top X_i \begin{bmatrix} u_i - u_i^\star \\ y_i - y_i^\star \end{bmatrix} \right\}. \tag{3.25}$$

The global constraint set $\mathcal{G}$ is unchanged.

Theorem 8 is directly applicable to this formulation by replacing the local constraint sets in (3.6) by those in (3.25).

Proposition 12. *Consider N subsystems interconnected according to* (3.3)*, with a global supply rate of the form* (3.23)*. Assume there exists a nonempty set $\mathcal{X}^\star \subseteq \mathbb{R}^n$ such that for each $x^\star \in \mathcal{X}^\star$ there is a unique $d^\star$ such that $f_i(x_i^\star, u_i^\star) = 0$ for $i = 1, \ldots, N$. Then, if there exist $X_1, \ldots, X_N$ satisfying*

$$\begin{aligned} &X_i \in \mathcal{L}_i^{EID} \quad \text{for } i = 1, \ldots, N \\ &(X_1, \ldots, X_N) \in \mathcal{G} \end{aligned} \tag{3.26}$$

then the interconnected system is EID with respect to the global supply rate.

3.4 Certification of Systems Satisfying IQCs

We extend this approach to systems that satisfy IQCs by redefining the local constraint sets as

$$\mathcal{L}_i^{IQC} := \left\{ X_i \;\middle|\; \Sigma_i \text{ satisfies the IQC } \Pi_i = \Psi_i^* X_i \Psi_i \right\} \tag{3.27}$$

where Ψ_i is a stable linear system specified by the analyst and X_i is a symmetric matrix to be determined. Let $(\hat{A}_i, \hat{B}_i, \hat{C}_i, \hat{D}_i)$ be a state space realization of Ψ_i for each $i = 1, \ldots, N$.

Rather than certify performance with respect to a global supply rate, we generalize this to certifying performance with respect to a global IQC, of the form $\Pi_{\mathrm{w}} := \Psi_{\mathrm{w}}^* W \Psi_{\mathrm{w}}$ where Ψ_{w} is a stable linear system with realization $(\hat{A}_{\mathrm{w}}, \hat{B}_{\mathrm{w}}, \hat{C}_{\mathrm{w}}, \hat{D}_{\mathrm{w}})$ and W is a real symmetric matrix, both specified by the analyst.

Let $\begin{bmatrix} y \\ d \end{bmatrix}$ be the input to a stable linear system Ψ with the state space realization:

$$\begin{aligned} \hat{A} &:= \operatorname{diag}(\hat{A}_1, \ldots, \hat{A}_N, \hat{A}_{\mathrm{w}}) \\ \hat{B} &:= \operatorname{diag}(\hat{B}_1, \ldots, \hat{B}_N, \hat{B}_{\mathrm{w}}) P_\pi \begin{bmatrix} M \\ I_p \end{bmatrix} \\ \hat{C} &:= \operatorname{diag}(\hat{C}_1, \ldots, \hat{C}_N, \hat{C}_{\mathrm{w}}) \\ \hat{D} &:= \operatorname{diag}(\hat{D}_1, \ldots, \hat{D}_N, \hat{D}_{\mathrm{w}}) P_\pi \begin{bmatrix} M \\ I_p \end{bmatrix}. \end{aligned} \tag{3.28}$$

Then the global constraint set is defined as

$$\mathcal{G}^{IQC} := \left\{ X_1, \ldots, X_N \;\middle|\; \exists\, P \succeq 0 \text{ such that } \begin{bmatrix} \hat{A}^\top P + P\hat{A} & P\hat{B} \\ \hat{B}^\top P & 0 \end{bmatrix} + \begin{bmatrix} \hat{C}^\top \\ \hat{D}^\top \end{bmatrix} Q \begin{bmatrix} \hat{C}^\top \\ \hat{D}^\top \end{bmatrix}^\top \preceq 0 \right\} \tag{3.29}$$

where $Q = \operatorname{diag}(X_1, \ldots, X_N, -W)$, as in (3.7).

Proposition 13. *Consider N subsystems interconnected according to* (3.3)*. If there exist $X_1, \ldots, X_N$ satisfying*

$$\begin{aligned} &X_i \in \mathcal{L}_i^{IQC} \quad \text{for } i = 1, \ldots, N \\ &(X_1, \ldots, X_N) \in \mathcal{G}^{IQC} \end{aligned} \tag{3.30}$$

then the interconnected system is EID with respect to the global IQC Π_W.

Proof. Let η be the state and z the output of Ψ. Defining $V(\eta) := \eta^\top P \eta$ gives

$$\dot{V}(\eta, y, d) = \begin{bmatrix} \eta \\ y \\ d \end{bmatrix}^\top \begin{bmatrix} \hat{A}^\top P + P\hat{A} & P\hat{B} \\ \hat{B}^\top P & 0 \end{bmatrix} \begin{bmatrix} \eta \\ y \\ d \end{bmatrix}.$$

The LMI in (3.29) is equivalent to

$$\dot{V}(\eta, y, d) + z^\top Q z \leq 0 \tag{3.31}$$

for all η, y, and d with $z = \hat{C}\eta + \hat{D}\,[\begin{smallmatrix} y \\ d \end{smallmatrix}]$. We partition z such that z_i is the output of Ψ_i and z_{w} is the output of Ψ_{w}. Then (3.31) becomes

$$\dot{V}(\eta, y, d) + \sum_{i=1}^{N} z_i^\top X_i z_i \leq z_{\mathrm{w}}^\top W z_{\mathrm{w}}. \tag{3.32}$$

Since each subsystem satisfies an IQC Π_i, we have $\dot{V}(x_i, \eta_i, u_i, y_i) \leq z_i^\top X_i z_i$. Adding this to (3.32) gives

$$\dot{V}(\eta, y, d) + \sum_{i=1}^{N} \dot{V}_i(x_i, \eta_i, u_i, y_i) \leq z_{\mathrm{w}}^\top W z_{\mathrm{w}}$$

certifying the interconnected system satisfies the global IQC Π_{w}. ∎

For computational considerations it is useful to understand the size of the LMI in (3.29). Suppose each subsystem has n_y outputs and n_u inputs and the subsystem IQCs are described by

$$\Psi_i(s) = \begin{bmatrix} \psi_i^1(s) \\ \vdots \\ \psi_i^{n_b}(s) \end{bmatrix} \otimes I_{n_y + n_u} \tag{3.33}$$

where $\otimes$ is the Kronecker product and ψ_i are scalar rational functions of degree q. The state dimension of Ψ (and matrix dimension of P) is $N n_b (n_u + n_y) q$ and the dimension of each X_i is $(n_b + 1)(n_u + n_y)$. For example, if $N = 30$, $q = 1$, $n_u = n_y = 1$, $n_b = 5$ then $P = P^\top \in \mathbb{R}^{300 \times 300}$ and each $X_i = X_i^\top \in \mathbb{R}^{10 \times 10}$. This results in $v = 46,800$ decision variables and $s = 330$ being the dimension of the LMI in the global constraint. While this is a large constraint it is still manageable with current SDP solvers.

3.5 Safety Certification

In this section we augment the performance certification framework to certify safety properties of the interconnected system. Specifically, we want to certify that all state trajectories of the interconnected system starting from the origin cannot intersect a given unsafe set $\mathcal{U}$ for any disturbance d with energy bounded by $\beta \in \mathbb{R}$. The disturbance d in Figure 3.1 has bounded energy if the L_2 norm satisfies

$$\|d\|^2 = \int_0^\infty |d(t)|^2 dt \leq \beta. \tag{3.34}$$

To achieve this goal, we certify that the interconnected system is dissipative with respect to the L_2 reachability supply rate $w(d, e) = \|d\|^2$. Expressed as a quadratic form as in (3.4) the matrix characterizing this supply rate is

$$W = \begin{bmatrix} I_m & 0 \\ 0 & 0 \end{bmatrix}. \tag{3.35}$$

If Theroem 8 holds with W in (3.35) then the storage function $V(x) = \sum_{i=1}^N V_i(x_i)$ satisfies $V(x) \leq \|d\|^2$. To certify safety for all d with $\|d\|^2 \leq \beta$, we need to guarantee that the sublevel set $\mathcal{V}_\beta := \{x \in \mathbb{R}^n : V(x) \leq \beta\}$ does not intersect the unsafe set $\mathcal{U}$; that is, its complement $\overline{\mathcal{V}}_\beta$ contains $\mathcal{U}$:

$$\mathcal{U} \subset \overline{\mathcal{V}}_\beta. \tag{3.36}$$

If each storage function V_i is a polynomial and $\mathcal{U}$ is a semialgebric set then we can formulate (3.36) as a SOS constraint. Let

$$\mathcal{U} = \{x \in \mathbb{R}^n \mid q_j(x) \geq 0 \text{ where } q_j \in \mathbb{R}[x] \text{ for } j = 1, \ldots, M\}. \tag{3.37}$$

Thus $\mathcal{V}_\beta$ and $\mathcal{U}$ are closed semialgebraic sets and the set containment constraint (3.36) is satisfied if there exists $\epsilon > 0$ and $s_j \in \Sigma[x]$ for $j = 1, \ldots, M$ such that

$$\sum_{i=1}^N V_i(x_i) - \beta - \epsilon - \sum_{j=1}^M s_j(x) q_j(x) \in \Sigma[x]. \tag{3.38}$$

To see that (3.38) guarantees (3.36) note that $x \in \mathcal{U}$ implies

$$\sum_{j=1}^M s_j(x) q_j(x) \geq 0$$

by definition of $\mathcal{U}$ and the fact that each s_j is SOS. Therefore, $V(x) - \beta - \epsilon \geq 0$ which implies $V(x) \geq \beta + \epsilon$, hence $x \in \overline{\mathcal{V}}_\beta$.

Proposition 14. *Consider N subsystems defined in* (3.1) *interconnected according to* (3.3)*, with a global supply rate parameterized by W in* (3.35)*. Suppose there exist $X_1, \ldots, X_N$ satisfying*

$$\begin{aligned} &X_i \in \mathcal{L}_i \quad \text{for } i = 1, \ldots, N \\ &(X_1, \ldots, X_N) \in \mathcal{G}. \end{aligned}$$

and there exists $\epsilon > 0$ and $s_j \in \Sigma[x]$ for $j = 1, \ldots, M$ such that

$$\sum_{i=1}^{N} V_i(x_i) - \beta - \epsilon - \sum_{j=1}^{M} s_j(x) q_j(x) \in \Sigma[x].$$

where each V_i certifies that $X_i \in \mathcal{L}_i$. Then, any state trajectory $x(t)$ with $x(0) = 0$ cannot intersect the unsafe set $\mathcal{U}$ in (3.37) *for any d with $\|d\|^2 \leq \beta$ for all $t \geq 0$.*

While Proposition 14 certifies $\mathcal{U} \subset \overline{\mathcal{V}}_\beta$ it can only be applied to moderately sized systems since it requires checking an SOS constraint involving all state variables of the interconnected system.

In order to improve the scalability of the safety certification technique we must make stronger assumptions about the unsafe set $\mathcal{U}$. Specifically, we assume that

$$\mathcal{U} = \cup_{i=1}^{N} \mathcal{U}_i \tag{3.39}$$

where each

$$\mathcal{U}_i = \{x \in \mathbb{R}^n \mid q_{ji}(x_i) \geq 0 \text{ where } q_{ji} \in \mathbb{R}[x_i] \text{ for } j = 1, \ldots, M_i\}.$$

With this assumption the SOS safety constraint in (3.38) can be written as the N decoupled constraints

$$V_i(x_i) - \beta - \epsilon - \sum_{j=1}^{M_i} s_{ji}(x_i) q_{ji}(x_i) \in \Sigma[x_i] \quad \text{for } i = 1, \ldots, N \tag{3.40}$$

and added to the local constraint sets. Specifically, we let the local constraint sets be

$$\mathcal{L}_i^{safe} := \left\{ X_i \;\middle|\; \begin{array}{l} \Sigma_i \text{ is dissipative w.r.t. } \begin{bmatrix} u_i \\ y_i \end{bmatrix}^\top X_i \begin{bmatrix} u_i \\ y_i \end{bmatrix} \text{ with storage function } V_i \text{ and} \\ \text{there exists } \epsilon > 0 \text{ and } s_{ji} \in \Sigma[x_i] \text{ for } j = 1, \ldots, M_i \text{ satisfying (3.40)} \end{array} \right\} \tag{3.41}$$

Proposition 15. *Consider N subsystems defined in* (3.1) *interconnected according to* (3.3)*, with a global supply rate characterized by W in* (3.35)*. If there exist $X_1, \ldots, X_N$ satisfying*

$$\begin{aligned} &X_i \in \mathcal{L}_i^{safe} \quad \text{for } i = 1, \ldots, N \\ &(X_1, \ldots, X_N) \in \mathcal{G} \end{aligned} \tag{3.42}$$

then any state trajectory $x(t)$ with $x(0) = 0$ cannot intersect the unsafe set $\mathcal{U}$ in (3.39) *for any d with $\|d\|^2 \leq \beta$ for all $t \geq 0$.*

Example 16. Consider the subsystems

$$\begin{aligned}\Sigma_1: \quad & \dot{x}_1 = -x_1^3 + u_1, \quad y_1 = x_1^3 \\ \Sigma_2: \quad & \dot{x}_2 = -x_2 + u_2, \quad y_2 = x_2\end{aligned}$$

interconnected by

$$\begin{bmatrix} u_1 \\ u_2 \end{bmatrix} = \begin{bmatrix} 0 & 1 & 1 & 0 \\ -1 & 0 & 0 & 1 \end{bmatrix} \begin{bmatrix} y_1 \\ y_2 \\ d_1 \\ d_2 \end{bmatrix}$$

where $d = \begin{bmatrix} d_1 \\ d_2 \end{bmatrix}$ are disturbances satisfying $\|d\|^2 \leq \beta$. The storage functions

$$V_1(x_1) = \frac{1}{2}x_1^4 \quad \text{and} \quad V_2(x_2) = x_2^2$$

certify the subsystems are output strictly passive with supply rates parameterized by

$$X_1 = \begin{bmatrix} 0 & 1 \\ 1 & -2 \end{bmatrix} \quad \text{and} \quad X_2 = \begin{bmatrix} 0 & 1 \\ 1 & -2 \end{bmatrix}.$$

Let

$$q_{11}(x_1) = x_1 - 1, \quad q_{12}(x_2) = x_2 - 0.8$$

and the unsafe set be $\mathcal{U} = \{x : q_{11}(x_1) \geq 0\} \cup \{x : q_{12}(x_2) \geq 0\}$.

Using Proposition 15 we certify that the system is safe for all d with $\|d\|^2 \leq 1.25$. Figure 3.2 shows the resulting level sets of the storage function for various values of β. For $\beta = 1.3$ it was not possible to certify safety of the system.

For the EID case minor modifications are required to certify safety and will be described in the following section. For the case where the subsystems satisfy IQCs it is straightforward to modify Proposition 14 or Proposition 15 to include the safety certification.

Extension to EID Systems

In order to extend this approach to EID systems we assume as in Section 3.3 that there exists a nonempty set $\mathcal{X}^\star$ of equilibrium points.

The safety constraints (3.38) or (3.40) must be modified since the subsystem storage functions depend on the unknown equilibrium $x^\star$. We also allow the unsafe set $\mathcal{U}$ to depend on $x^\star$; for example, we may consider the system safe if all trajectories remain within a distance of the equilibrium. This can be accomplished by letting the polynomials q_j that characterize the unsafe set $\mathcal{U}$ depend on $x^\star$.

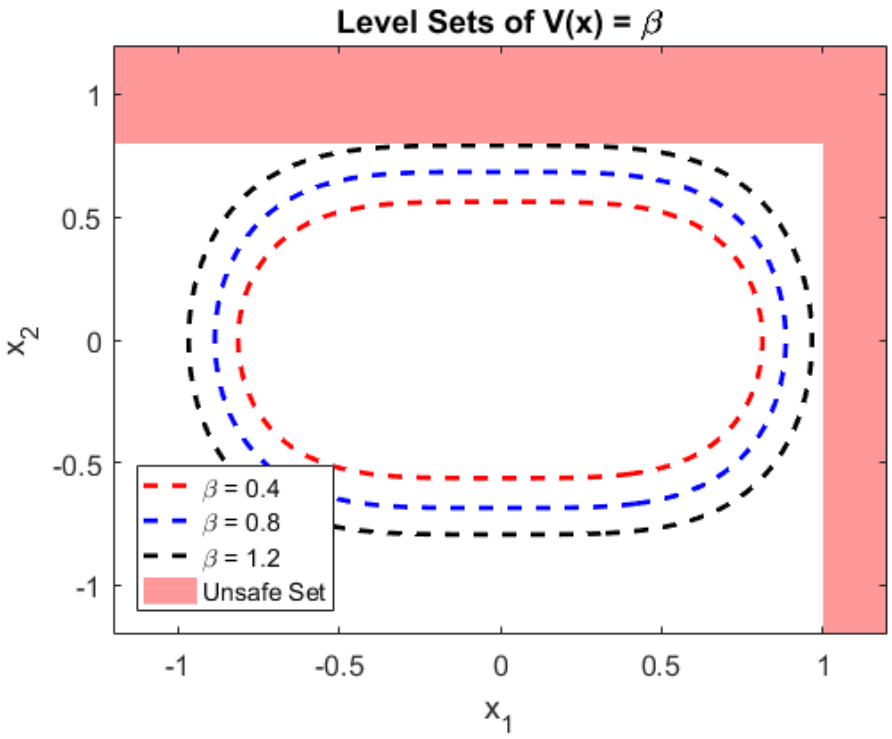

Figure 3.2: Level sets of $V(x) = V_1(x_1) + V_2(x_2) = \beta$. For increasing values of $\beta \leq 1.25$ the level sets approach but do not intersect the unsafe set.

The set containment constraint (3.36) is satisfied if there exists $\epsilon > 0$, $s_j \in \Sigma[x, x^\star]$, $j = 1, \ldots, M$, and $r_i \in \mathbb{R}[x_i, x_i^\star, u_i, u_i^\star]$, $i = 1, \ldots, N$ such that

$$\sum_{i=1}^{N} V_i(x_i, x_i^\star) - \beta - \epsilon - \sum_{j=1}^{M} s_j(x, x^\star) q_j(x, x^\star) - \sum_{i=1}^{N} r_i(x_i, x_i^\star, u_i, u_i^\star) f_i(x_i^\star, u_i^\star) \in \Sigma[x, x^\star, u, u^\star]. \quad (3.43)$$

Note that $x^\star$ and $u^\star$ in (3.43) are variables and not assumed to satisfy $f(x^\star, u^\star) = 0$. Instead, the r_k terms ensure that whenever $f(x^\star, u^\star) = 0$ then

$$\sum_{i=1}^{N} V_i(x_i, x_i^\star) - \beta - \epsilon - \sum_{j=1}^{M} s_j(x, x^\star) q_j(x, x^\star) \in \Sigma[x, x^\star] \quad (3.44)$$

as desired.

Therefore, to certify safety we can modify Proposition (14) to require that each subsystem is EID and the safety constraint (3.38) is replaced with (3.43). Then, trajectories starting from $x(0) = x^\star$ cannot intersect the unsafe set $\mathcal{U}$ for any d with $\|d\|^2 \leq \beta$.

Similarly, for the case where

$$\mathcal{U} = \cup_{i=1}^{N} \mathcal{U}_i \tag{3.45}$$

the safety constraint becomes the N decoupled constraints

$$V_i(x_i, x_i^\star) - \beta - \epsilon - \sum_{j=1}^{M_i} s_{ji}(x_i, x_i^\star) q_{ji}(x_i, x_i^\star) - \sum_{i=1}^{N} r_i(x_i, x_i^\star, u_i, u_i^\star) f_i(x_i^\star, u_i^\star) \in \Sigma[x_i, x_i^\star, u_i, u_i^\star] \quad \text{for } i = 1, \ldots, N. \tag{3.46}$$

Then, we can modify Proposition 15 by requiring each subsystem to be EID with storage function V_i that satisfies (3.46) for $i = 1, \ldots, N$. Then, trajectories starting from $x(0) = x^\star$ cannot intersect the unsafe set $\mathcal{U}$ for any d with $\|d\|^2 \leq \beta$.

Extension to Nonzero Initial Conditions

The previous safety certifications all guaranteed safety of trajectories starting from the equilibrium point (e.g. $x(0) = 0$ or $x(0) = x^\star$). It is straightforward to extend these results to the case where the initial state belongs to a semialgebraic set rather than being located at the equilibrium. Suppose the initial state is contained in the set

$$\mathcal{I} := \{x \in \mathbb{R}^n : w_\ell(x) \geq 0 \text{ where } w_\ell \in \mathbb{R}[x] \text{ for } \ell = 1, \ldots, L\}. \tag{3.47}$$

If $\mathcal{I} \subset \mathcal{V}_\alpha$ and the interconnected system is dissipative with respect to the L_2 reachability supply rate (3.35) then the state trajectory $x(t)$ is contained in the sublevel set $\mathcal{V}_{\alpha+\beta}$ for all d with $\|d\|^2 \leq \beta$, $x(0) \in \mathcal{I}$, and $t \geq 0$. Using SOS techniques we can certify $\mathcal{I} \subset \mathcal{V}_\alpha$ if

$$t_\ell \in \Sigma[x] \quad \text{for } \ell = 1, \ldots, L$$
$$-\left(\sum_{i=1}^{N} V_i(x_i) - \alpha\right) - \sum_{\ell=1}^{L} t_\ell(x) w_\ell(x) \in \Sigma[x]$$

holds. Therefore, the system is safe if the level set $\mathcal{V}_{\alpha+\beta}$ does not intersect the unsafe set $\mathcal{U}$. To guarantee this the safety constraints (3.38) or (3.40) must hold with β replaced by $\beta + \alpha$.

3.6 Chapter Summary

In this chapter a compositional approach to stability and performance certification of interconnected systems was presented. For the case of linear subsystems, we have shown this approach is equivalent to searching for a separable storage function whereas for nonlinear

systems this approach may be conservative since we are characterizing the subsystem properties with quadratic supply rates. We extended this framework to certify safety under finite energy disturbances by requiring the interconnected system to be dissipative with respect to the L_2 reachability supply rate and adding safety constraints guaranteeing that the a level set of the resulting storage function does not intersect an unsafe set.

Chapter 4

Performance Certification via Distributed Optimization

In this chapter we apply ADMM to decouple and efficiently solve the certification problems posed in Chapter 3. ADMM is a distributed optimization technique that allows the decomposition of an optimization problem into smaller subproblems [1] that are iteratively solved in a coordinated fashion to find a solution to the original problem. It has been shown to perform well for many large-scale engineering applications [1], [42], [43].

The ADMM algorithm decouples the performance certification problem into local problems for each subsystem and a global problem. In the algorithm the local problems each receive a proposed supply rate from the global problem and solves an optimization problem certifying dissipativity of the corresponding subsystem with a supply rate similar to the proposed one. The global problem, with knowledge of the interconnection M and the updated supply rates from the local problems, solves an optimization problem to certify dissipativity of the interconnected system and proposes new supply rates. The algorithm iterates until supply rates are found that certify the desired global properties.

In this chapter, we first present the general ADMM algorithm and then apply it to the certification problem. We describe the algorithm in terms of the local and global constraints sets, $(\mathcal{L}_1, \ldots \mathcal{L}_N)$ and $\mathcal{G}$ respectively, so that it can be directly applied to any of the certification problems reported in Chapter 3.

After presenting the algorithm, we describe its convergence properties and present a relaxed exit criterion that can reduce the number of iterations required to find a solution. The convergence performance of the ADMM algorithm is also compared to other common distributed optimization techniques on a large-scale linear example.

4.1 Alternating Direction Method of Multipliers (ADMM)

In general, ADMM is used to solve problems of the form

$$\begin{aligned} \text{minimize} \quad & f(x) + g(z) \\ \text{subject to} \quad & Ax + Bz = c \end{aligned} \tag{4.1}$$

where x and z are vector decision variables and f and g are extended real valued functions. The scaled ADMM algorithm is given by

$$\begin{aligned} x^{k+1} &= \arg\min_x f(x) + \frac{\rho}{2}\|Ax + Bz^k - c + \lambda^k\|_2^2 \\ z^{k+1} &= \arg\min_z g(z) + \frac{\rho}{2}\|Ax^{k+1} + Bz - c + \lambda^k\|_2^2 \\ \lambda^{k+1} &= Ax^{k+1} + Bz^{k+1} - c + \lambda^k \end{aligned}$$

where λ is a scaled dual variable. The regularization parameter ρ is a free parameter that typically effects the convergence rate of ADMM. However, for feasibility problems, where f and g are indicator functions, this parameter has no effect.

The certification problem in (3.9) may be put into this form by defining the following indicator functions:

$$\mathbb{I}_{\mathcal{L}_i}(X_i) := \begin{cases} 0 & X_i \in \mathcal{L}_i \\ \infty & \text{otherwise} \end{cases}$$

$$\mathbb{I}_{\mathcal{G}}(X_1, \ldots, X_N) := \begin{cases} 0 & (X_1, \ldots, X_N) \in \mathcal{G} \\ \infty & \text{otherwise} \end{cases}$$

and introducing the auxiliary variable Z_i for each subsystem. This allows us to rewrite (3.9) as an optimization problem in the canonical form (4.1):

$$\begin{aligned} \underset{(X_{1:N}, Z_{1:N})}{\text{minimize}} \quad & \sum_{i=1}^{N} \mathbb{I}_{\mathcal{L}_i}(X_i) + \mathbb{I}_{\mathcal{G}}(Z_1, \ldots, Z_N) \\ \text{subject to} \quad & X_i - Z_i = 0 \quad \text{for } i = 1, \ldots, N \end{aligned} \tag{4.2}$$

where $X_{1:N} := (X_1, \ldots, X_N)$. Since the other certification problems in Chapter 3 are also defined in terms of local and global constraints set they can also be put in this form.

The transformation of the feasibility problem (3.9) to the optimization problem (4.2) with indicator functions is commonly used in optimization theory [1] to allow decomposition of problems. As will be seen, in the ADMM algorithm the indicator functions in the objectives will be transformed to constraints that the subproblems must satisfy.

Note that the first term in the objective of (4.2) is separable and the constraints are decoupled. Therefore, the ADMM algorithm takes on the following parallelized form:

1. X-updates: for each $i = 1, \dots N$, solve the local problem:

$$X_i^{k+1} = \underset{X \in \mathcal{L}_i}{\arg\min} \left\| X - Z_i^k + \Lambda_i^k \right\|_F^2$$

2. Z-update: if $(X_1^{k+1}, \dots, X_N^{k+1}) \in \mathcal{G}$, then we have found a solution to (3.9), so terminate the algorithm. Otherwise, solve the global problem:

$$(Z_1^{k+1}, \dots, Z_N^{k+1}) = \underset{Z_{1:N} \in \mathcal{G}}{\arg\min} \sum_{i=1}^{N} \left\| X_i^{k+1} - Z_i + \Lambda_i^k \right\|_F^2$$

3. Λ-update: Update Λ and return to step 1.

$$\Lambda_i^{k+1} = X_i^{k+1} - Z_i^{k+1} + \Lambda_i^k$$

Figure 4.1 depicts the parallelizable nature of the ADMM algorithm. The local SDP or SOS problems are solved independently to determine the supply rate $X_i \in \mathcal{L}_i$ that is closest, in the Frobenius norm sense, to $\Lambda_i - Z_i$. These supply rates are then passed to the global problem to determine the supply rates $(Z_1, \dots, Z_N) \in \mathcal{G}$ that are closest to $X_i + \Lambda_i$. The Λ-update then plays a role analogous to integral control to drive $X_i - Z_i$ to zero.

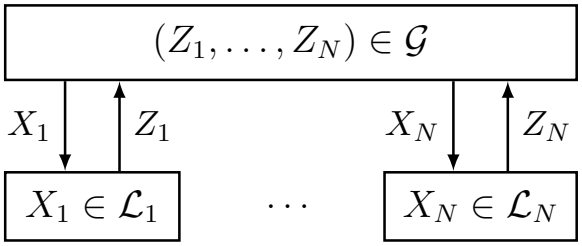

Figure 4.1: The parallelizable nature of ADMM where the local supply rates X_i are updated individually based on the subsystem properties and the global supply rates Z_i are updated simultaneously.

4.2 Convergence of ADMM

In this section we present the convergence properties of ADMM in general and applied to the certification problem. In order to do this we first define the epigraph of a function f as

$$\operatorname{epi}(f) := \left\{ (x, t) \in \mathbb{R}^{n+1} \mid f(x) \leq t \text{ for all } t \in \mathbb{R} \right\}.$$

An extended real-valued function $f : \mathbb{R}^n \to \mathbb{R} \cup \{\infty\}$ is closed, convex, and proper if and only if the epigraph of f is closed, convex, and nonempty.

Theorem 17. *If the extended real-valued functions f and g in (4.1) are closed, proper, and convex and the Lagrangian has a saddle point then as $k \to \infty$ the objective $f(x^k) + g(z^k)$ converges to the optimal value, the dual variable v^k converges to the dual optimal point $v^\star$, and the residual $Ax + Bz - c$ converges to zero [1]. Furthermore, if A and B are full column rank then the decision variables x^k and z^k are guaranteed to converge to $x^\star$ and $z^\star$ as $k \to \infty$ [44].*

Since the local and global constraint sets in (3.9) are convex and assumed to be nonempty the indicator functions $\mathbb{I}_{\mathcal{L}_i}$ and $\mathbb{I}_{\mathcal{G}}$ are closed, convex, and proper. If the intersection of the local and global constraint sets is non-empty then a feasible point $(X^\star, Z^\star)$ exists. By Slater's condition strong duality holds. Therefore, there exists a dual optimal point $\Lambda^\star$ such that the Lagrangian has a saddle point [45]. Therefore, for our application ADMM is guaranteed to find a feasible point as $k \to \infty$. A feasible point is typically found in a finite number of iterations, but if the interior of the feasible set is empty the algorithm may asymptotically approach a feasible point and reach it only in the limit. This behavior is demonstrated in the vehicle platoon example in Section 5.4.

4.3 Relaxed Exit Criterion for ADMM

Prior to the Z-update in each iteration of the ADMM algorithm we check if the local supply rates $(X_1^{k+1}, \ldots, X_N^{k+1}) \in \mathcal{G}$ and if so terminate the algorithm. By making a minor modification to this exit criterion it may be possible to significantly reduce the number of iterations required.

Note that the ADMM algorithm generates a sequence of supply rates X_i^q for $q = 1, \ldots, k+1$ that certify dissipativity for the i-th subsystem. Since a system is dissipative with respect to any conic combination of valid supply rates, we can instead check if a combination of the sequence of supply rates are in the global constraint $\mathcal{G}$. Therefore, if there exists $p_{i,q} \geq 0$ for $i = 1, \ldots, N$ and $q = 1, \ldots, k+1$ such that

$$\left(\sum_{q=1}^{k+1} p_{1,q} X_{1,q}, \ldots, \sum_{q=1}^{k+1} p_{N,q} X_{N,q} \right) \in \mathcal{G} \tag{4.3}$$

then the certification is achieved and the algorithm can be terminated. Alternatively, one may only consider a subset of recent supply rates rather than the whole sequence $q = 1, \cdots, k+1$ to reduce the number of decision variables.

This modification does not affect the iterations of the ADMM algorithm, only the exit criterion. Thus the algorithm is still guaranteed to converge, but the number of iterations can be significantly reduced.

Example 18. An interconnection of 100 two-state nonlinear SISO systems was generated. For each test the subsystem parameters and interconnection were chosen randomly but constrained so that the system had L_2 gain less then or equal to one. On 50 instances of

this problem the standard ADMM algorithm required on average 14.7 iterations. With the modified exit criterion this average dropped to 4.8.

4.4 Comparison to other Distributed Optimization Techniques

While we have found that ADMM works well for the performance certification problem, many other distributed optimization methods could also be used to solve this problem. We briefly describe a couple common methods and compare their performance with ADMM on a simple example.

Dual decomposition and the projected subgradient method presented in [1] was used in [34] to certify stability of an interconnected system by searching over the L_2 gain supply rates and in [46] to verify the safety of a system using barrier certificates. Under mild conditions on the stepsize sequence the subgradient method is guaranteed to converge to a optimal solution in the limit [47]. Unlike ADMM, this method typically requires careful tuning of the stepsize schedule and regularization parameter for different problems to get acceptable performance.

Projection methods [48], [49] can also be applied to this problem. A natural way of viewing (3.9) is that we are seeking to find a point that lies in the intersection of several sets. Note that $\mathcal{G}$ is a convex set. If all the $\mathcal{L}_i$ sets are convex as well, we may use projection methods. The simplest such method is the *alternating projection* method [48]. We tested this method as well as *Dykstra's method* [49], another popular projection method. These methods are guaranteed to converge monotonically, though the convergence rates may be very slow.

Example 19. In order to compare the different distributed optimization algorithms, we randomly generated $N = 50$ stable LTI subsystems, each with 3 states, 2 inputs, and 2 outputs. The subsystem state-space equations (2.1) then take the form

$$\Sigma_i : \qquad \begin{aligned} \dot{x}_i &= A_i x_i + B_i u_i \\ y_i &= C_i x_i + D_i u_i \end{aligned} \qquad \text{for } i = 1, \ldots, N$$

Each Σ_i was scaled so that its L_2-norm was equal to 0.95. A random interconnection matrix M was also generated with 5% of its entries nonzero. We then scaled M so that its spectral norm satisfies $\|M\| = 0.95$. The interconnected system has two inputs and two outputs that were also randomly chosen. Due to the scalings mentioned above, the interconnected system will be stable and have L_2-gain less than 1. Further random scalings $\Psi = \text{diag}(\Psi_1, \ldots, \Psi_N)$ and $\Phi = \text{diag}(\Phi_1, \ldots, \Phi_N)$ were used to transform the interconnection of Figure 3.1 into that of Figure 4.2. These final scalings do not change the closed-loop map from d to e, but they conceal the fact that the interconnection was constructed so that it satisfies the small gain theorem [50].

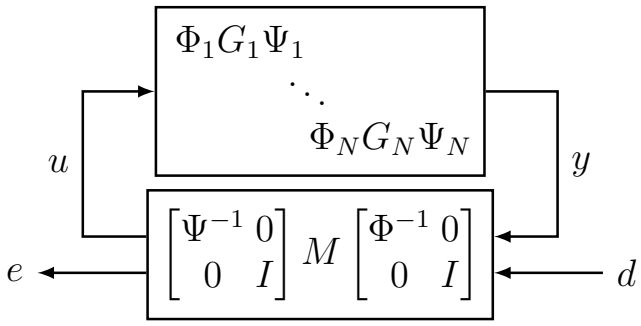

Figure 4.2: Scaling of the interconnected system of Figure 3.1 that leaves the closed-loop map unchanged.

We restricted our search to quadratic storage functions. Therefore, the $\mathcal{L}_i$ sets (3.6) are

$$\mathcal{L}_i := \left\{ X_i, P_i \;\middle|\; P_i \succeq 0, \begin{bmatrix} A_i^\top P_i + P_i A_i & P_i B_i \\ B_i^\top P_i & 0 \end{bmatrix} - \begin{bmatrix} 0 & I \\ C_i & D_i \end{bmatrix}^\top X_i \begin{bmatrix} 0 & I \\ C_i & D_i \end{bmatrix} \preceq 0 \right\}$$

The global supply rate was set as $w(u, y) = |u|^2 - |y|^2$ which certifies the L_2 gain of the system is less than or equal to 1.

Figure 4.3 shows a typical convergence plot comparing the various methods. Each method was implemented in MATLAB using the CVX toolbox [51] and SeDuMi [26] to solve the optimization problems. For each method, we plot the largest eigenvalue of the $\mathcal{G}$-constraint as a function of iteration count. When this value becomes negative, all eigenvalues are negative and the $\mathcal{G}$-constraint is satisfied; a feasible point has been found. The iterative methods were initialized using $\Lambda^0 = I$ and $X_i^0 = Z_i^0 = -I$, as applicable.

We now make a few remarks regarding these result. For the particular example plotted in Figure 4.3, the ADMM method converges in 15 iterations. Similar traces are obtained for the projected subgradient method, though the number of iterations required to find a feasible point turned out to be very sensitive to initial conditions, stepsize schedule, and regularization parameter. With a stepsize of $\alpha_k = (100 + k)^{-1}$, a feasible point was found in 187 iterations, but when the stepsizes are increased slightly to $\alpha_k = (50 + k)^{-1}$, no feasible point was found after 1000 iterations.

Finally, the alternating method and Dykstra's method exhibited a monotonically decreasing behavior typical of projection methods; they steadily approached the boundary of the feasible set without ever intersecting it.

Note that in Figure 4.3, the x-axis measures iterations rather than time or floating-point operations. Iteration count is a fair metric in this case, because all methods compared have a similar structure. Specifically, each iteration consists of parallelizable local steps involving the $\mathcal{L}_i$ constraints, and a global step involving the $\mathcal{G}$ constraint.

These results suggest that ADMM is more computationally efficient than other distributed optimization techniques for this problem. However, our primary concern is that the algorithm is robust. In order to test this, we generated 1000 random instances of the

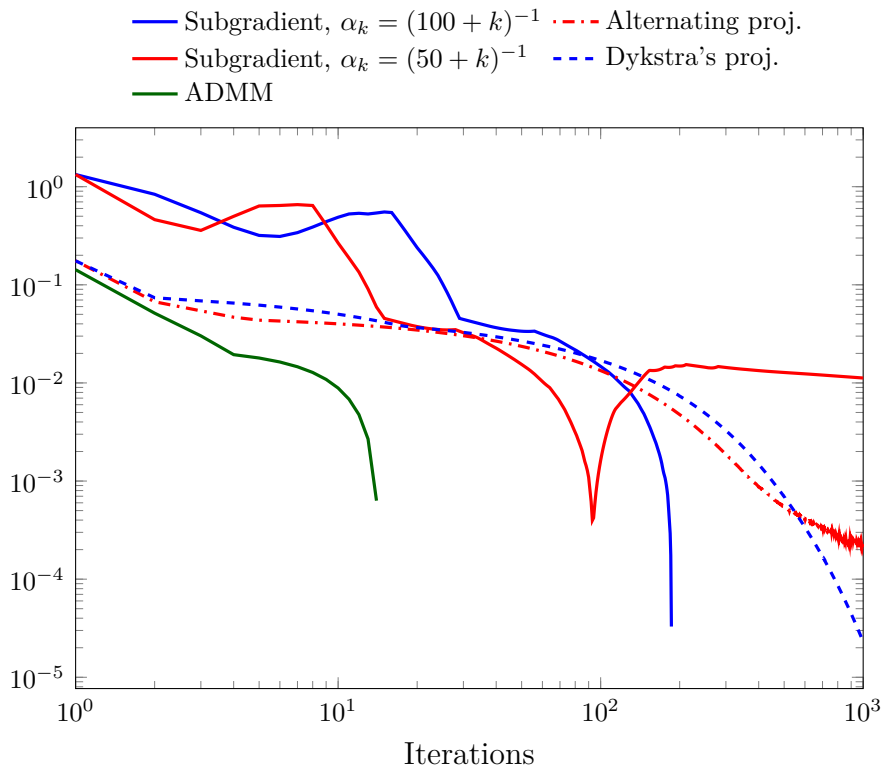

Figure 4.3: Plot of the largest eigenvalue for five different iterative methods. Feasibility is achieved when all eigenvalues are negative. ADMM converged in 15 iterations, while the other methods took significantly longer or failed to converge after 1000 iterations.

interconnected system described earlier and used ADMM to certify performance of each system. Figure 4.4 shows a cumulative frequency plot of the number of iterations required to certify performance. Only one of the 1000 systems tested required more than 40 iterations (it required 74 iterations), and 90% of systems tested required 16 iterations or fewer.

4.5 Chapter Summary

In this chapter the general ADMM algorithm was presented and applied to the certification problems described in Chapter 3. The primary benefit of this algorithm is it allows to decompose our problem into local and global subproblems that can be solved iteratively. We showed that for the certification problem the ADMM algorithm is guaranteed to converge if a solution exists and presented a relaxed exit criterion to reduce the number of iterations of the algorithm required. Finally, we demonstrated that for a simple example it performs significantly better than other distributed optimization techniques, like dual decomposition or Dykstra's Projection method.

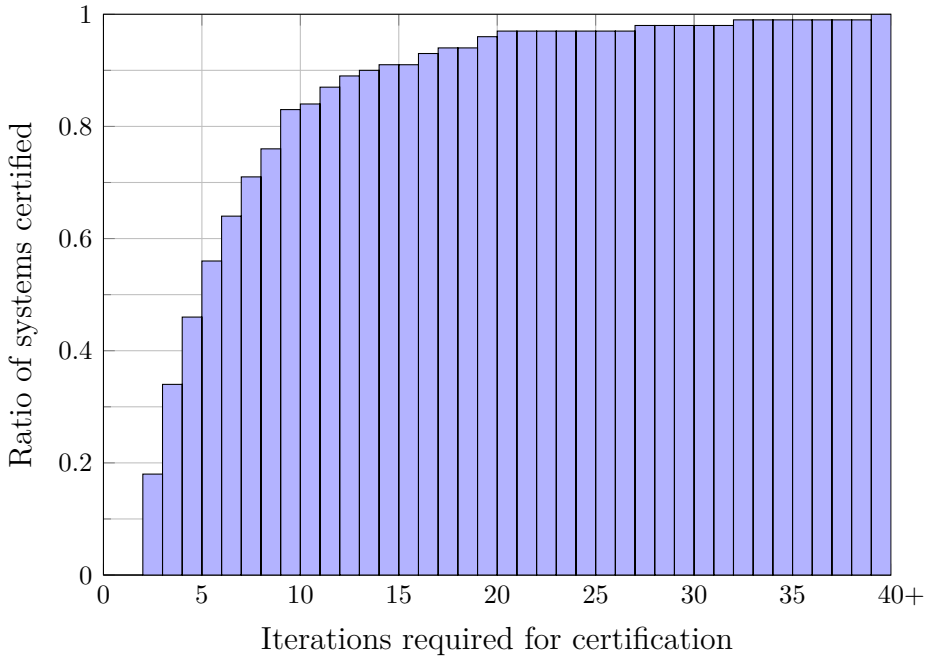

Figure 4.4: Cumulative plot showing the fraction of 1000 total trials that required at most a given number of iterations to find a feasible solution using ADMM. For example, the fastest trials found a feasible point in 4 iterations. Also, 90% of trials succeeded in 16 iterations or fewer.

Chapter 5

Large-Scale Examples

In this section we present multiple examples demonstrating the stability, performance, and safety certification using the ADMM algorithm in Chapter 4. First, two examples with linear systems are presented. The first example demonstrates the algorithms ability to reliably certify stability for a large-scale problem with a small feasible region. The second example demonstrates the benefits of characterizing the subsystem properties with IQCs. The next example demonstrates the scalable nature of the algorithm for a large interconnection of nonlinear systems and compares it to directly searching for a separable storage function. Finally, we apply this approach to certify performance and safety of a vehicle platoon.

For all examples, the Computations were performed in MATLAB using the SOSOPT toolbox [24] to formulate SOS programs and the CVX toolbox [51] to formulate SDP problems. The resulting SDPs were solved with MOSEK [25] or SeDuMi [26].

5.1 Skew-symmetric Interconnection Structure

For this example 50 linear subsystems of the following form were generated:

$$\Sigma_i : \begin{cases} \dot{x}_i = \begin{bmatrix} -\epsilon_i & 1 \\ -1 & -\epsilon_i \end{bmatrix} x_i + \begin{bmatrix} 0 \\ 1 \end{bmatrix} u_i \\ y_i = \begin{bmatrix} 0 & 1 \end{bmatrix} x_i \end{cases}$$

The decay rate ϵ_i was chosen from a uniform distribution over $\big[0, 0.1\big]$. Each subsystem is passive, but has large L_2 gain due to the small decay rates ϵ_i. The interconnection matrix M is skew-symmetric with the following form:

$$M = \begin{bmatrix} 0 & M_0 \\ -M_0^\top & 0 \end{bmatrix}$$

where each element of M_0 was chosen randomly from a standard normal distribution. This structure arises in communication networks and multiagent systems [52]–[54]. Skew-symmetry

of M along with the passivity of the subsystems guarantees stability without any restriction on the L_2-gain of the subsystems or the spectral norm of M. In contrast, a large norm (e.g. due to the size of M) and the subsystem gains prevent stability certification by the small-gain theorem.

The formulation was tested on 100 random instances of the skew-symmetric interconnected system. In all instances, the ADMM algorithm certified stability in at most 65 iterations and 90% of cases required fewer than 47 iterations (see Figure 5.1). Although we structured this example such that certification is possible with passivity, we did not bias the algorithm with this prior knowledge, and demonstrated its ability to converge to a narrow feasible set in a large-scale interconnection. We emphasize, however, that the main interest in the algorithm is when useful structural properties of the interconnection and compatible subsystem properties are not apparent to the analyst.

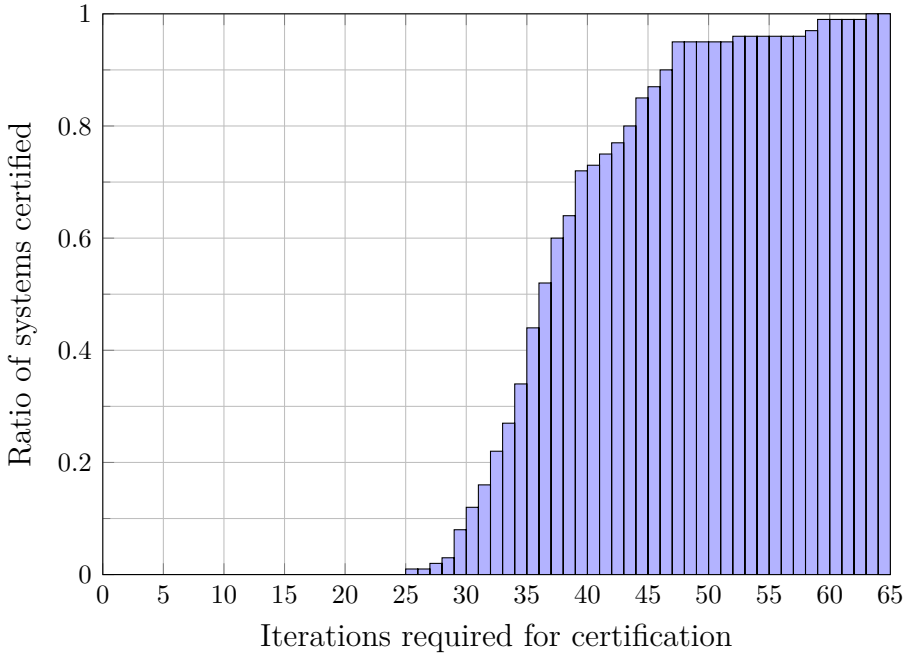

Figure 5.1: Cumulative plot showing the fraction of 100 total trials that required at most a given number of iterations to certify stability using ADMM.

5.2 IQC Example

This example, while very simple, demonstrates the advantage of using IQCs instead of dissipativity. Consider the two subsystems

$$\Sigma_1(s) = \frac{1}{s+1} \quad \text{and} \quad \Sigma_2(s) = \frac{2}{5s+1}$$

interconnected by

$$M = \begin{bmatrix} 0 & -1 & 1 \\ 1 & 0 & 0 \\ 1 & 0 & 0 \end{bmatrix}.$$

The L_2-gain of the interconnected (linear) system is approximately 0.862. However, using duality certificates, one can show that by using the compositional framework with only dissipativity properties of the subsystems it is not possible to certify the L_2-gain of the interconnected system is less than 1. By contrast, using IQCs described by

$$\Psi(s) = \begin{bmatrix} \psi_0(s) \\ \vdots \\ \psi_K(s) \end{bmatrix} \otimes I_2 \text{ where } \psi_k(s) = \left(\frac{1}{s+2}\right)^k$$

with $K = 3$ to characterize the subsystem properties, the ADMM algorithm certifies the L_2-gain of the interconnected system is less than or equal to 0.863. The IQCs in this case are more powerful because they capture the frequency dependent behavior of the individual subsystems where dissipativity is only able to certify properties that hold for all frequencies.

5.3 Large-scale Rational Polynomial System

In this example we analyze the interconnection of N, 2-state rational polynomial subsystems. Each subsystem is described by:

$$H : \begin{cases} \dot{x}_1 = x_2 \\ \dot{x}_2 = \dfrac{-ax_2 - bx_1^3 + u}{1 + cx_2^2} \\ y = x_2 \end{cases} \tag{5.1}$$

where $a, b, c > 0$ are parameters of the subsystem. The positive-definite storage function

$$V(x) := \frac{ab}{2}x_1^4 + \frac{ac}{2}x_2^4 + ax_2^2$$

with the supply rate

$$w(u, y) := u^2 - a^2y^2$$

certify that the L_2-gain of H is less than or equal to a^{-1}.

Clearly, *a*ny interconnection of these subsystems, with an interconnection matrix whose spectral norm is less than a, will have L_2-gain less than 1. This insight allows us to construct large-scale examples as described by the following steps:

1. Randomly choose parameters (a_i, b_i, c_i) from a uniform distribution on $(1, 2) \times (0, 1) \times (0.5, 2)$ for $i = 1, \ldots, N$. These constitute the parameters of each subsystem H_i for $i = 1, \ldots, N$.

2. Denote $\gamma := \max_i a_i^{-1}$.

3. Choose each entry of $S \in \mathbb{R}^{m \times p}$ from a standard normal distribution. If desired sparsity can be added to the interconnection by selectively zeroing out particular entries of S.

4. Compute $\beta = \inf_B \bar{\sigma}(BMB^{-1})$ where $B = \text{diag}(b_1, \ldots, b_N, I_d)$, $b_i > 0$ for $i = 1, \ldots, N$ and redefine
$$S := \frac{0.99}{\gamma\beta} S.$$
This guarantees the spectral norm of the interconnection is less than γ.

5. Randomly choose nonzero, diagonal scalings
$$\Psi = \text{diag}(\Psi_1, \ldots, \Psi_N)$$
where $\Psi_i \in \mathbb{R}^{m_i \times m_i}$ for $i = 1, \ldots, N$ and
$$\Phi = \text{diag}(\Phi_1, \ldots, \Phi_N)$$
where $\Phi_i \in \mathbb{R}^{p_i \times p_i}$ for $i = 1, \ldots, N$.

6. Define the final subsystems as $\Sigma_i := \Phi_i H_i \Psi_i$ and the interconnection as
$$M := \begin{bmatrix} \Psi^{-1} & 0 \\ 0 & I_d \end{bmatrix} S \begin{bmatrix} \Phi^{-1} & 0 \\ 0 & I_d \end{bmatrix}.$$

The scalings introduced in step 5 alter the gain properties of the subsystems and interconnection disguising the simple construction that guarantees the L_2-gain of the interconnected system is less than 1. Figure 5.2 below illustrates the interconnection that the algorithm must attempt to certify.

We generated 200 random instances of this interconnected system, each with $N = 100$ subsystems. The ADMM algorithm was applied to certify the L_2-gain of the interconnection is less than or equal to 1. SOS programming was used to search for quartic storage functions to certify dissipativity of the subsystems. Each storage function consists of all monomials up to degree 4. The algorithm succeeded for all 200 tests, requiring at most 48 iterations and less than 15 for 90% of the tests as shown in Figure 5.3.

Using this example we also were able to compare the computational performance of our method to directly searching for a separable storage function via SOS programming. As discussed in Section 2.6 using SOS programming on a system with 200 states is not possible. Therefore, we tested this approach with different numbers of polynomial or rational polynomial subsystems and compared it to the ADMM algorithm.

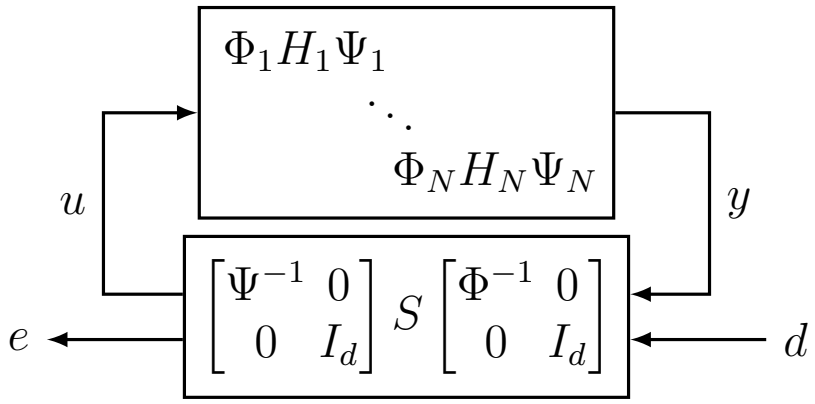

Figure 5.2: Scaling of the interconnected system of Figure 3.1.

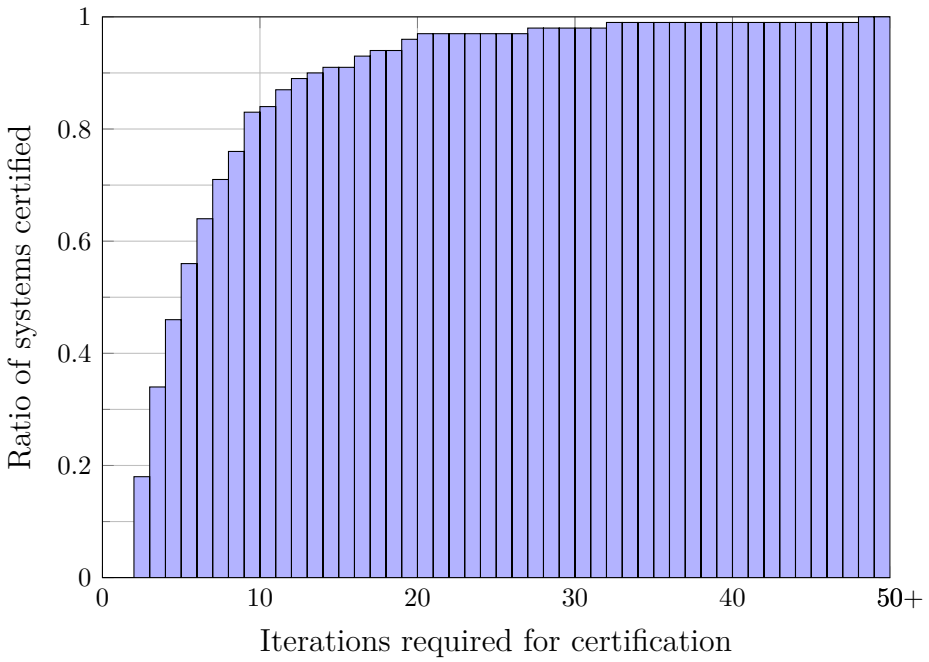

Figure 5.3: Cumulative plot showing the fraction of 200 total trials that required at most a given number of iterations to certify dissipativity using ADMM.

The subsystems and interconnection were generated as described above. For the polynomial subsystems the coefficient c in (5.1) was set to 0. Since the number of iterations for the ADMM algorithm may vary, 100 tests for each system size were performed. Figure 5.4 shows the average time for the ADMM algorithm to find a solution compared to the time to directly search for a separable storage function.

As can be seen for moderately sized systems the ADMM algorithm outperforms conventional approaches. Directly searching for a separable storage function became computa-

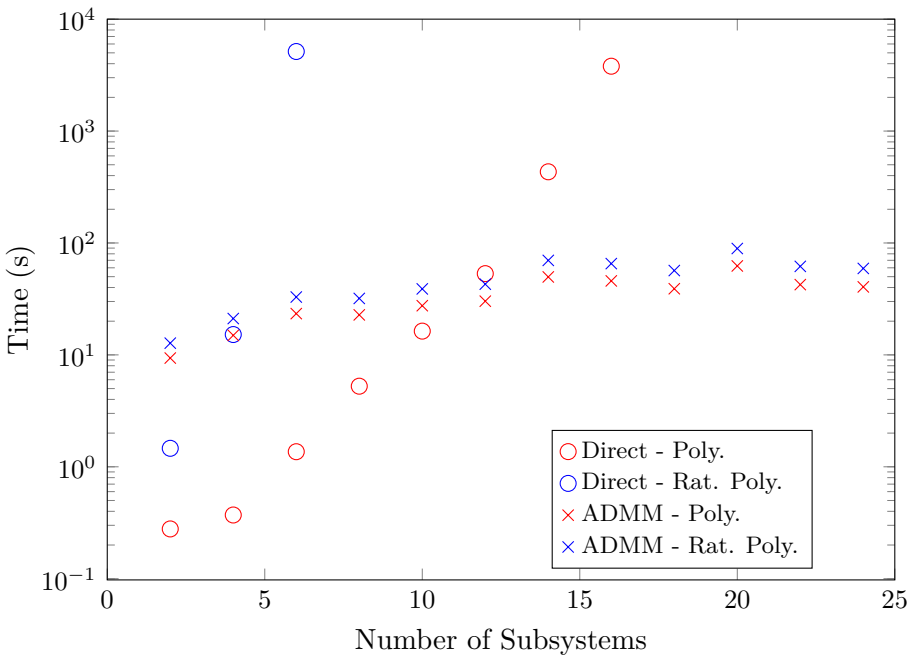

Figure 5.4: Runtime of the proposed method using ADMM compared to directly finding a separable storage function. Directly searching for a separable storage function became computationally intractable for systems with more than 16 polynomial subsystems and more than 6 rational subsystems.

tionally intractable for systems with more than 16 polynomial subsystems and more than 6 rational subsystems, while the ADMM algorithm has been used to certify properties for systems with 200 rational polynomial subsystems.

5.4 Vehicle Platoon Performance Certification

In this example we analyze the L_2-gain properties of a vehicle platoon [13], [55]. We consider a platoon with N vehicles where the dynamics of the i^{th} vehicle are described by

$$\Sigma_i : \begin{cases} \dot{v}_i(t) = -v_i(t) + v_i^{\text{nom}} + u_i(t) \\ y_i(t) = v_i(t) \end{cases} \qquad i = 1, \ldots, N \tag{5.2}$$

where v_i is the vehicle velocity and v_i^{nom} is the nominal velocity. In the absence of a control input u_i each vehicle tends to its nominal velocity.

Each vehicle uses the relative distance between itself and a subset of the other vehicles to regulate its velocity. The subsets are represented by a connected, bidirectional, acyclic graph with L links interconnecting the N vehicles. In Figure 5.5, the links are shown as dotted lines.

Letting p_ℓ be the relative displacement between the vehicles connected by link ℓ gives $\dot{p}_\ell = v_i - v_j$ where i is the leading node and j is the trailing node. We define $D \in \mathbb{R}^{N\times L}$ as

$$D_{i\ell} := \begin{cases} 1 & \text{if } i \text{ is the leading node of edge } \ell \\ -1 & \text{if } i \text{ is the trailing node of edge } \ell \\ 0 & \text{otherwise.} \end{cases} \tag{5.3}$$

Thus, $D^\top$ maps the velocities of the vehicles to the relative velocities across each link:

$$\dot{p} = D^\top v.$$

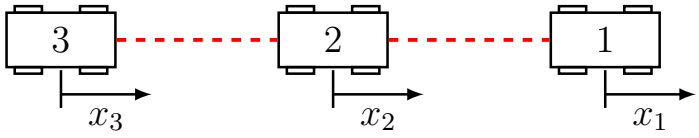

Figure 5.5: Vehicle platoon. Each vehicle measures the relative distance of all vehicles connected to it by a dotted line.

We consider a set of control laws for velocity regulation that encompass those analyzed in [13], [55]. Specifically, we let

$$u_i = -\sum_{\ell=1}^{L} D_{i\ell}\phi_\ell(p_\ell) \tag{5.4}$$

where $\phi_\ell : \mathbb{R} \to \mathbb{R}$ can be any function that is increasing and surjective. The assumptions on ϕ ensure the existence of an equilibrium point [13], but the value of the equilibrium point is unknown. Defining $\Phi := \mathrm{diag}(\phi_1, \ldots, \phi_L)$, we represent the system as the block diagram in Figure 5.6.

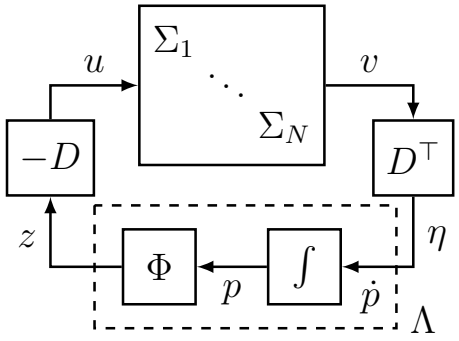

Figure 5.6: Block diagram of the vehicle platoon dynamics.

The map Λ from η to z, indicated by the dashed box in Figure 5.6, is diagonal; each $\dot{p}_\ell$ is integrated and the corresponding ϕ_ℓ is applied. Thus, we define $\Lambda := \operatorname{diag}(\Lambda_1, \ldots, \Lambda_L)$, where Λ_ℓ is

$$\Lambda_\ell : \begin{cases} \dot{p}_\ell = \eta_\ell \\ z_\ell = \phi_\ell(p_\ell) \end{cases} \qquad \ell = 1, \ldots, L \tag{5.5}$$

with input η_ℓ and output z_ℓ. By diagonally concatenating $\Sigma := \operatorname{diag}(\Sigma_1, \ldots, \Sigma_N)$ with Λ we can transform this system into Figure 5.7.

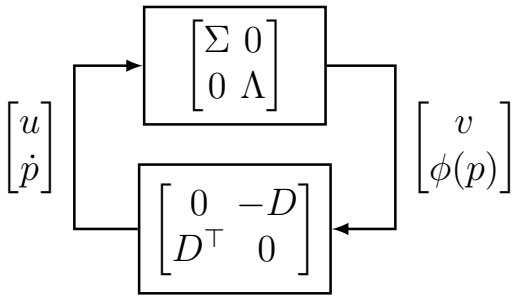

Figure 5.7: Figure 5.6 transformed into the form of Figure 3.1.

An equilibrium $(v^\star, p^\star)$ is guaranteed to exist, but it depends on the unknown functions ϕ_ℓ. Therefore, we will exploit the EID properties of the subsystems to establish the desired global property without explicit knowledge of the equilibrium.

For each Λ_ℓ subsystem the dissipativity properties depend on the unknown ϕ_ℓ function. However, it is not difficult to show that Λ_i is EID with respect to the following supply rate

$$\begin{bmatrix} \eta_\ell - \eta_\ell^\star \\ z_\ell - z_\ell^\star \end{bmatrix}^\top \begin{bmatrix} 0 & 1 \\ 1 & 0 \end{bmatrix} \begin{bmatrix} \eta_\ell - \eta_\ell^\star \\ z_\ell - z_\ell^\star \end{bmatrix} \tag{5.6}$$

for any function $\phi_\ell : \mathbb{R} \to \mathbb{R}$ that is increasing and surjective. This property can be proven by using the storage function

$$V_\ell(p_\ell) = 2 \int_{p_\ell^\star}^{p_\ell} [\phi_\ell(\theta) - \phi_\ell(p_\ell^\star)] \, d\theta$$

and the property

$$(p_\ell - p_\ell^\star)[\phi_\ell(p_\ell) - \phi_\ell(p_\ell^\star)] \geq 0$$

which follows because ϕ_ℓ is increasing. Therefore, instead of searching over supply rates for the Λ_ℓ subsystems in the ADMM algorithm, we fix (5.6) as the supply rate so that the algorithm does not rely on the ϕ_ℓ functions or their associated equilibrium points.

For the simulation, we used $N = 20$ and each vehicle's nominal velocity was randomly chosen. A linear topology was used as in Figure 5.5. That is, each vehicle measures the distance to the vehicle in front of it and the vehicle behind it. We investigated how a

force disturbance applied to the trailing vehicle would affect the velocity of the lead vehicle. Specifically, we augmented the interconnection matrix M (see Figure 3.1) such that the disturbance d is applied to the last vehicle:

$$\dot{v}_N = -v_N + v_N^{\text{nom}} + u_N + d$$

and the output e is the velocity of the first vehicle v_1. We then certified the L_2-gain from d to e is no greater than γ using the supply rate

$$\begin{bmatrix} d \\ e - e^\star \end{bmatrix}^\top \begin{bmatrix} 1 & 0 \\ 0 & -\gamma^{-2} \end{bmatrix} \begin{bmatrix} d \\ e - e^\star \end{bmatrix}.$$

A bisection search was used to find that $\gamma_{\min} = 0.71$ was the smallest value that could be certified. Since our method searches over a restricted class of possible storage functions it may be conservative. To bound this conservatism, we performed an ad-hoc search over linear ϕ_ℓ functions, seeking a worst-case L_2-gain. The result was that $\gamma_{\min} \geq 0.49$.

In this problem the interior of the feasible set is empty. Letting X^{jk} be the entry in the j-th row and k-th column of X, the local subproblems have the constraints

$$X_i^{11} \geq 0 \text{ for } i = 1, \ldots, N$$

while the global problem has the constraint

$$D^\top \text{diag}(Z_1^{11}, \ldots, Z_N^{11}) D \leq 0.$$

The only solution that satisfies both of these constraints is

$$X_i^{11} = Z_i^{11} = 0 \text{ for } i = 1, \ldots, N$$

which also implies that

$$X_i^{12} = X_i^{21} = 1 \text{ for } i = 1, \ldots, N.$$

Thus, the intersection of the $\mathcal{G}$ and $\mathcal{L}_i$ sets having an empty interior results in the ADMM algorithm oscillating between $X_i^{11} > 0$ for the local problems and $Z_i^{11} < 0$ for the global problem, leading to slow convergence and finding a feasible solution (i.e. $X_i^{11} = Z_i^{11} = 0$) in the limit.

The difficulties arising from hidden equality constraints in SDP problems are well known and there are procedures for automatically detecting these [56]. Unfortunately, it is not clear how to apply these ideas here, because the equality constraint is only present when the local and global constraints are considered simultaneously. We addressed this issue by setting $X_i^{11} = 0$ and $X_i^{12} = X_i^{21} = 1$, effectively removing those variables from the optimization. The feasible region of the resulting problem has a nonempty interior, and the ADMM algorithm converges in a few iterations.

5.5 Vehicle Platoon Safety Example

We also illustrate the safety certification procedure on the vehicle platoon. Recall that v_i for $i = 1, \ldots, N$ is the velocity of the i-th vehicle and p_ℓ for $\ell = 1, \ldots, L$ is the relative position of the vehicles connected by the ℓ-th link.

We consider an additive disturbance $(d_1, \ldots, d_N)$ on the velocity dynamics (5.2) of each vehicle and wish to find a L_2 norm bound $\|d\|^2 \leq \beta$ such that the disturbance will not cause a collision. Thus, we select the unsafe set to be

$$\mathcal{U} = \cup_{\ell=1}^{L} \mathcal{U}_\ell \quad \text{where} \quad \mathcal{U}_\ell = \{(v, p) : \ |p_\ell| \leq \gamma\} \tag{5.7}$$

with a prescribed safety margin $\gamma > 0$. If the vehicles are guaranteed to not enter the unsafe set $\mathcal{U}$ then they will always stay a distance of γ away from each other preventing the possibility of a collision.

In order to perform the safety certification we let the control law be as in (5.4) with

$$\phi_\ell(p_\ell) = (p_\ell - p_0)^{1/3}$$

for $\ell = 1, \ldots, L$ where $p_0 > 0$. Since ϕ_ℓ is increasing and onto, a unique equilibrium point exists.

The Λ_ℓ subsystems are integrators with input η_ℓ and output $\phi_\ell(p_\ell) = (p_\ell - p_0)^{1/3}$. The storage functions

$$V_\ell(p_\ell, p_\ell^\star) = \alpha_\ell \left(\frac{3}{2}(p_\ell - p_0)^{4/3} - 2(p_\ell - p_0)(p_\ell^\star - p_0)^{4/3} + \frac{1}{2}(p_\ell^\star - p_0)^{1/3} \right)$$

for $\alpha_\ell > 0$ certify equilibrium independent passivity since

$$\begin{aligned} \nabla_{p_\ell} V_\ell(p_\ell, p_\ell^\star)\eta_\ell &= ((p_\ell - p_0)^{1/3} - (p_\ell^\star - p_0)^{1/3})w_\ell \\ &= \alpha_\ell \begin{bmatrix} \eta_\ell - \eta_\ell^\star \\ \phi_\ell(p_\ell) - \phi_\ell(p_\ell^\star) \end{bmatrix}^\top \begin{bmatrix} 0 & 1 \\ 1 & 0 \end{bmatrix} \begin{bmatrix} \eta_\ell - \eta_\ell^\star \\ \phi_\ell(p_\ell) - \phi_\ell(p_\ell^\star) \end{bmatrix} \end{aligned}$$

where $\eta_\ell^\star = 0$. As in the previous example we will fix the supply rates for the Λ_ℓ subsystems, but we will allow the ADMM algorithm to search over the positive scalings $(\alpha_1, \ldots, \alpha_L)$ to certify safety. The algorithm searches for both storage functions and supply rates for the Σ_i subsystems.

As a numerical example consider a formation of $N = 3$ vehicles as in Figure 5.5. The unsafe set

$$\mathcal{U} := \{(v, p) : |p_1| \leq 5\} \cup \{(v, p) : |p_2| \leq 5\}$$

is the union of two sets; therefore, we include a constraint of the form (3.43) in each of the local constraint sets for the Λ_i subsystems. We let $v_1^0 = 9$, $v_2^0 = 10$, $v_3^0 = 11$, and $p_0 = 20$. Assuming the system is initialized at the equilibrium and a disturbance d is applied to the third vehicle, the ADMM algorithm was able to certify safety of the vehicle platoon for all

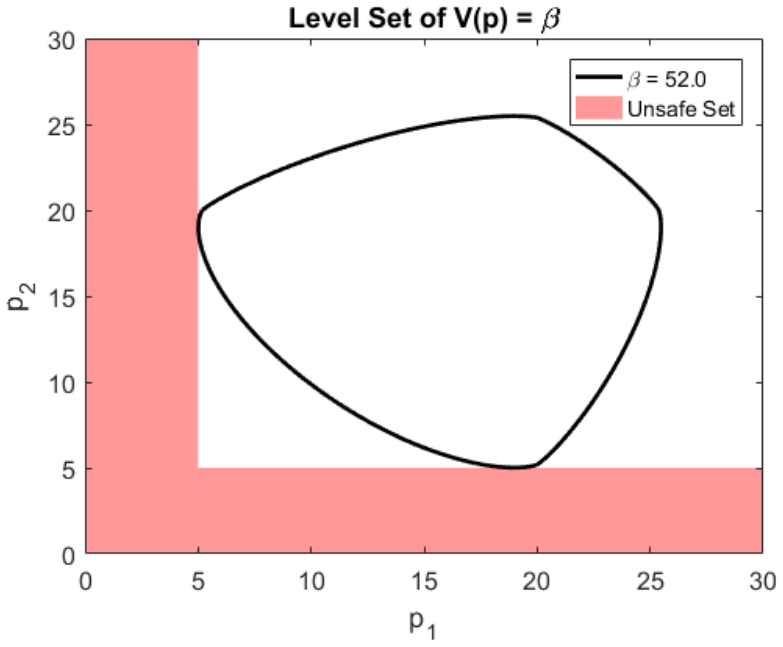

Figure 5.8: Level set of V for $\beta = 52.0$.

disturbances d such that $\|d\|^2 \leq 52.0$. The unsafe set and the level set of the storage function $V(p) = V_1(p_1, p_1^\star) + V_2(p_2, p_2^\star)$ for $\beta = 52.0$ is shown in Figure 5.8.

Note that it is not obvious how to apply the SOS techniques to the functions ϕ_ℓ and R_ℓ since they have fractional powers. To remedy this we replace $(p_\ell - p_0)^{1/3}$ and $(p_\ell^\star - p_0)^{1/3}$ with the auxiliary variables y_ℓ and $y_\ell^\star$, respectively, and include the polynomial equality constraints $(y_\ell)^3 = p_\ell - p_0$ and $(y_\ell^\star)^3 = p_\ell^\star - p_0$ in the SOS program. More information about applying SOS techniques to nonpolynomial systems can be found in [57].

Chapter 6

Symmetry Reduction

In this chapter we exploit symmetries in the interconnection matrix M to provide a dimensionality reduction in the performance certification. If the subsystems possess similar dissipativity properties then the conservatism introduced by the reduction is minimal. We demonstrate how to incorporate this reduction into the ADMM algorithm presented in Chapter 4.

Symmetries often occur naturally in interconnected systems such as ring oscillators, vehicle platoons, and robot swarms. Symmetry in the interconnection matrix M, defined by invariance under specific row and column permutations, allows the subsystems to be partitioned into equivalence classes. If the subsystems within an equivalence class share common dissipativity properties, the number of decision variables in the global constraint can be reduced. In some cases a reduction in the dimension of the linear matrix inequality (LMI) defining the global constraint is also possible. Taken together, these reductions can significantly reduce the computational time for analysis, and allow treatment of very large systems.

In general it may be difficult to determine all of the symmetries present in M, but specific instances of symmetry are readily apparent in many physical systems, like vehicle platoons or biological networks [58], where M can be interpreted as the adjacency matrix of a weighted directed graph. In some cases systems have a symmetric structure but nonidentical weights in the interconnection M prevent exploitation of this symmetry. We demonstrate that it is possible to diagonally scale M to recover this symmetry and then apply the symmetry reduction to the scaled system.

Symmetry reduction techniques have been widely applied; here we briefly summarize the results that are most relevant. In [59] stability certification of large interconnections with subsystems is achieved by checking the stability of a reduced, equivalent system. This approach requires that all of the subsystems are identical and are identically interconnected, i.e. every subsystem is connected to its neighbors in the same fashion. Symmetry reduction techniques are used in [60] to reduce the complexity of general SDP and SOS problems. These results have been applied in many areas including controller synthesis for symmetric linear systems in [61] and the fastest mixing problem in reversible Markov chains with graph

symmetries in [62]. Symmetries in the network topology have been associated in [63] with uncontrollability of networked consensus dynamics.

The approach put forth here is unique in that it does not require the subsystems to be identical or even have similar dynamics. The only requirement is that they share dissipativity properties. Furthermore, no restrictions on the interconnection are required. Reference [60] exploits symmetry in the LMI constraint and objective of the SDP; however, this may be difficult to detect. By contrast, in our approach the graph representation of the interconnection readily exposes symmetries. If the subsystems in an equivalence class share common dissipative properties these symmetries can be imposed on the global constraint reducing the number of decision variables.

In this chapter, we first define symmetries of interconnected systems via the notion of automorphisms from graph theory and describe the reduction for interconnections of dissipative systems. We demonstrate this on the vehicle platoon model presented in Section 5.4 and a large-scale cyclic interconnection of nonlinear subsystems. After these examples we present an extension of the theory for subsystems that satisfy integral quadratic constraints (IQC).

For simplicity of notation, we address the case where each subsystem is SISO (*i.e.*, $m_i = p_i = 1$, $i = 1, ..., N$) although the results are generalizable to MIMO systems (see Remark 27).

6.1 Interconnection Symmetries

To characterize the symmetry properties we adapt the notion of *automorphism* from graph theory [64] to our interconnected system with inputs e and outputs d. We represent the interconnected system as an incidence graph (Figure 6.1) where the edges are interconnections and the vertices V_N, V_D, and V_E are the subsystems, disturbance inputs, and exogenous outputs, respectively. We characterize an automorphism by matrices R_N, R_D, and R_E that permute the vertices of the graph while preserving its structure.

Definition 20. Consider the interconnection defined by the matrix M in (3.3). An *automorphism* is a tuple (R_N, R_D, R_E) where $R_N \in \mathbb{R}^{N\times N}$, $R_D \in \mathbb{R}^{p_d \times p_d}$, and $R_E \in \mathbb{R}^{m_e \times m_e}$ are permutation matrices such that the following equalities hold:

$$R_N M_{11} = M_{11} R_N \qquad R_N M_{12} = M_{12} R_D \qquad R_E M_{21} = M_{21} R_N \qquad R_E M_{22} = M_{22} R_D. \tag{6.1}$$

The set of all automorphisms of the interconnection M forms a group, called the *automorphism group*:

$$Aut(M) = \left\{ (R_N, R_D, R_E) \mid (6.1) \text{ holds} \right\}. \tag{6.2}$$

Definition 21. Given the automorphism group $Aut(M)$, the *orbit* of index $i \in V_N = \{1, ..., N\}$ is defined as:

$$O_i = \left\{ j \in V_N \;\middle|\; R_N q_i = q_j \text{ for some } (R_N, R_D, R_E) \in Aut(M) \right\} \tag{6.3}$$

where $q_i \in \mathbb{R}^{N\times 1}$ is the i-th unit vector.

Hence, two indices i, j are in the same orbit if there exists a permutation in $Aut(M)$ that permutes subsystem Σ_i with Σ_j. The orbits form an *equivalence class* given by the *equivalence relation* $\sim$, where

$$i \sim j \quad \text{if} \quad j \in O_i. \tag{6.4}$$

Let r be the number of distinct orbits, labeled as $\hat{O}_1, ..., \hat{O}_r$.

The automorphisms represent symmetries in the incidence graph $\mathcal{M}(V, E)$ of the interconnection matrix M. The vertex set of $\mathcal{M}(V, E)$ is

$$V = V_N \cup V_D \cup V_E \tag{6.5}$$

where

$$V_N = \{1, ..., N\}$$

corresponds to the subsystems Σ_i, $i = 1, ..., N$, and similarly,

$$V_D = \{N + 1, ..., N + p_d\}$$

corresponds to the disturbance inputs d_l, $l = 1, ..., p_d$, and

$$V_E = \{N + p_d + 1, ..., N + p_d + m_e\}$$

corresponds to the performance outputs e_k, $k = 1, ..., m_e$. The set of edges is

$$E = E_N \cup E_D \cup E_E \cup E_O \tag{6.6}$$

where E_N includes the edges between Σ_i and Σ_j with weight $\{M_{11}\}_{ij}$; the edges E_D from V_D to V_N represent the effect of disturbance d_l in Σ_i with input weight $\{M_{12}\}_{il}$; the edges E_E from V_N to V_E represent the effect of Σ_i in the output e_k with weight $\{M_{21}\}_{ki}$; and the edges E_O from V_D to V_E represent the throughput of the disturbance d_k on the output e_l with weight $\{M_{22}\}_{kl}$.

As an illustration, consider the cyclic network with six subsystems $\Sigma_1, ..., \Sigma_6$, one disturbance d_1, and three performance outputs e_1, e_2, e_3, with incidence graph depicted in Figure 6.1a. Since the graph is symmetric with respect to the vertical axis, it remains unchanged when 2 permutes with 6, 3 with 5, and 8 with 10. The automorphism group is given by $R_i = (R_N^i, R_D^i, R_E^i)$, for $i = 1, 2$:

$$R_1 = (I_6, 1, I_3) \quad \text{and} \quad R_2 = \left(\begin{bmatrix} 1 & 0 & 0 & 0 & 0 & 0 \\ 0 & 0 & 0 & 0 & 0 & 1 \\ 0 & 0 & 0 & 0 & 1 & 0 \\ 0 & 0 & 0 & 1 & 0 & 0 \\ 0 & 0 & 1 & 0 & 0 & 0 \\ 0 & 1 & 0 & 0 & 0 & 0 \end{bmatrix}, 1, \begin{bmatrix} 0 & 0 & 1 \\ 0 & 1 & 0 \\ 1 & 0 & 0 \end{bmatrix} \right).$$

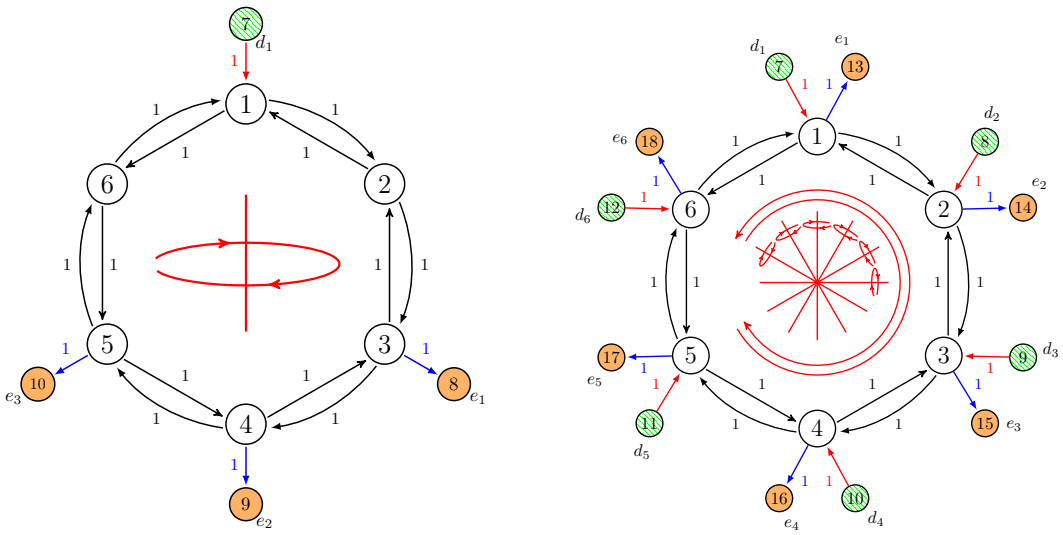

(a) (b)

Figure 6.1: Graph representation of cyclic networks with six subsystems. White vertices represent the subsystems Σ_i, green dashed vertices represent the disturbances d_l, and orange filled vertices represent the outputs e_k.

The four distinct orbits are $\hat{O}_1 = \{1\}$, $\hat{O}_2 = \{2, 6\}$, $\hat{O}_3 = \{3, 5\}$, $\hat{O}_4 = \{4\}$.

In Figure 6.1b each subsystem has a disturbance input performance output pair, and $M_{12} = M_{21} = I_N$. Thus, definition (6.1) implies that $R_D = R_E = R_N$, and the automorphisms are determined by R_N alone. The graph now exhibits rotational symmetry as well as symmetry with respect to all axes that are angled by integer multiples of 30^o. Thus all subsystems permute with each other (as well as all disturbances and outputs) and there is only one orbit: $\hat{O}_1 = \{1, ..., 6\}$.

Remark 22. The full automorphism group of the interconnection may be hard to compute [65]. However, we can still make use of subgroups corresponding to symmetries that are easy to identify. The reduction discussed in the next section is valid for any subgroup of $Aut(M)$ although the reduction may not be as extensive.

6.2 Symmetry Reduction for Performance Certification

In this section, we use the automorphism group of the interconnection matrix M to reduce the dimensionality of the LMI in the global constraint set $\mathcal{G}$ in (3.7) used in Theorem 8. We present these results for the case when the subsystems are dissipative and we certify dissipativity of the interconnected system, but they are directly applicable if the subsystems

are EID and we want to certify EID of the interconnected system. In Section 6.8 we generalize these result for subsystems that satisfy IQCs.

For convenience, we restate the LMI in the global constraint set:

$$\begin{bmatrix} M \\ I_p \end{bmatrix}^\top P_\pi^\top Q P_\pi \begin{bmatrix} M \\ I_p \end{bmatrix} \preceq 0 \tag{6.7}$$

where $Q = \mathrm{diag}(X_1, \ldots, X_N, -W)$ and P_π is the permutation matrix defined in (3.8).

Lemma 23. *If* (6.7) *holds for* $(X_1, ..., X_N, W)$ *then it also holds for* $(\tilde{X}_1, ..., \tilde{X}_N, \tilde{W})$*, where*

$$\tilde{X}_i := \frac{1}{|O_i|} \sum_{j \in O_i} X_j \tag{6.8}$$

and

$$\tilde{W} := \frac{1}{k} \sum_{i=1}^{k} \begin{bmatrix} R_D^i & 0 \\ 0 & R_E^i \end{bmatrix}^\top W \begin{bmatrix} R_D^i & 0 \\ 0 & R_E^i \end{bmatrix} \tag{6.9}$$

with $k = |Aut(M)|$ *and* $(R_N^i, R_D^i, R_E^i) \in Aut(M)$.

Proof. Let $R_L := \mathrm{diag}(R_N, R_E)$ and $R_R := \mathrm{diag}(R_N, R_D)$ be constructed from an automorphism $(R_N, R_D, R_E) \in Aut(M)$. Since the matrices R_N, R_E, R_D are orthonormal, the following holds for M and P_π,

$$\begin{bmatrix} M \\ I_p \end{bmatrix} = \begin{bmatrix} R_L & 0 \\ 0 & R_R \end{bmatrix} \begin{bmatrix} M \\ I_p \end{bmatrix} R_R^\top \quad \text{and} \quad P_\pi \begin{bmatrix} R_L & 0 \\ 0 & R_R \end{bmatrix} = S P_\pi$$

where

$$S = \mathrm{diag}(R_N \otimes I_2, R_D, R_E) \tag{6.10}$$

Then, the following LMI equivalence holds:

$$\begin{bmatrix} M \\ I_p \end{bmatrix}^\top P_\pi^\top Q P_\pi \begin{bmatrix} M \\ I_p \end{bmatrix} \preceq 0 \quad \Leftrightarrow \quad \begin{bmatrix} M \\ I_p \end{bmatrix}^\top P_\pi^\top S^\top Q S P_\pi \begin{bmatrix} M \\ I_p \end{bmatrix} \preceq 0. \tag{6.11}$$

Since Q is block diagonal

$$S^\top Q S = \left[\begin{array}{ccc|c} X_{R_N(1)} & & & \\ & \ddots & & 0 \\ & & X_{R_N(N)} & \\ \hline & 0 & & -\hat{W} \end{array}\right]$$

with

$$\hat{W} = \begin{bmatrix} R_D & 0 \\ 0 & R_E \end{bmatrix}^\top W \begin{bmatrix} R_D & 0 \\ 0 & R_E \end{bmatrix}$$

where the subscripts $R_N(i)$ represent the subsystem to which i gets permuted. Finally, since the equivalence in (6.11) holds for all automorphisms in $Aut(M)$, we take the mean over all automorphisms to obtain:

$$\begin{bmatrix} M \\ I_p \end{bmatrix}^\top P_\pi^\top Q P_\pi \begin{bmatrix} M \\ I_p \end{bmatrix} \preceq 0 \quad \Leftrightarrow \quad \begin{bmatrix} M \\ I_p \end{bmatrix}^\top P_\pi^\top \underbrace{\frac{1}{k}\sum_{i=1}^{k} S_i^\top Q S_i}_{:=\tilde{Q}} P_\pi \begin{bmatrix} M \\ I_p \end{bmatrix} \preceq 0 \tag{6.12}$$

where $k = |Aut(M)|$ and each block in $\tilde{Q}$ becomes

$$\tilde{X}_i = \frac{1}{|O_i|}\sum_{j \in O_i} X_j \quad \text{and} \quad \tilde{W} = \frac{1}{k}\sum_{i=1}^{m} \hat{W}_i$$

with $\tilde{X}_i = \tilde{X}_j$ for $i \sim j$. ∎

This lemma implies that (6.7), when feasible, admits a solution satisfying

$$\tilde{X}_i = \tilde{X}_j \quad \text{if} \quad i \sim j. \tag{6.13}$$

Thus, we may search for one common variable for subsystems in the same orbit. In particular, when M is vertex-transitive (i.e., all the vertices in V_N, V_D, and V_E permute with each other as in Figure 6.1b) there is only one orbit $\hat{O}_1 = V_N$ and the number of matrix decision variables X_i reduces to one.

Note, however, that in this reduction W is replaced with $\tilde{W}$ in (6.9). Since W specifies the desired performance, we ask that W be invariant under $Aut(M)$, so that $W = \tilde{W}$.

Assumption 24. *The matrix W is invariant under $Aut(M)$; that is,*

$$\begin{bmatrix} R_D & 0 \\ 0 & R_E \end{bmatrix} W = W \begin{bmatrix} R_D & 0 \\ 0 & R_E \end{bmatrix} \quad \textit{for all} \quad (R_N, R_D, R_E) \in Aut(M). \tag{6.14}$$

As an example, suppose we want to certify an L_2-gain bound in the network of Figure 6.1a with the global supply rate

$$w(d,e) = \|d_1\|^2 - \frac{1}{\gamma_1^2}\|e_1\|^2 - \frac{1}{\gamma_2^2}\|e_2\|^2 - \frac{1}{\gamma_3^2}\|e_3\|^2.$$

If we seek the same gain bound for e_1 and e_3, $\gamma_1 = \gamma_3$, then the corresponding W is invariant under $Aut(M)$ because the global supply rate is unchanged under the automorphism that permutes e_1 and e_3.

The combination of Lemma 23 with Assumption 24 leads to the following main result:

Theorem 25. *If* (6.7) *holds with* $(X_1, ..., X_N)$ *and Assumption 24 is satisfied, then* (6.7) *also holds with* $(\tilde{X}_1, ..., \tilde{X}_N)$ *where* $\tilde{X}_i = \tilde{X}_j$ *for* $i \sim j$.

Theorem 25 states that the feasibility of the LMI in (6.7) is not compromised if we reduce the search space to identical supply rates for subsystems in the same orbit. For identical subsystems, or more generally subsystems that are all dissipative with respect to the same set of supply rates, this does not add any conservatism. Otherwise, demanding the subsystems are dissipative with respect to a common supply rate may introduce conservatism. However, this conservatism is minimal if the subsystems share similar dissipativity properties such as passivity or finite L_2-gain.

In addition to this result, the contrapositive of Lemma 23 provides an infeasibility certificate:

Corollary 26. *If there is no* $(\tilde{X}_1, ..., \tilde{X}_N, \tilde{W})$ *satisfying* (6.7) *with* $\tilde{X}_i = \tilde{X}_j$ *for* $i \sim j$, *then no other* $(X_1, ..., X_N, W)$ *satisfying* (6.7) *exists.*

Remark 27. For MIMO systems, the definition of automorphism in (6.1) changes to the tuple (R_U, R_Y, R_D, R_E), such that $R_U M_{11} = M_{11} R_Y$, where $M_{11} \in \mathbb{R}^{m_N \times p_N}$, $R_U \in \mathbb{R}^{m_N \times m_N}$, and $R_Y \in \mathbb{R}^{p_N \times p_N}$ with $m_N := \sum_{i=1}^{N} m_i$ and $p_N := \sum_{i=1}^{N} p_i$. Instead of interpreting the automorphism as a permutation on the subsystems, we now look for permutations of inputs and outputs for each subsystem. Moreover, note that $X_i \in \mathbb{R}^{(m_i+p_i)\times(m_i+p_i)}$ and that (6.13) still holds, but the labeling of u_i and y_i must be chosen appropriately in order to obtain $\tilde{X}_i$ as in Lemma 23.

6.3 Recovering Symmetry with Weight Balancing

In practice the *unweighted* incidence graph of M may possess symmetries which are lost in the weighted graph because the edges are not compatibly weighted. As an example see Figure 6.2a where the apparent rotational symmetry is broken unless the weights g_i are identical for each i, and the same holds for g_{d_i} and g_{e_i}. In this case symmetry can be recovered by transforming M into an interconnection $\hat{M}$ with weight redistributions on the edges of M. Indeed, our performance certificate remains valid under the transformation

$$\hat{M} := \begin{bmatrix} D_N & 0 \\ 0 & D_E \end{bmatrix}^{-1} M \begin{bmatrix} D_N & 0 \\ 0 & D_D \end{bmatrix}, \tag{6.15}$$

where $D_N \in \mathbb{C}^{N\times N}$, $D_D \in \mathbb{C}^{p_d \times p_d}$, and $D_E \in \mathbb{C}^{m_e \times m_e}$ are diagonal and invertible.

Lemma 28. *The LMI in* (6.7) *is satisfied by* $(X_1, ..., X_N, W)$ *with the interconnection matrix* M *if and only if it is satisfied by* $(\hat{X}_1, ..., \hat{X}_N, \hat{W})$ *with the interconnection matrix* $\hat{M}$, *where* $\hat{X}_i = |\{D_N\}_i|^2 X_i$ *and*

$$\hat{W} = \begin{bmatrix} D_D & 0 \\ 0 & D_E \end{bmatrix}^{*} W \begin{bmatrix} D_D & 0 \\ 0 & D_E \end{bmatrix}. \tag{6.16}$$

An application of Lemma 28 is illustrated in Figure 6.2 where the graph in Figure 6.2a is transformed into the vertex-transitive graph in Figure 6.2b with the weight balancing matrices:

$$\begin{aligned} D_N &= \operatorname{diag}\left(1, \frac{g_2 g_3}{r^2}, \frac{g_3}{r}\right) \\ D_D &= \operatorname{diag}\left(\frac{1}{g_{d_1}}, \frac{g_2 g_3}{g_{d_2} r^2}, \frac{g_3}{g_{d_3} r}\right) \\ D_E &= \operatorname{diag}\left(g_{e_1}, \frac{g_2 g_3 g_{e_2}}{r^2}, \frac{g_3 g_{e_3}}{r}\right), \end{aligned} \tag{6.17}$$

where $r = (g_1 g_2 g_3)^{\frac{1}{3}}$. Thus, the decision variables in (6.7) can be reduced to a single matrix variable. When $g_1 g_2 g_3 < 0$, these matrices are complex and the weights throughout the cycle can be balanced to $r = |g_1 g_2 g_3|^{\frac{1}{3}} e^{-i\frac{\pi}{3}}$.

6.4 Symmetry Reduction with ADMM

In this section we demonstrate how the ADMM algorithm presented in Section 4.1 can be modified to take into account the symmetry reduction techniques. This further improves the scalability and computational efficiency of this approach.

In Section 4.1 we posed the performance certification problem as the optimization problem

$$\begin{aligned} \underset{(X_{1:N}, Z_{1:N})}{\text{minimize}} \quad & \sum_{i=1}^{N} \mathbb{I}_{\mathcal{L}_i}(X_i) + \mathbb{I}_{\mathcal{G}}(Z_1, \ldots, Z_N) \\ \text{subject to} \quad & X_i - Z_i = 0 \quad \text{for } i = 1, \ldots, N \end{aligned} \tag{6.18}$$

where $X_{1:N} := (X_1, \ldots, X_N)$. From Theorem 25, problem (6.18) can be reduced to

$$\begin{aligned} \underset{(X_{1:N}, Z_{1:N})}{\text{minimize}} \quad & \sum_{i=1}^{N} \mathbb{I}_{\mathcal{L}_i}(X_i) + \mathbb{I}_{\mathcal{G}}(Z_1, \ldots, Z_N) \\ \text{subject to} \quad & Z_i = Z_j \quad \text{for } i \sim j \\ & X_i = Z_i \quad \text{for } i = 1, \ldots, N \end{aligned} \tag{6.19}$$

where the equality constraint $Z_i = Z_j$ for $i \sim j$ reduces the number of independent decision variables.

Then the ADMM algorithm for (6.19) becomes:

1. X-updates: for each i, solve the local problem:

$$X_i^{k+1} = \underset{X \in \mathcal{L}_i}{\arg\min} \left\| X - Z_i^k + \Lambda_i^k \right\|_F^2$$

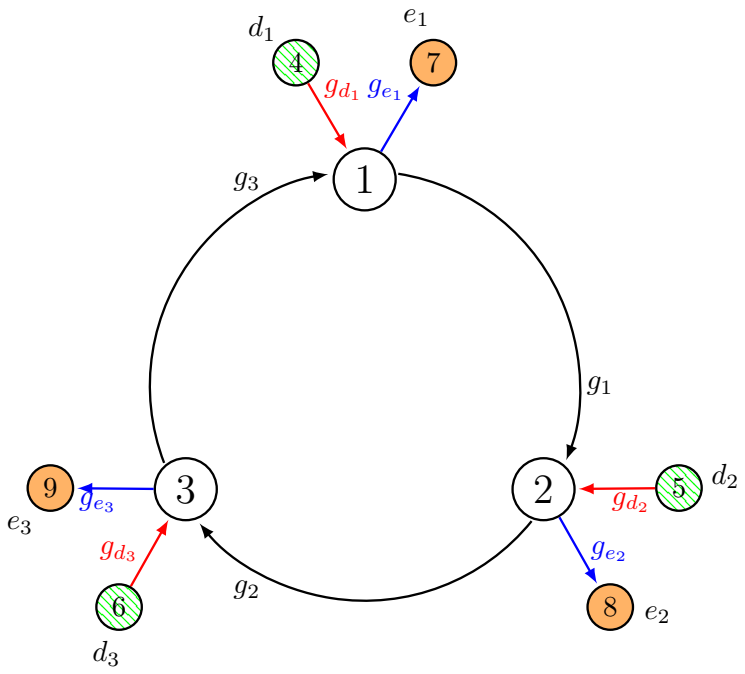

(a) Original interconnection with trivial $Aut(M)$.

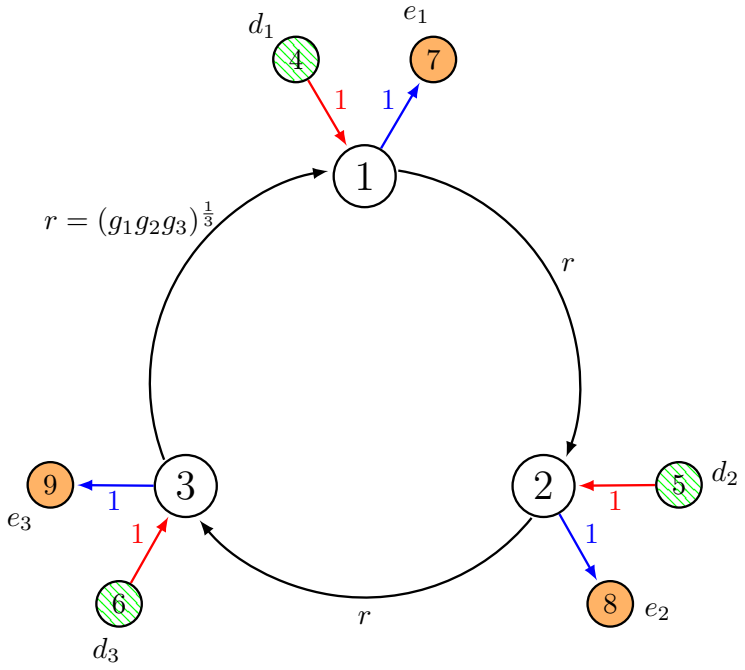

(b) Balanced interconnection with a unique orbit $O_1 = V_N$

Figure 6.2: Balancing the weights of the original interconnection M as in (6.15), with (6.17).

2. Z-update: solve the global problem:

$$(Z_1^{k+1}, \ldots, Z_N^{k+1}) = \underset{Z_{1:N} \in \mathcal{G}}{\arg\min} \sum_{i=1}^{N} \left\| X_i^{k+1} - Z_i + \Lambda_i^k \right\|_F^2$$
$$\text{subject to} \quad Z_i = Z_j \text{ for } i \sim j$$

3. Λ-update: If $Z_i^{k+1} \in \mathcal{L}_i$ for $i = 1, \ldots, N$ then terminate the algorithm. Otherwise, update Λ and return to step 1.

$$\Lambda_i^{k+1} = X_i^{k+1} - Z_i^{k+1} + \Lambda_i^k$$

Once $(Z_1, \ldots, Z_N)$ satisfy the local constraints then the performance of the system is certified and the algorithm may be terminated. However, for a large number of subsystems, it may be undesirable to check this condition on every iteration. Instead, one could check the convergence of the primal and dual residuals, defined as $r_i^{k+1} := X_i^{k+1} - Z_i^{k+1}$ and $s_i^{k+1} := Z_i^{k+1} - Z_i^k$, respectively. With these modifications the ADMM algorithm is still guaranteed to converge as $k \to \infty$ if a feasible point exists as described in Section 4.2.

6.5 Reducing the Global LMI to a Quotient LMI

In Section 6.2 we showed how symmetries in the interconnected system allows us to reduce the number of decision variables in the global LMI constraint (6.7), from $X_1, ..., X_N$ to $(\tilde{X}_1, ..., \tilde{X}_N)$ with $\tilde{X}_i = \tilde{X}_j$ for $i \sim j$. In this section we exploit the symmetry further to reduce the dimension of (6.7).

First, we define

$$A := \begin{bmatrix} M \\ I_p \end{bmatrix}^\top P_\pi^\top \tilde{Q} P_\pi \begin{bmatrix} M \\ I_p \end{bmatrix} \tag{6.20}$$

where $\tilde{Q} = \frac{1}{k} \sum_{i=1}^{k} S_i^\top Q S_i$ as in (6.12). Then, we define $T_I := \text{diag}(T_N, T_D)$ and $T_O := \text{diag}(T_N, T_E)$ where

$$\{T_N\}_{ij} = \begin{cases} 1 & \text{if vertex } i \in V_N \text{ is in orbit } j \\ 0 & \text{otherwise.} \end{cases}$$

T_D and T_E are defined similarly for the vertices in V_D and V_E and their orbits.

For the example in Figure 6.1a, we have:

$$T_N = \begin{bmatrix} 1 & 0 & 0 & 0 \\ 0 & 1 & 0 & 0 \\ 0 & 0 & 1 & 0 \\ 0 & 0 & 0 & 1 \\ 0 & 0 & 1 & 0 \\ 0 & 1 & 0 & 0 \end{bmatrix} \qquad T_D = 1 \qquad T_E = \begin{bmatrix} 1 & 0 \\ 0 & 1 \\ 1 & 0 \end{bmatrix}$$

The symmetry in the interconnection matrix implies that $MT_I = T_O\overline{M}$ where

$$\overline{M} := (T_O^\top T_O)^{-1} T_O^\top M T_I$$

is the *quotient* interconnection matrix. Due to the symmetry of $\tilde{Q}$ the matrix A in (6.20) is also symmetric and $AT_I = T_I\overline{A}$ where

$$\begin{aligned}\overline{A} &:= (T_I^\top T_I)^{-1} T_I^\top A T_I \\ &= (T_I^\top T_I)^{-1} \begin{bmatrix} \overline{M} \\ I \end{bmatrix}^\top \overline{P}_\pi^\top \overline{Q}\, \overline{P}_\pi \begin{bmatrix} \overline{M} \\ I \end{bmatrix}\end{aligned}$$

with

$$\begin{aligned}\overline{P}_\pi &:= (T_S^\top T_S)^{-1} T_S^\top P_\pi T \\ \overline{Q} &:= T_S^\top Q T_S\end{aligned}$$

where $T := \mathrm{diag}(T_O, T_I)$ and $T_S := \mathrm{diag}(T_N \otimes I_2, T_D, T_E)$. Under certain conditions on the matrix A we show that if $\overline{A}$ is negative semidefinite then A is also negative semidefinite. This is beneficial because the dimension of the LMI $A \preceq 0$ is

$$s = p_d + \sum_{i=1}^{N} p_i$$

and can be replaced by the *quotient* LMI $\overline{A} \preceq 0$ of dimension

$$s = r_d + \sum_{i=1}^{r_N} p_i$$

where r_d and r_N are the number of orbits in V_D and V_N, respectively.

First, we define the concept of a *quasi-positive* matrix:

Definition 29. A matrix N is said to be *quasi-positive* if $\{N\}_{ij} \geq 0$ for $i \neq j$.

Proposition 30. *If A is a quasi-positive matrix then*

$$A \preceq 0 \;\Leftrightarrow \lambda_{max}(\overline{A}) \leq 0. \tag{6.21}$$

Proof. Since A is symmetric, it is enough to show that largest eigenvalue of A is nonpositive if and only the largest eigenvalue of $\overline{A}$ is also nonpositive. Thus, due to quasi-positiveness of A, the proof follows from the following claim.

Lemma 31. *The largest eigenvalue of $\overline{A}$ is equal to the largest eigenvalue of A.*

Proof. First, we show that all eigenvalues of $\overline{A}$ are also eigenvalues of A. Letting $\overline{A}\overline{v} = \lambda\overline{v}$ and $v = T_I\bar{v}$ we have

$$Av = AT_I\overline{v} = T_I\overline{A}\overline{v} = \lambda T_I\overline{v} = \lambda v. \tag{6.22}$$

Then, since A is quasi-positive, it follows from the Perron-Frobenius Theorem that $\lambda_{max}(A)$ has an associated eigenvector that is positive, i.e., $v_M > 0$. Since v_M is positive, the vector $\overline{v}_M = (T_I^\top T_I)^{-1}T_I^\top v_M$ is nonzero and we can show it is an eigenvector of $\overline{A}$:

$$\begin{aligned}\overline{A}\overline{v}_M &= (T_I^\top T_I)^{-1}T_I^\top AT_I\overline{v}_M = (T_I^\top T_I)^{-1}T_I^\top AT_I(T_I^\top T_I)^{-1}T_I^\top v_M \\ &= (T_I^\top T_I)^{-1}\overline{A}^\top T_I^\top v_M = \left((T_I^\top T_I)^{-1}T_I^\top\right)\lambda_{max}v_M = \lambda_{max}\overline{v}_M.\end{aligned} \tag{6.23}$$

The third and fourth equalities hold since $T_I^\top A = T_T^\top A^\top = \overline{A}_I^\top T_I^\top$. We conclude that $\lambda_{max}(A) = \lambda_{max}(\overline{A})$. ∎

Therefore, if A is quasi-positive we can replace the constraint $A \preceq 0$ in the global constraint set $\mathcal{G}$ with $\overline{A} \preceq 0$. The following are sufficient conditions on the subsystem supply rates that guarantee the quasi-positiveness property of the matrix A.

Lemma 32. *Let the interconnection matrix M be nonnegative, with $M_{22} \equiv 0$, and consider quadratic supply rates parameterized by $X_1, \ldots, X_N$ and W of the form:*

$$X_i = \begin{bmatrix} Q_i & S_i \\ S_i^\top & R_i \end{bmatrix} \text{ for } i = 1, ..., N \quad \text{and} \quad W = \begin{bmatrix} Q_0 & S_0 \\ S_0^\top & R_0 \end{bmatrix}.$$

Then, the following conditions on X_i and W guarantee the quasi-positiveness of A in (6.20)*:*

- *For $k \neq l$, $\{R_i\}_{kl} \geq 0$ (i.e. all nondiagonal elements of R_i are nonnegative);*
- *Q_i, S_i are nonnegative;*
- *For $k \neq l$, $\{Q_0\}_{kl} \leq 0$, $\{R_0\}_{kl} \leq 0$ (all nondiagonal elements of Q_0 and R_0 are nonpositive);*
- *S_0 is nonpositive.*

Additionally, if $M_{22} \neq 0$ then R_0 must be nonpositive.

6.6 Large Scale Polynomial Example

In the following example we consider the case where the dynamics of each subsystem have the same structure, but depend on parameters which may differ. Assuming the parameter values lie in known bounds, we certify that the subsystems are dissipative with respect to a supply rate for all possible parameter values. This methodology could also be applied to systems with uncertain or unknown parameters.

Consider a system of the form

$$\begin{aligned} \dot{x} &= f(x,u,\delta) \qquad f(0,0,\delta) = 0 \\ y &= h(x,u,\delta) \qquad h(0,0,\delta) = 0 \\ \delta &\in \Delta \end{aligned} \tag{6.24}$$

where $\Delta := \{\delta \in \mathbb{R}^d \mid q_i(\delta) \leq 0 \text{ for } i = 1,\ldots,n_q\}$ is a closed semialgebriac set and $q_i : \mathbb{R}^d \to \mathbb{R}$ are real polynomials. The system is *robustly dissipative* with respect to a supply rate w if it is dissipative with respect to w for all parameters $\delta \in \Delta$. A sufficient condition for robust dissipativity is the existence of a differentiable and nonnegative storage function $V : \mathbb{R}^n \to \mathbb{R}_+$ and nonnegative functions $r_i : \mathbb{R}^{n+m+d} \to \mathbb{R}_+$ such that

$$\nabla V(x)^\top f(x,u,\delta) - w(u,y) - \sum_{i=1}^{n_q} r_i(x,u,\delta) q_i(\delta) \leq 0 \tag{6.25}$$

for all $x \in \mathbb{R}^n$, $u \in \mathbb{R}^m$, $\delta \in \mathbb{R}^d$, and $y = h(x,u,\delta)$. Similarly to standard dissipativity, this problem can also be cast as an SOS program for systems with linear or polynomial dynamics.

Suppose multiple subsystems are contained in an orbit under the action of the interconnection automorphism group. Then it is possible to search simultaneously for a supply rate and storage function certifying robust dissipativity for all the subsystems in the orbit. This significantly reduces the complexity of the problem and is especially beneficial when many similar subsystems are in the same orbit.

As an example consider a cyclically interconnected system of $N = 100$ subsystems where each subsystem has a disturbance input and performance output as in Figure 6.1b. The N subsystems are described by

$$\Sigma_i : \begin{cases} \dot{x}_1(t) = x_2(t) \\ \dot{x}_2(t) = \dfrac{-a_i x_2(t) - b_i x_1(t)^3 + u_i(t) + d_i(t)}{1 + c_i x_2(t)^2} \\ y_i(t) = e_i(t) = x_2(t) \end{cases}$$

where $a_i, b_i, c_i > 0$ are parameters, $d_i(t)$ is the input disturbance, and $e_i(t)$ the exogenous output. The parameters a_i, b_i, and c_i are chosen uniformly from the interval $[1.1,\ 1.2]$ so that the subsystems are all different.

We certify an L_2-gain bound from d to e using three different methods:

1. ADMM without symmetry reduction,
2. ADMM with symmetry reduction, and
3. robust analysis with symmetry reduction.

In the first two methods we certify dissipativity of each subsystem individually since the parameter values are different for each subsystem. For the robust analysis we certify robust dissipativity of all the subsystems simultaneously for all possible parameter values in the interval [1.11.2]. For each method subsystem dissipativity or robust dissipativity is certified via SOS programming to search for a quartic storage function.

Without symmetry reduction, the ADMM algorithm certifies that the system has L_2-gain less than 0.58. By taking advantage of the interconnection symmetry the number of supply rate matrices reduces from 100 to 1, thus reducing the number of decision variables in the global constraint from 300 to 3, one for each unique entry in the supply rate matrix $X_i = X_i^\top \in \mathbb{R}^{2\times 2}$. In this case ADMM certifies the system has L_2-gain less than 0.64. While this bound is more conservative, solving the global constraint takes $25 - 30\%$ less time, specifically, 5.0 seconds on average compared to 7.1 seconds for each iteration of the ADMM algorithm (for this case 12 iterations were required).

For the robust analysis, each subsystem has uncertain parameters a_i, b_i, and c_i contained in the interval [1.1, 1.2]. Since each subsystem has the same dynamics and uncertainty we can find a supply rate for all the subsystems by solving one instance of the robust dissipativity condition (6.25). Therefore, decomposing the problem and solving it iteratively is not necessary. Solving the local and global constraints simultaneously took less than 10 seconds and certified the L_2-gain of the system is less than 0.64.

In this example we demonstrated that the symmetry reduction with ADMM provides a modest reduction in the solution time of the global constraint. The reason a more significant reduction is not achieved is because the computational complexity of solving an SDP depends primarily on the number of decision variables v and the dimension of the semidefinite cone s as described in Section 2.7. For the global constraint (6.7) the number of decision variables and size of the SDP cone are given by

$$v = \frac{1}{2}\sum_{i=1}^{N}(p_i + m_i + 1)(p_i + m_i)$$

and

$$s = p_d + \sum_{i=1}^{N} p_i.$$

The symmetry reduction applied greatly reduces v but s is unchanged.

In Section 6.5 it is shown that under certain conditions it is possible to also reduce the dimension of the SDP cone, s. Specifically, by exploiting the symmetry in the global LMI (6.7) with $\tilde{Q} = \frac{1}{k}\sum_{i=1}^{k} S_i^\top Q S_i$, where S_i is as in (6.10) the LMI will have the same symmetric structure as M. Then, if the left hand side of the LMI is quasi-positive the certification of the LMI (6.7) can be reduced to an equivalent *quotient* LMI of dimension

$$s = r_d + \sum_{i=1}^{r_N} p_i$$

where r_d and r_N are the number of orbits in V_D and V_N, respectively. If the LMI is quasi-positive this reduction does not add any additional conservatism. Otherwise, it is often possible to restrict the structure of the subsystem supply rates such that the LMI is quasi-positive, but depending on the subsystems and interconnection this may introduce conservatism.

The left hand side of the LMI in (6.7) is quasi-positive for this interconnection if the local supply rate matrices are of the form

$$X_i = \begin{bmatrix} x_{11}^i & x_{12}^i \\ x_{12}^i & -x_{22}^i \end{bmatrix} \tag{6.26}$$

where $x_{11}^i,\ x_{12}^i,\ x_{22}^i \geq 0$. Therefore, by constraining the local supply rates to be of this form the dimension of the LMI in the global constraint can be reduced from 200 to 2. This reduction combined with the ADMM algorithm allows the global problem to be solved in less than 0.1 seconds. For the robust analysis case the local and global problems are both independent of the number of subsystems and can be solved simultaneously in less than 0.5 seconds. Restricting the supply rates to the form in 6.26 did not add any conservatism for this example. Both the ADMM and robust analysis methods found a L_2-gain bound of 0.64.

Table 6.1 compares the size of the problem for each solution method. Specifically, N is the number of local problems that must be solved, v is the number of decision variables in the global constraint LMI, and s is the dimension of the LMI.

Method	N	v	s
ADMM	100	300	200
ADMM + Sym. Reduction	100	3	200
ADMM + Quotient Reduction	100	3	2
Robust Analysis + Sym. Reduction	1	3	200
Robust Analysis + Quotient Reduction	1	3	2

Table 6.1: Size comparison for various certification methods.

6.7 Vehicle Platoon Example

In this example we apply the symmetry reduction techniques to the vehicle platoon example presented in Section 5.4. Recall, the dynamics of each vehicle are

$$\Sigma_i : \begin{cases} \dot{v}_i(t) = -v_i(t) + v_i^{\text{nom}} + u_i(t) \\ y_i(t) = v_i(t) \end{cases} \qquad i = 1, \ldots, N$$

where v_i is the vehicle velocity, v_i^{nom} is the nominal velocity, and u_i is the control input.

The interconnection of vehicles is represented by a connected, bidirectional, acyclic graph with L links interconnecting the N vehicles as in Figure 6.3 (top), where d_1 is an additive

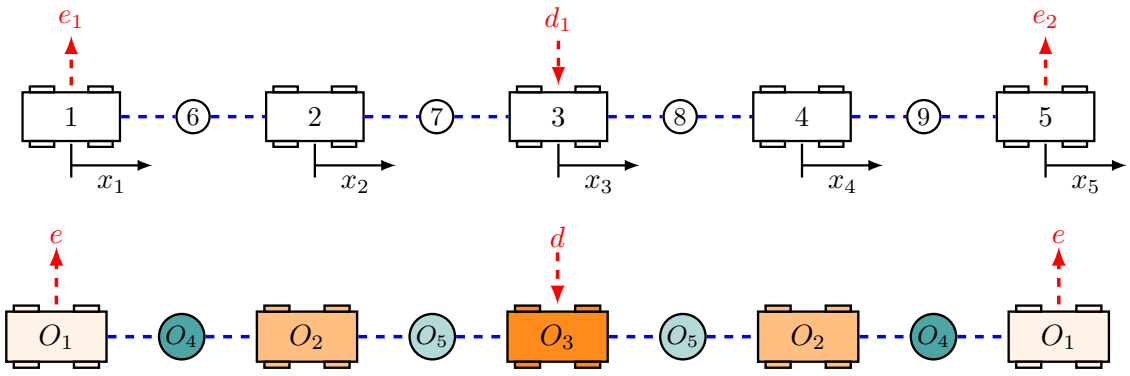

Figure 6.3: Vehicle platoon with linear topology. Each vehicle measures the relative distance of all vehicles connected to it by a link (dotted line) (top). Reduction due to the symmetry along the middle vehicle (bottom).

disturbance on u_3, and e_i are the performance outputs which measure the velocity of the respective vehicles.

The relative displacement p_ℓ between the vehicles connected by link ℓ is related to the individual vehicle velocities v_i by the incidence matrix D defined in (5.3) so that

$$\dot{p}(t) = D^\top v(t). \tag{6.27}$$

We consider the same class of control laws as in Section 5.4:

$$u_i(t) = -\sum_{\ell=1}^{L} D_{i\ell}\phi_\ell(p_\ell(t))$$

where $\phi_\ell : \mathbb{R} \to \mathbb{R}$ is increasing and surjective, but otherwise unknown. This assumption guarantees the existence of an equilibrium point $(p^\star, v^\star)$ for the interconnected system [13]. Letting Λ_ℓ be the link subsystems as in (5.5) with input η_ℓ and output z_ℓ. Each Λ_ℓ subsystem is EID with respect to the supply rate

$$\begin{bmatrix} \eta_\ell - \eta_\ell^\star \\ z_\ell - z_\ell^\star \end{bmatrix}^\top \begin{bmatrix} 0 & 1 \\ 1 & 0 \end{bmatrix} \begin{bmatrix} \eta_\ell - \eta_\ell^\star \\ z_\ell - z_\ell^\star \end{bmatrix}.$$

as was shown in Section 5.4. In the following computations the supply rates of each Λ_ℓ are fixed and the supply rates of each Σ_i are decision variables.

The interconnected system can then be represented as in the block diagram in Figure 5.7 where $\Sigma = \operatorname{diag}(\Sigma_1, \ldots, \Sigma_N)$ and $\Lambda = \operatorname{diag}(\Lambda_1, \ldots, \Lambda_L)$.

We now exploit the symmetric topology of the vehicle platoon using the results of the previous sections. Consider a platoon of $N = 201$ vehicles with symmetry as depicted in Figure 6.3 and each vehicle's nominal velocity randomly chosen. To numerically test our

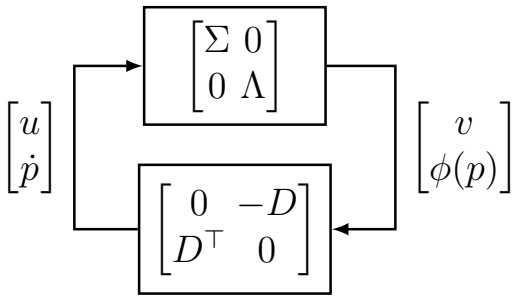

Figure 6.4: Vehcile Platoon example transformed into the form of Figure 3.1.

reduction algorithm we apply a disturbance d to the 51-st vehicle and investigate the L_2 gain from d to the velocities of the first and last vehicles, designated as the performance variables e_1 and e_2. This configuration allows us to exploit the symmetry of the interconnection about the center vehicle (Figure 6.3) reducing the number of unique supply rates in the global LMI constraint from 201 to 101. Since X_i for each vehicle has three unique entries, the number of decision variables reduces from 603 to 303.

Using the ADMM algorithm and the symmetry reduction we certify that the L_2-gain from d to e is no greater than 1. In fact, the ADMM algorithm without symmetry reduction cannot certify a smaller gain; hence, for this example the symmetry reduction does not add conservatism. The symmetry reduction reduces the average time required to solve the global problem from 18.4 to 8.1 seconds[1].

This further reduction described in Section 6.5 can also be applied to the vehicle platoon example with interconnection as in Figure 6.3. For this case the supply rates X_i considered are of the form

$$X_i = \begin{bmatrix} 0 & x_{12}^i \\ x_{12}^i & -x_{22}^i \end{bmatrix}$$

where $x_{12}^i, x_{22}^i \geq 0$ which guarantees the left hand side of the LMI in (6.7) is quasi-positive. Then, in addition to the reduction in the number of decision variables, the dimension of the global LMI can also be reduced from 402 (201 vehicles, 200 links, and 1 disturbance) to 202 (101 vehicles, 100 links, and 1 disturbance) without introducing additional conservatism. This reduces the average time required to solve the global LMI constraint to 3.8 seconds.

Another interesting example of a symmetric topology is a two-lane interconnection where, in addition to communicating with the vehicles in front and behind, each vehicle also communicates with the three adjacent vehicles in the other lane, as depicted in Figure 6.5. In this example, there exists a symmetry along the longitudinal line dividing the two lanes. This allows the reduction of the problem to a single lane linear platoon topology, *i.e.*, 1 and 6 are in O_1, 2 and 7 are in O_2, 3 and 8 are in O_3, and so on. For $N = 200$ vehicles the number of unique supply rates is reduced from 200 to 100 giving a similar reduction in the number of decision variables and the computation time as the previous example.

[1]Computations were performed in MATLAB on a desktop computer with a 2.8 GHz Intel i7-860 processor. The SDP was solved with SDPT3 [27].

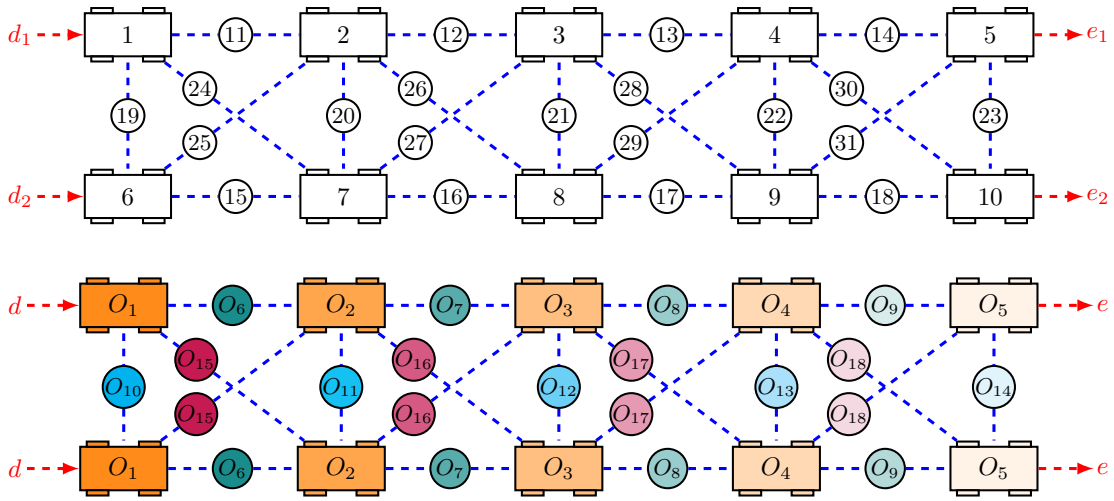

Figure 6.5: Two-lane vehicle platoon (top), and respective symmetry reduction (bottom).

6.8 Extension to Integral Quadratic Constraints

The symmetry reduction presented in Section 6.2 can be extended to the performance certification of an interconnected system with respect to a global IQC of the form

$$\Pi_W := \Psi_W^* W \Psi_W$$

where Ψ_W is a stable linear system with realization $(\hat{A}_W, \hat{B}_W, \hat{C}_W, \hat{D}_W)$, and W is a real symmetric matrix, both specified by the user. In this case we certify that each subsystem satisfies an IQC

$$\Pi_i = \Psi_i^* X_i \Psi_i$$

where Ψ_i is a stable linear system with state space realization $(\hat{A}_i, \hat{B}_i, \hat{C}_i, \hat{D}_i)$ and X_i is a real symmetric matrix.

Then the performance of the interconnected system is certified if $X_1, \dots X_N$ are in the global constraint set $\mathcal{G}^{IQC}$ defined in (3.29). As in Section 6.2 we would like to use the symmetry of the interconnected system to reduce the number of decision variables in the LMI constraint in the global constraint set $\mathcal{G}^{IQC}$. For convenience we restate the LMI:

$$\begin{bmatrix} \hat{A}^\top P + P\hat{A} & P\hat{B} \\ \hat{B}^\top P & 0 \end{bmatrix} + \begin{bmatrix} \hat{C}^\top \\ \hat{D}^\top \end{bmatrix} Q \begin{bmatrix} \hat{C}^\top \\ \hat{D}^\top \end{bmatrix}^\top \preceq 0 \tag{6.28}$$

where $Q = \mathrm{diag}(X_1, ..., X_N, -W)$ and $(\hat{A}, \hat{B}, \hat{C}, \hat{D})$ are defined in (3.28).

Under the following assumptions, the automorphisms of the interconnection matrix M provide a dimensionality reduction in the number of decision variables of the global constraint (6.28).

Assumption 33. *The state space realizations for the stable linear system Ψ_i, $i = 1, ..., N$, used in the IQCs $\Pi_i = \Psi_i^* X_i \Psi_i$, and given by $(\hat{A}_i, \hat{B}_i, \hat{C}_i, \hat{D}_i)$ are identical for systems in the same orbit, under the action of $Aut(M)$.*

Assumption 34. *The state space realization for the stable linear system Ψ_W given by $(\hat{A}_W, \hat{B}_W, \hat{C}_W, \hat{D}_W)$ is symmetric with respect to the input permutations $R_U = \mathrm{diag}(R_D, R_E)$, i.e., there exist permutation matrices R_X and R_Y such that*

$$\hat{A}_W R_X = R_X \hat{A}_W, \quad \hat{B}_W R_U = R_X \hat{B}_W, \quad \hat{C}_W R_X = R_Y \hat{C}_W, \quad \hat{D}_W R_U = R_Y \hat{D}_W. \tag{6.29}$$

The next Corollary is the IQC counterpart of Lemma 23. To simplify the notation, we assume that the state space realizations of each Ψ_i for $i = 1, ..., N$ have the same dimension, where $\hat{A}_i \in \mathbb{R}^{q \times q}$, $\hat{B}_i \in \mathbb{R}^{q \times 2}$, $\hat{C}_i \in \mathbb{R}^{l \times q}$, and $\hat{D}_i \in \mathbb{R}^{l \times 2}$. The Corollary still holds when the dimensions are different but the matrices S_X and S_Y need to be appropriately modified.

Corollary 35. *Let the Assumptions (33) and (34) hold. If the LMI defined in (6.28) is satisfied by $(X_1, ..., X_N, W)$ with $P \succeq 0$ then it is also satisfied by $(\tilde{X}_1, ..., \tilde{X}_N, \tilde{W})$, with $\tilde{X}_i = \tilde{X}_j$ if $i \sim j$, and*

$$\overline{P} = \frac{1}{k} \sum_{i=1}^{m} S_X^{iT} P S_X^i$$

where $S_X^i = \mathrm{diag}(R_N^i \otimes I_q, R_X^i)$, $(R_N^i, R_U^i) \in Aut(M)$, and R_X^i is as in (6.29).

Remark 36. The size of P depends on the dimension of the state space realization of the IQCs and therefore can be very large. Corollary 35 shows that $\overline{P}$ and $\overline{Q}$ are also solutions of the LMI in (6.28) that have repeated elements. The reduction on the number of variables for the block diagonal matrix $\overline{Q}$ is the same as before. The diagonal variables of $\overline{P}$ repeat in a similar way, *i.e.*, $\{\overline{P}\}_{kk} = \{\overline{P}\}_{ll}$ if elements $k, l \in (V_N, V_D, V_E)$ are in the same orbit. The off-diagonal elements of $\overline{P}$ repeat with the following pattern: $\{\overline{P}\}_{ij} = \{\overline{P}\}_{kl}$ if there exists a permutation $R := (R_N, R_X)$ consistent with $Aut(M)$ such that $Re_i = e_k$ and $Re_j = e_l$ or such that $Re_i = e_l$ and $Re_j = e_k$.

Proof. [Corollary 35] First note that due to the Assumptions above, the following holds for each automorphism in $Aut(M)$:

$$\begin{bmatrix} \hat{C}^\top \\ \hat{D}^\top \end{bmatrix}^\top = S_Y \begin{bmatrix} \hat{C}^\top \\ \hat{D}^\top \end{bmatrix}^\top \begin{bmatrix} S_X^\top & 0 \\ 0 & R_R^\top \end{bmatrix}$$

where $S_Y := \mathrm{diag}(R_N \otimes I_l, R_Y)$ and

$$\begin{bmatrix} A^\top P + PA & PB \\ B^\top P & 0 \end{bmatrix} = \begin{bmatrix} S_X & 0 \\ 0 & R_R \end{bmatrix} \begin{bmatrix} \hat{A}^\top \overline{P} + \overline{P} \hat{A} & \overline{P} \hat{B} \\ \hat{B}^\top \overline{P} & 0 \end{bmatrix} \begin{bmatrix} S_X^\top & 0 \\ 0 & R_R^\top \end{bmatrix}$$

where $R_R := \mathrm{diag}(R_N \otimes 2, R_U)$. Then, the proof follows from the equivalence

$$\begin{bmatrix} \hat{A}^\top P + P\hat{A} & P\hat{B} \\ \hat{B}^\top P & 0 \end{bmatrix} + \begin{bmatrix} \hat{C}^\top \\ \hat{D}^\top \end{bmatrix} Q \begin{bmatrix} \hat{C}^\top \\ \hat{D}^\top \end{bmatrix}^\top \preceq 0 \tag{6.30}$$

if and only if

$$\begin{bmatrix} \hat{A}^\top \overline{P} + \overline{P}\hat{A} & \overline{P}\hat{B} \\ \hat{B}^\top \overline{P} & 0 \end{bmatrix} + \begin{bmatrix} \hat{C}^\top \\ \hat{D}^\top \end{bmatrix} \overline{Q} \begin{bmatrix} \hat{C}^\top \\ \hat{D}^\top \end{bmatrix}^\top \preceq 0 \tag{6.31}$$

with $\overline{Q} = S_Y^\top Q S_Y$. ∎

6.9 Chapter Summary

Symmetry reduction techniques were applied to performance certification of interconnected dissipative systems. By reducing the number of decision variables and dimension of the global constraint the computational performance and scalability is significantly improved. We demonstrated the reduction, combined with distributed optimization and robust dissipativity, allows the analysis of very large interconnections without introducing excessive conservatism. Finally, we show that this approach can be extended to the case where the subsystems satisfy IQCs.

Chapter 7

Passivity-based Formation Control for UAVs with a Suspended Load

In this chapter, we present a passivity-based formation control strategy for multiple unmanned aerial vehicles (UAVs), specifically multicopters, transporting a suspended payload as in Figure 7.1. Many potential applications for this have been proposed, including package delivery and transportation, fire extinguishing, and geo-surveying and mine detection as in [66], [67].

Using multiple UAVs for this task is advantageous because it provides a higher load carrying capacity as well as having better control over the position and orientation of the suspended load. This is especially important in applications like geo-surveying where it is necessary to maintain the suspended load at a certain orientation relative to the ground. A multiple UAV configuration also reduces the effect of disturbances like wind on the motion of the suspended load. This is especially important for search and rescue or rendezvous operations as in [68] where precise position control is necessary.

Cooperative control of multiple UAVs carrying a suspended load has been studied under many different scenarios. For example, [67], [69] assume external cameras are available to provide accurate position measurements of the UAVs and the payload, which limits the applicability of these approaches for large scale, outdoor environments. Alternatively, in [68], [70]–[72] sensors onboard the UAVs are used to measure the relative positions of the UAVs and the payload, and use only these measurements to maintain a constant formation.

We assume that the UAVs only measure their relative positions and not the position of the suspended load. We treat each UAV and the suspended load as individual subsystems and propose a passivity based formation control strategy similar to that in [73], [74] to stabilize the interconnected system. For each UAV we propose an internal control law rendering the system output strictly passive between the input, the force from the cables and formation control law, and the output, the velocity error. Similar to the control law in the vehicle platoon example in Section 5.4 the formation control law can be interpreted as virtual springs between the UAVs. The connection between the UAVs and the suspended load is modeled as a physical spring representing the cable. We extend the framework in [74] to allow for the

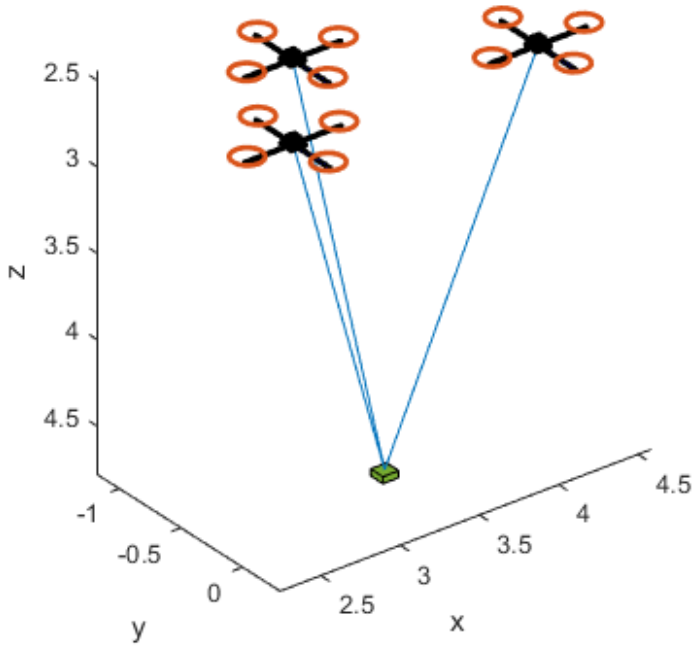

Figure 7.1: Multiple UAVs carrying a suspended load.

suspended load and compensate for its effect on the UAVs.

First, we model the dynamics of the UAVs, suspended load, and cables between the UAVs and the load. Then, in Section 7.2 we propose an internal feedback control law for each UAV and a formation control law that regulates the relative position between each UAV. We show that with this control strategy the interconnected system has a similar structure to the vehicle platoon example in Section 5.4. In Section 7.3 we show that the interconnected system has a continuum of equilibria and prove stability for all equilibrium points where the cables supporting the suspended load are in tension. Finally, we present simulation results using the proposed control strategy for a system with 3 UAVs.

7.1 System Dynamics

We consider N UAVs that are cooperatively carrying a suspended load. The desired formation of the UAVs and the load in the $x-y$ plane are represented by an undirected graph as in Figure 7.2. We let $\eta_i \in \mathbb{R}^3$, $i = 1, \ldots, N$ and η_{N+1} be the position of the UAVs and the suspended load, respectively.

For each dotted edge $\ell = 1, \ldots, T$ in the graph between UAVs we assign one vertex to be the head if it is clockwise from the other vertex. Therefore, for the configuration in Figure 7.2 vertex 1 is the head and vertex 2 is the tail along edge 1. Solid edges $\ell = T+1, \ldots, E$ represent the cable between the UAV and the load. We assign the UAV vertex to be the

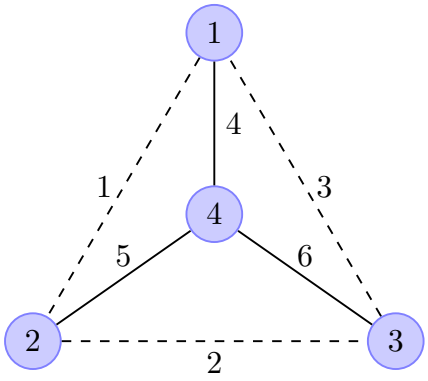

Figure 7.2: Undirected graph of UAVs $(1, 2, 3)$ and the suspended load 4.

head and the load vertex the tail. The incidence matrix, given by

$$M_{il} = \begin{cases} 1 & \text{if vertex } i \text{ is the head of edge } \ell \\ -1 & \text{if vertex } i \text{ is the tail of edge } \ell \\ 0 & \text{otherwise,} \end{cases} \tag{7.1}$$

will be used to characterize the interconnection topology.

Along each edge $\ell = 1, \ldots, E$ we define the relative position as $r_\ell(t) := \eta_i(t) - \eta_j(t) \in \mathbb{R}^3$ where i and j correspond to the head and tail vertices, respectively, of the ℓ-th edge.

Since the input and output of the UAVs and the suspended load is in three dimensions the matrix $D := M \otimes I_3$ maps the position of the UAVs to the relative positions $r_\ell(t) \in \mathbb{R}^3$ along each edge $\ell = 1, \ldots, E$ by

$$r = D^\top \eta. \tag{7.2}$$

As an example for the formation described in Figure 7.1 we have

$$M = \begin{bmatrix} 1 & 0 & -1 & 1 & 0 & 0 \\ -1 & 1 & 0 & 0 & 1 & 0 \\ 0 & -1 & 1 & 0 & 0 & 1 \\ 0 & 0 & 0 & -1 & -1 & -1 \end{bmatrix}$$

and

$$\begin{bmatrix} r_1 \\ r_2 \\ r_3 \\ r_4 \\ r_5 \\ r_6 \end{bmatrix} = D^\top \eta = \begin{bmatrix} \eta_1 - \eta_2 \\ \eta_2 - \eta_3 \\ \eta_3 - \eta_1 \\ \eta_1 - \eta_4 \\ \eta_2 - \eta_4 \\ \eta_3 - \eta_4 \end{bmatrix}.$$

The dynamics of each UAV are described by point mass models, as in [70], [75], of the form

$$m_i \dot{v}_i(t) = -m_i g + u_i^L(t) + \tau_i(t) \qquad i = 1, \ldots, N \tag{7.3}$$

with state $v_i(t) \in \mathbb{R}^3$, control input $\tau_i(t) \in \mathbb{R}^3$, mass m_i, and acceleration due to gravity $g \in \mathbb{R}^3$. The force applied to the UAV through the cable connected to the suspended load is $u_i^L(t) \in \mathbb{R}^3$. For each UAV an internal feedback controller will be used to compensate for this unknown force.

The dynamics of the suspended load are

$$m_L \dot{v}_{N+1}(t) = -m_L g + u_{N+1}(t) \tag{7.4}$$

with state $v_{N+1}(t) \in \mathbb{R}^3$, mass m_L, acceleration due to gravity g, and input $u_{N+1}(t) \in \mathbb{R}^3$ which is the sum of the forces applied to the load by the UAVs through the cables.

The edges $\ell = 1, \ldots, T$ between UAVs do not represent a physical connection so in Section 7.2 a control law is proposed that acts as virtual springs oriented along the edges between the UAVs. The edges $\ell = T+1, \ldots, E$ between the UAVs and the load represent a flexible cable. The force transferred along this cable is modeled by a function $h_\ell : \mathbb{R}^3 \to \mathbb{R}^3$ which takes the form

$$h_\ell(r_\ell) = \sigma_\ell(\|r_\ell\|) \frac{1}{\|r_\ell\|} r_\ell \tag{7.5}$$

where we assume $\sigma_\ell : \mathbb{R}_+ \to \mathbb{R}$ is strictly increasing and onto for $\ell = T+1, \ldots, E$. This function can be interpreted as a spring acting between the UAV and the suspended load.

7.2 Control Strategy

In this section, we describe an internal feedback control for each UAV that renders it EID and compensates for the vertical force applied to it by the suspended load. Then, a formation control strategy is presented that regulates the relative position of the UAVs in the x, y, and z coordinates independently.

Internal Feedback Control

We propose a passivity based design where the internal feedback for each UAV is

$$\tau_i(t) = m_i g + v^d - v_i(t) - \delta_i(t) + u_i^f(t) \tag{7.6}$$

where $m_i g$ compensates for the effect of gravity on the UAV, v^d is the desired velocity of the formation, and u_i^f is the formation control force which will regulate the relative positions of the UAVs as described in Section 7.2. The component $\delta_i(t)$ is updated by

$$\dot{\delta}_i(t) = v_i(t) - v^d \qquad \delta_i(0) = \hat{\delta}_i \tag{7.7}$$

where $\hat{\delta}_i$ is an estimate of the bias force applied to each UAV. The purpose of δ is to compensate for the vertical force applied to each UAV by the suspended load as well as compensate for other unmodeled bias forces like wind.

With this control strategy the UAV dynamics are

$$\begin{aligned} m_i \dot{v}_i(t) &= -v_i(t) + v^d - \delta_i(t) + u_i(t) \\ \dot{\delta}_i(t) &= v_i(t) - v^d \end{aligned} \tag{7.8}$$

where $u_i = u_i^f + u_i^L$ is the sum of the formation control force u_i^f and the force from the suspended load u_i^L. In Section 7.3 we show that this choice of τ guarantees that the system (7.8) is equilibrium independent output strictly passive from the input u_i to the output v_i.

Formation Control

The interconnected system can be represented as the block diagram in Figure 7.3. The Σ_i subsystems mapping u_i to v_i are the UAV ($i = 1, \ldots, N$) and suspended load ($i = N + 1$) subsystems and the Λ_ℓ subsystems mapping w_ℓ to $y_\ell = h(r_\ell)$ for $\ell = 1, \ldots, E$ are the edge subsystems.

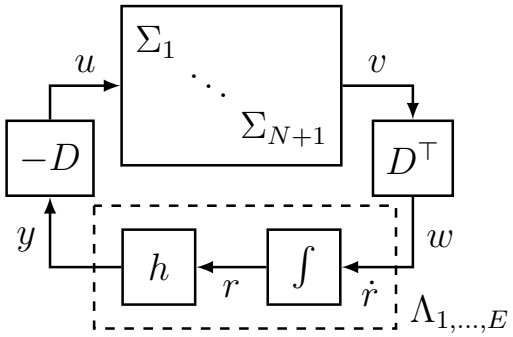

Figure 7.3: Block diagram of the vehicle platoon dynamics.

As depicted in Figure 7.3 we express the edge subsystems as

$$\begin{aligned} \dot{r}_\ell &= w_\ell \\ y_\ell &= h_\ell(r_\ell) \end{aligned} \tag{7.9}$$

where $w \triangleq D^\top v$ is the input to the edge subsystems and y is the output. For the edges $\ell = 1, \ldots, T$ the functions h_ℓ characterize the formation control strategy, while for the edges $\ell = T + 1, \ldots, E$ they model the cable connecting the UAVs and the suspended load.

The formation control strategy, which requires measurement of the relative positions of the UAVs, is described by the functions $h_\ell : \mathbb{R}^3 \to \mathbb{R}^3$ of the form

$$h_\ell(r_\ell) = \begin{bmatrix} \sigma_\ell^x(r_\ell^x) \\ \sigma_\ell^y(r_\ell^y) \\ \sigma_\ell^z(r_\ell^z) \end{bmatrix} \tag{7.10}$$

for each edge $\ell = 1, \dots, T$ between UAVs. Similarly to (7.5) we assume that $\sigma_\ell^x, \sigma_\ell^y, \sigma_\ell^z : \mathbb{R} \to \mathbb{R}$ are strictly increasing and onto for $\ell = 1, \dots, T$. This control law can be interpreted as three virtual springs for each edge connecting UAVs that act independently in each coordinate.

The input to the UAVs is then

$$u = -D \begin{bmatrix} h_1(r_1) \\ \vdots \\ h_E(r_E) \end{bmatrix} \tag{7.11}$$

where h_ℓ are given by (7.10) for $\ell = 1, \dots, T$ and by (7.5) for $\ell = T+1, \dots, E$. Therefore, the input applied to the i-th subsystem is

$$u_i = -\sum_{\ell=1}^{E} D_{il} h_\ell(r_\ell) \tag{7.12}$$

which depends only on locally available measurements because $D_{il} \neq 0$ only when vertex i is the head or tail of edge ℓ.

7.3 Stability Analysis

We analyze the stability properties of the system and proposed control laws using a compositional approach. Specifically, for each subsystem (i.e. UAV, load, or edge) we find a storage function certifying that it is EID. From these storage functions we then obtain a Lyapunov function for the interconnected system.

For each UAV $i = 1, \dots N$, described by (7.8), the storage function

$$S_i(v_i, \bar{v}_i, \delta_i, \bar{\delta}_i) = \frac{m_i}{2}\|v_i - \bar{v}_i\|^2 + \frac{1}{2}\|\delta_i - \bar{\delta}_i\|^2 \tag{7.13}$$

certifies equilibrium independent output strict passivity since

$$\begin{aligned} \dot{S}_i(v_i, \bar{v}_i, \delta_i, \bar{\delta}_i) &= (v_i - \bar{v}_i)^\top(-v_i + v^d - \delta_i + u_i) + (\delta_i - \bar{\delta}_i)^\top(v_i - v^d) \\ &= -\|v_i - \bar{v}_i\|^2 + (v_i - \bar{v}_i)^\top(u_i - \delta_i) + (v_i - \bar{v}_i)^\top(\delta_i - \bar{u}_i) \\ &= -\|v_i - \bar{v}_i\|^2 + (v_i - \bar{v}_i)^\top(u_i - \bar{u}_i) \end{aligned}$$

where we have used $\bar{v}_i = v^d$ and $\bar{u}_i = \bar{\delta}_i$ in the second equality.

For the suspended load, described by (7.4), the storage function

$$S_L(v_{N+1}, \bar{v}_{N+1}) = \frac{m_L}{2}\|v_{N+1} - \bar{v}_{N+1}\|^2 \tag{7.14}$$

can be used to show that it is equilibrium independent passive since

$$\begin{aligned}\dot{S}_L(v_{N+1}, \bar{v}_{N+1}) &= (v_{N+1} - \bar{v}_{N+1})^\top(-m_L g + u_{N+1}) \\ &= (v_{N+1} - \bar{v}_{N+1})^\top(u_{N+1} - \bar{u}_{N+1})\end{aligned}$$

where $\bar{u}_{N+1} = m_L g$.

For each edge $\ell = 1, \ldots, T$, described by (7.9) with the control strategy in (7.10), the storage function is

$$\begin{aligned}R_\ell(r_\ell, \bar{r}_\ell) &= \int_{\bar{r}_\ell}^{r_\ell} (h_\ell(\zeta) - h_\ell(\bar{r}_\ell))d\zeta \\ &= \sum_{i \in \{x,y,z\}} \int_{\bar{r}_\ell^i}^{r_\ell^i} (\sigma_\ell^i(\zeta^i) - \sigma_\ell^i(\bar{r}_\ell^i))d\zeta^i\end{aligned} \tag{7.15}$$

where the second equality holds since the curl of h_ℓ in (7.10) is zero implying path independence of the integral. The storage function R_ℓ is zero for $r_\ell = \bar{r}_\ell$ and strictly positive for all $r_\ell \neq \bar{r}_\ell$ since σ_ℓ^x, σ_ℓ^y, and σ_ℓ^z are strictly increasing and onto for $\ell = 1, \ldots, T$. This storage function certifies each subsystem is equilibrium independent passive since

$$\begin{aligned}\dot{R}_\ell(r_\ell, \bar{r}_\ell) &= \begin{bmatrix} \sigma_\ell^x(r_\ell^x) - \sigma_\ell^x(\bar{r}_\ell^x) \\ \sigma_\ell^y(r_\ell^y) - \sigma_\ell^y(\bar{r}_\ell^y) \\ \sigma_\ell^x(r_\ell^z) - \sigma_\ell^z(\bar{r}_\ell^z) \end{bmatrix}^\top w_\ell \\ &= (h_\ell(r_\ell) - h_\ell(\bar{r}_\ell))^\top(w_\ell - \bar{w}_\ell)\end{aligned}$$

where $\bar{w}_\ell = 0$.

For each edge $\ell = T+1, \ldots, E$, described by (7.9) and (7.5), the storage function is

$$R_\ell(r_\ell, \bar{r}_\ell) = \int_{\|\bar{r}_\ell\|}^{\|r_\ell\|} \sigma_\ell(\zeta)d\zeta - \sigma_\ell(\|\bar{r}\|)\frac{\bar{r}_\ell^\top(r_\ell - \bar{r}_\ell)}{\|\bar{r}_\ell\|}. \tag{7.16}$$

Clearly, $R_\ell(\bar{r}_\ell, \bar{r}_\ell) = 0$ and by calculating the Hessian of R_ℓ we can show that it is positive definite in a neighborhood of $\bar{r}_\ell$.

The gradient of the storage function is

$$\begin{aligned}\nabla_{r_\ell} R_\ell(r_\ell, \bar{r}_\ell) &= \sigma_\ell(\|r_\ell\|)\frac{r_\ell}{\|r_\ell\|} - \sigma_\ell(\|\bar{r}_\ell\|)\frac{\bar{r}_\ell}{\|\bar{r}_\ell\|} \\ &= h_\ell(r_\ell) - h_\ell(\bar{r}_\ell)\end{aligned}$$

and the Hessian is

$$\begin{aligned}H_{r_\ell} R_\ell(r_\ell, \bar{r}_\ell) &= \nabla_{r_\ell}\left(\sigma_\ell(\|r_\ell\|)\frac{r_\ell^\top}{\|r_\ell\|}\right) \\ &= \frac{\sigma_\ell(\|r_\ell\|)}{\|r_\ell\|} I_3 + \nabla_{r_\ell}\left(\frac{\sigma_\ell(\|r_\ell\|)}{\|r_\ell\|}\right) r_\ell^\top \\ &= \frac{\sigma_\ell(\|r_\ell\|)}{\|r_\ell\|} I_3 + \left(\sigma_\ell'(\|r_\ell\|) - \frac{\sigma_\ell(\|r_\ell\|)}{\|r_\ell\|}\right)\frac{1}{r_\ell^\top r_\ell} r_\ell r_\ell^\top\end{aligned}$$

where $I_n \in \mathbb{R}^{n\times n}$ is the identity matrix. Note that the Hessian is the sum of a scaled identity matrix and a rank one matrix. Therefore, the eigenvalues of the Hessian are

$$\frac{\sigma_\ell(\|r_\ell\|)}{\|r_\ell\|}$$

with multiplicity 2 and

$$\frac{\sigma_\ell(\|r_\ell\|)}{\|r_\ell\|} + \left(\sigma'_\ell(\|r_\ell\|) - \frac{\sigma_\ell(\|r_\ell\|)}{\|r_\ell\|}\right) = \sigma'_\ell(\|r_\ell\|)$$

with multiplicity 1. Thus, if

$$\sigma_\ell(\|\bar{r}_\ell\|) > 0 \;\text{ and }\; \sigma'_\ell(\|\bar{r}_\ell\|) > 0 \tag{7.17}$$

then the Hessian is positive definite at $\bar{r}_\ell$ which implies that $R_\ell(r_\ell, \bar{r}_\ell) > 0$ for all $r_\ell \neq \bar{r}_\ell$ in a neighborhood of $\bar{r}_\ell$. The first condition, $\sigma_\ell(\|\bar{r}_\ell\|) > 0$, holds whenever the spring is in tension and the second condition, $\sigma'_\ell(\|\bar{r}_\ell\|) > 0$, always holds since σ_ℓ is increasing.

The Lie derivative of this storage function is

$$\dot{R}_\ell(r_\ell, \bar{r}_\ell) = (h_\ell(r_\ell) - h_\ell(\bar{r}_\ell))^\top (w_\ell - \bar{w}_\ell)$$

where $\bar{w}_\ell = 0$. Therefore, this storage function certifies the edge subsystems are equilibrium independent passive in a neighborhood of $\bar{r}_\ell$ for any $\bar{r}_\ell$ satisfying $\sigma_\ell(\|\bar{r}_\ell\|) > 0$.

In order to characterize the equilibrium points of the system we must consider configurations with specific numbers of UAVs. For example with N = 2, the set of equilibria of the interconnected system in Figure 7.3 with the UAV, edge, and load subsystems described by (7.8), (7.9), and (7.4) respectively, is given by

$$\mathcal{E} = \left\{ (\bar{v}, \bar{\delta}, \bar{r}) \;\middle|\; \begin{array}{r} \bar{v}_i = v^d \text{ for } i = 1, \ldots, 3 \\ m_L g = h_2(\bar{r}_2) + h_3(\bar{r}_3) \\ \bar{\delta} = \begin{bmatrix} -h_1(\bar{r}_2 - \bar{r}_3) - h_2(\bar{r}_2) \\ h_1(\bar{r}_2 - \bar{r}_3) - h_3(\bar{r}_3) \end{bmatrix} \end{array} \right\}.$$

where the geometric relation $\bar{r}_1 = \bar{r}_2 - \bar{r}_3$ is used in the last equation. Since the functions $h_1, \ldots, h_3$ are increasing and onto in each coordinate there exists a unique $\bar{\delta}$ for all values of $\bar{r}_2$ and $\bar{r}_3$. Therefore, there is an equilibrium point for any r_2 and r_3 satisfying $m_L g = h_2(r_2) + h_3(r_3)$. For configurations with $N > 2$ UAVs the set of equilibria $\mathcal{E}$ is of a similar form and is a continuum of points.

Theorem 37. *Any equilibrium point $(\bar{v}, \bar{\delta}, \bar{r}) \in \mathcal{E}$ of the interconnected system in Figure 7.3 that satisfies $\sigma_\ell(\|\bar{r}_\ell\|) > 0$ for $\ell = T+1, \ldots, E$ is stable.*

Proof. By combining the subsystem storage functions (7.13)-(7.16) we get the candidate Lyapunov function

$$V(v,\delta,r)=\sum_{i=1}^{N}S_i(v_i,\bar{v}_i,\delta_i,\bar{\delta}_i)+S_L(v_{N+1},\bar{v}_{N+1})+\sum_{\ell=1}^{E}R_\ell(r_\ell,\bar{r}_\ell). \tag{7.18}$$

for any equilibrium point $(\bar{v},\bar{\delta},\bar{r})\in\mathcal{E}$. By the definitions of the subsystem storage functions $V(\bar{v},\bar{\delta},\bar{r})=0$ and V is positive definite for all v, δ, and r_ℓ for $\ell=1,\ldots,T$. Furthermore, since $\sigma_\ell(\|\bar{r}_\ell\|)>0$ for $\ell=T+1,\ldots,E$ then there will exist an open set $\mathcal{R}$ containing $(\bar{r}_{T+1},\ldots,\bar{r}_E)$ such that

$$V(\bar{v},\bar{\delta},\bar{r})=0 \text{ and } V(\bar{v},\bar{\delta},r)>0$$

for any $\{(r_{T+1},\ldots,r_E)\in\mathcal{R}\mid r_\ell\neq\bar{r}_\ell \text{ for } \ell=T+1,\ldots,E\}$.

The Lie derivative of V is

$$\begin{aligned}
\dot{V}(v,\delta,r)&=\sum_{i=1}^{N}\left(-\|v_i-\bar{v}_i\|^2+(v_i-\bar{v}_i)^\top(u_i-\bar{u}_i)\right)\\
&\quad+(v_{N+1}-\bar{v}_{N+1})^\top(u_{N+1}-\bar{u}_{N+1})+\sum_{\ell=1}^{E}(h_\ell(r_\ell)-h_\ell(\bar{r}_\ell))^\top(w_\ell-\bar{w}_\ell)\\
&=-\sum_{i=1}^{N}\|v_i-\bar{v}_i\|^2+(v-\bar{v})^\top(u-\bar{u})+(h(r)-h(\bar{r}))^\top(w-\bar{w})\\
&=-\sum_{i=1}^{N}\|v_i-\bar{v}_i\|^2-(v-\bar{v})^\top D(h(r)-h(\bar{r}))+(v-\bar{v})^\top D(h(r)-h(\bar{r}))\\
&=-\sum_{i=1}^{N}\|v_i-\bar{v}_i\|^2\leq 0
\end{aligned}$$

where the third inequality follows from $u=-Dh(r)$ and $w=D^\top v$. Hence, any equilibrium point $(\bar{v},\bar{\delta},\bar{r})$ satisfying $\sigma_\ell(\|\bar{r}_\ell\|)>0$ for $\ell=T+1,\ldots,E$ is stable. ∎

Remark 38. The assumption that $\sigma_\ell(\|\bar{r}_\ell\|)>0$ for $\ell=T+1,\ldots,E$ is not restrictive because it is only true when the cables between the UAVs and the load are in tension. This condition is expected in normal operation and desired so that there is no slack in the cables.

7.4 Example

As an example, consider the configuration in Figure 7.2 with $N=3$ UAVs carrying the suspended load. Let each UAV have a mass $m=2$ kg, and the load have mass $m_L=3$ kg. In addition to the reaction force from the load, the UAVs are also affected by a constant wind in the x-direction with a magnitude of 4 m/s.

For $N = 3$, a fully connected graph between all UAVs consists of three links and the resulting control incidence matrix M_c is given by

$$M_c = \begin{bmatrix} 1 & 0 & -1 \\ -1 & 1 & 0 \\ 0 & -1 & 1 \end{bmatrix} \tag{7.19}$$

Suppose we want the three UAVs to form a triangle with each side having length $\Delta \in \mathbb{R}$. We let $\eta_i^d \in \mathbb{R}^3$ for $i = 1, \ldots, N$ represent the desired positions of the UAVs and assume that

$$\eta_1^d = \begin{bmatrix} 0 \\ 0 \\ 0 \end{bmatrix}.$$

Then a set of possible desired positions of the UAVs are described by

$$\eta_2^d = \begin{bmatrix} \Delta \\ 0 \\ 0 \end{bmatrix} \quad \text{and} \quad \eta_3^d = \begin{bmatrix} \Delta/2 \\ \sqrt{\Delta^2 - \Delta^2/2^2} \\ 0 \end{bmatrix}.$$

The desired relative positions $r_\ell^d \in \mathbb{R}^3$ are then given by

$$\begin{bmatrix} r_1^d \\ r_2^d \\ r_3^d \end{bmatrix} = (M_c \otimes I_3)^\top \begin{bmatrix} \eta_1^d \\ \eta_2^d \\ \eta_3^d \end{bmatrix}. \tag{7.20}$$

We then design h_ℓ as described in Section 7.2. Specifically, we choose the formation control feedback function h_ℓ for $\ell = 1, \ldots, T$ to be

$$h_\ell(r_\ell) = k(r_\ell - r_\ell^d) \tag{7.21}$$

with $k = 8$. Since k is positive h_ℓ is strictly increasing and onto.

Note that without the suspended load the relative positions r_ℓ of the UAVs would converge to the desired relative positions r_ℓ^d. However, the force from the suspended load will pull the UAVs slightly closer together, so the equilibrium $\bar{r}_\ell$ for the links between the UAVs will be slightly different from r_ℓ^d.

The force between the load and the UAVs are modeled by Hooke's law as

$$\sigma_\ell(||r_\ell||) = \gamma(||r_\ell|| - L_\ell) \tag{7.22}$$

for $\ell = T + 1, \ldots, E$, where $L_\ell = 2$ is the nominal length of the wire at link ℓ. The wires are modeled as relatively stiff springs with $\gamma = 100$.

We let the initial positions of the UAVs be

$$\eta_1^0 = \begin{bmatrix} 0 \\ 0 \\ 0 \end{bmatrix}, \quad \eta_2^0 = \begin{bmatrix} 3 \\ 0 \\ 0 \end{bmatrix}, \quad \eta_3^0 = \begin{bmatrix} 0 \\ 1 \\ 0 \end{bmatrix},$$

the desired formation be given by (7.20) with $\Delta = 2$, and the desired velocity be

$$v^d = \begin{bmatrix} 0 \\ 0 \\ 0 \end{bmatrix}.$$

The results of the simulation can be seen in Figures 7.4-7.7. The relative movements of the three UAVs can be seen in Figure 7.4, where the star represents the initial position, and the UAV drawing is the final position. As can be seen, they approach the desired relative formation, and the velocity error $|v_i(t) - v^d(t)|$ converges to zero in Figure 7.5. From Figure 7.6 we see that the distance between the UAVs converge to a constant value, but as expected, it is slightly less than Δ.

Figure 7.7 shows estimates of the mass of the suspended load and wind bias, which converge to the true values. The estimated mass of the suspended load is calculated by summing the z-components of δ_i, while the estimated wind bias is the average of the xy-components.

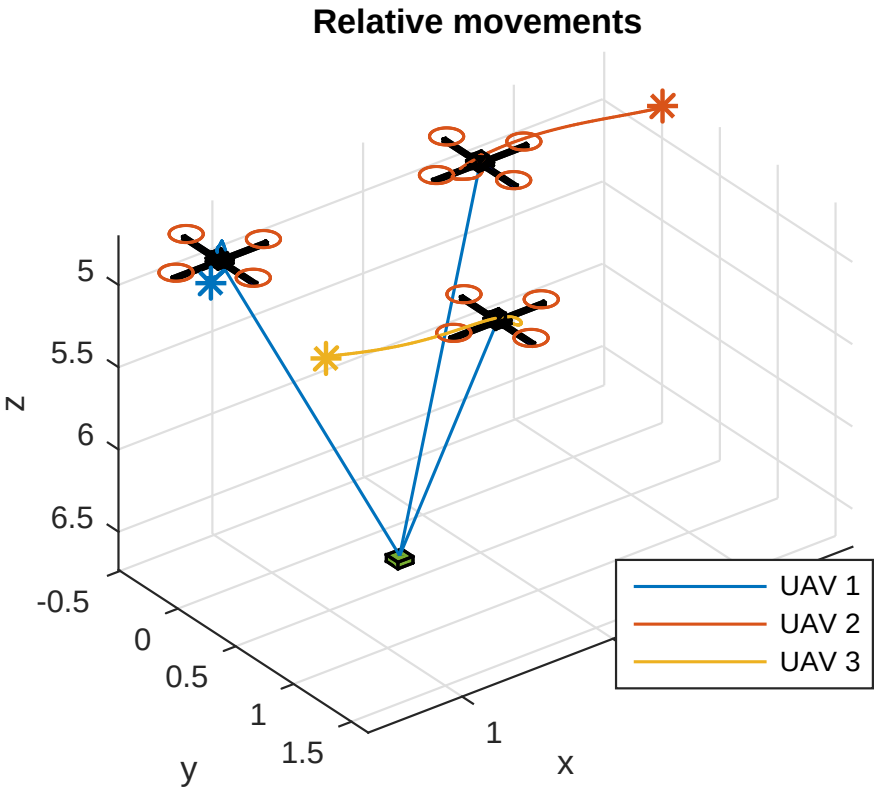

Figure 7.4: Position of the three UAVs and the suspended load.

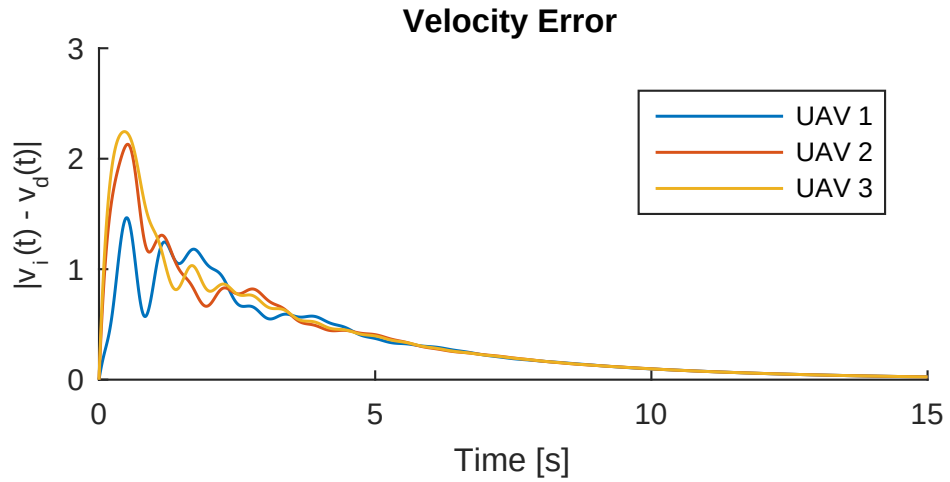

Figure 7.5: The velocity error relative to the desired velocity v^d for each UAV.

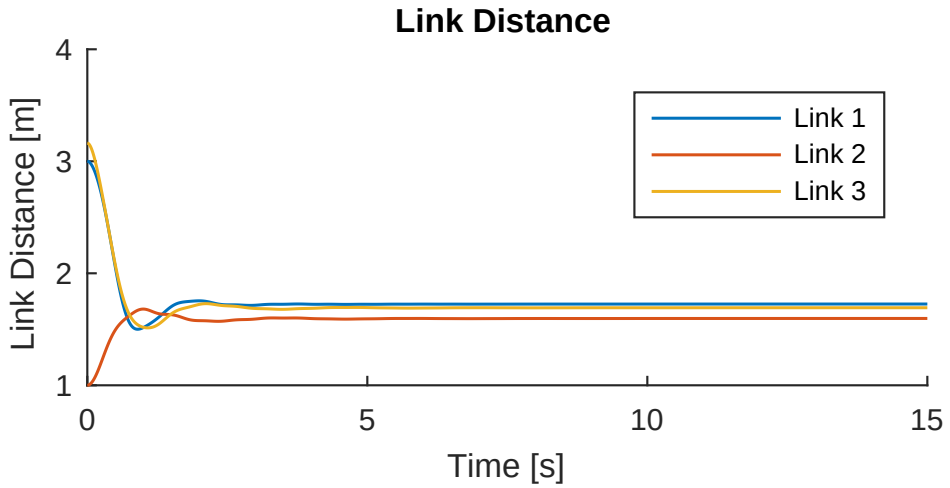

Figure 7.6: Distance between each UAV.

7.5 Chapter Summary

In this chapter, passivity-based control design was applied to a system of multiple UAVs carrying a suspended load. The proposed control strategy regulates the relative position between the UAVs and compensates for the vertical force applied by the suspended load. We prove that the equilibrium points of the system when the cables are in tension are stable and provide simulation results demonstrating the performance of the control strategy.

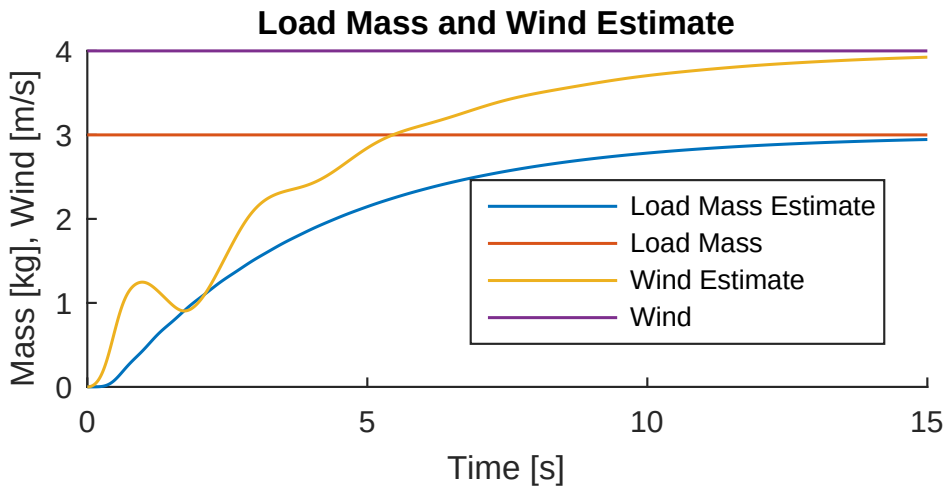

Figure 7.7: Load and bias estimates, as calculated from the integral terms δ_i of each UAV.

Chapter 8

Conclusion

In this dissertation a compositional approach to stability, performance, and safety certification of interconnected systems was presented. This approach is necessary because modern computational tools to analyze nonlinear systems are not scalable to large-scale systems. The problem is formulated as local constraints for each subsystem and a global constraint that only involves the subsystem properties and the interconnection structure.

Using ADMM we are able to decompose this problem into subproblems for each constraint. The local subproblems use the notions of dissipativity, EID, or IQCs to characterize the input-output properties of the corresponding subsystem. The global problem depends on the properties certified by the local problems and the interconnection structure and attempts to certify global properties of the interconnected system. By iteratively solving these problems as described in Section 4.1 convergence to a feasible solution is guaranteed.

We demonstrated that this approach is reliable and scalable; allowing the analysis of very large nonlinear interconnected systems that are beyond the reach of conventional analysis techniques. It is unique from conventional approaches in that it searches over the properties of the individual subsystems in a coordinated fashion to find properties that are most propitious for certifying the desired properties of the interconnected system.

Furthermore, it was shown that by taking advantage of symmetries in large-scale interconnected systems that the performance and scalability of these approaches can be further improved. Specifically, we are able to reduce the number of decision variables and, in some cases, the dimension of the LMI constraint in the global problem. These reductions provide significant reductions in the computational time required to certify properties of these systems and allow the analysis of even larger interconnected systems.

Bibliography

[1] S. Boyd, N. Parikh, E. Chu, B. Peleato, and J. Eckstein, "Distributed optimization and statistical learning via the alternating direction method of multipliers," *Foundations and Trends in Machine Learning*, vol. 3, no. 1, pp. 1–122, 2011.

[2] J. C. Willems, "Dissipative dynamical systems part i: General theory," *Archive for Rational Mechanics and Analysis*, vol. 45, no. 5, pp. 321–351, 1972.

[3] ——, "Dissipative dynamical systems part ii: Linear systems with quadratic supply rates," *Archive for Rational Mechanics and Analysis*, vol. 45, no. 5, pp. 352–393, 1972.

[4] J. Anderson, A. Teixeira, H. Sandberg, and A. Papachristodoulou, "Dynamical system decomposition using dissipation inequalities," in *IEEE Conference on Decision and Control*, 2011, pp. 211–216.

[5] S. Dashkovskiy, B. Rüffer, and F. Wirth, "An ISS small gain theorem for general networks," *Mathematics of Control, Signals, and Systems*, vol. 19, no. 2, pp. 93–122, 2007.

[6] N. Sandell, Jr., P. Varaiya, M. Athans, and M. Safonov, "Survey of decentralized control methods for large scale systems," *IEEE Transactions on Automatic Control*, vol. 23, no. 2, pp. 108–128, 1978.

[7] M. Vidyasagar, *Input-output analysis of large-scale interconnected systems: decomposition, well-posedness, and stability*. Springer-Verlag, 1981.

[8] C. Meissen, L. Lessard, M. Arcak, and A. Packard, "Compositional performance certification of interconnected systems using ADMM," *Automatica*, vol. 61, pp. 55–63, 2015.

[9] M. Arcak, C. Meissen, and A. Packard, *Networks of Dissipative Systems: Compositional Certification of Stability, Performance, and Safety*, ser. SpringerBriefs in Control, Automation and Robotics. Springer, 2016.

[10] C. Meissen, L. Lessard, and A. Packard, "Performance certification of interconnected systems using decomposition techniques," in *American Control Conference*, 2014, pp. 5030–5036.

[11] A. R. Ferreira, C. Meissen, M. Arcak, and A. Packard, "Symmetry reduction for performance certification of interconnected systems," *IEEE Transactions on Control of Network Systems*, 2016.

[12] C. Meissen, K. Klausen, M. Arcak, T. Fossen, and A. Packard, "Passivity-based formation control for UAVs with a suspended load," *IFAC World Congress*, 2017.

[13] M. Bürger, D. Zelazo, and F. Allgöwer, "Duality and network theory in passivity-based cooperative control," *Automatica*, vol. 50, no. 8, pp. 2051–2061, 2014.

[14] G. Hines, M. Arcak, and A. Packard, "Equilibrium-independent passivity: A new defintion and numerical certification," in *Automatica*, 2011, pp. 1949–1956.

[15] A. Megretski and A. Rantzer, "System analysis via integral quadratic constraints," *IEEE Transactions on Automatic Control*, vol. 42, no. 6, pp. 819–830, 1997.

[16] P. Seiler, "Stability analysis with dissipation inequalities and integral quadratic constraints," *IEEE Transactions on Automatic Control*, 2015.

[17] J. Veenman and C. W. Scherer, "Stability analysis with integral quadratic constraints: A dissipativity based proof," in *IEEE Conference on Decision and Control*, 2013, pp. 3770–3775.

[18] P. A. Parrilo, "Semidefinite programming relaxations for semialgebraic problems," *Mathematical Programming*, vol. 96, no. 2, pp. 293–320, 2003.

[19] B. Reznick, "Some concrete aspects of hilbert's 17th problem," *Contemporary Mathematics*, vol. 253, pp. 251–272, 2000.

[20] P. Parrilo, "Structured semidefinite programs and semialgebraic geometry methods in robustness and optimization," PhD thesis, California Institute of Tech., 2000.

[21] M. Choi, T. Lam, and B. Reznick, "Sums of squares of real polynomials," *Proceedings of Symposia in Pure Mathematics*, vol. 58, no. 2, pp. 103–126, 1995.

[22] J. Löfberg, "Yalmip : A toolbox for modeling and optimization in MATLAB," in *Proceedings of the CACSD Conference*, Taipei, Taiwan, 2004.

[23] A. Papachristodoulou, J. Anderson, G. Valmorbida, S. Prajna, P. Seiler, and P. A. Parrilo, *SOSTOOLS: Sum of squares optimization toolbox for MATLAB*, `http://arxiv.org/abs/1310.4716`, 2013.

[24] P. Seiler, "SOSOPT: A toolbox for polynomial optimization," in *arXiv:1308.1889*, `http://www.aem.umn.edu/~AerospaceControl`, 2013.

[25] M. ApS, *The MOSEK optimization toolbox for MATLAB manual. version 7.1 (revision 28)*. 2015. [Online]. Available: `%5Curl%7Bhttp://docs.mosek.com/7.1/toolbox/index.html%7D`.

[26] J. F. Sturm, "Using SeDuMi 1.02, a Matlab toolbox for optimization over symmetric cones," *Optimization Methods and Software*, vol. 11, no. 1-4, pp. 625–653, Jan. 1, 1999.

[27] K. Toh, M. Todd, and R. Tutuncu, "SDPT3 — a Matlab software package for semidefinite programming," *Optimization Methods and Software*, vol. 11, pp. 545–581, 1999.

[28] L. Vanderberghe and S. Boyd, "Semidefinite programming," *SIAM Review*, vol. 38, no. 1, pp. 49–95, 1996.

[29] R. D. Monteiro and P. Zanjácomo, "Implementation of primal-dual methods for semidefinite programming based on Monteiro and Tsuchiya Newton directions and their variants," *Optimization Methods and Software*, vol. 11, no. 1-4, pp. 91–140, 1999.

[30] R. D. Monteiro, "First- and second-order methods for semidefinite programming," *Mathematical Programming*, vol. 1-2, no. 97, pp. 209–244, 2003.

[31] K. Gatermann and P. A. Parrilo, "Symmetry groups, semidefinite programs, and sums of squares," *J. Pure Appl. Algebra*, vol. 192, no. 1-3, pp. 95–128, 2004.

[32] S. Khoshfetrat Pakazad, A. Hansson, M. S. Andersen, and A. Rantzer, "Distributed robustness analysis of interconnected uncertain systems using chordal decomposition," *ArXiv e-prints*, 2014. eprint: 1402.2066.

[33] R. Mason and A. Papachristodoulou, "Chordal sparsity, decomposing SDPs and the Lyapunov equation," in *American Control Conference (ACC), 2014*, Jun. 2014, pp. 531–537. DOI: 10.1109/ACC.2014.6859255.

[34] U. Topcu, A. Packard, and R. Murray, "Compositional stability analysis based on dual decomposition," in *IEEE Conference on Decision and Control*, 2009, pp. 1175–1180.

[35] S. Coogan and M. Arcak, "A dissipativity approach to safety verification for interconnected systems," *Automatic Control, IEEE Transactions on*, vol. 60, no. 6, pp. 1722–1727, Jun. 2015.

[36] S. Prajna, A. Jadbabaie, and G. Pappas, "A framework for worst-case and stochastic safety verification using barrier certificates," *IEEE Transactions on Automatic Control*, vol. 52, no. 8, pp. 1415–1428, 2007.

[37] F. Blanchini, "Set invariance in control," *Automatica*, vol. 35, no. 11, pp. 1747–1767, 1999.

[38] P. Moylan and D. Hill, "Stability criteria for large-scale systems," *IEEE Transactions on Automatic Control*, vol. 23, pp. 143–149, 2 1978.

[39] H. Khalil, *Nonlinear Systems (3rd Edition)*. Englewood Cliffs, NJ: Prentice Hall, 2002.

[40] J. E. Colgate and N. Hogan, "Robust control of dynamically interacting systems," *International Journal of Control*, vol. 48, no. 1, pp. 65–88, 1988.

[41] F. Kerber and A. van der Schaft, "Compositional properties of passivity," in *IEEE Conference on Decision and Control*, 2011, pp. 4628–4633.

[42] J. F. C. Mota, J. M. F. Xavier, P. M. Q. Aguiar, and M. Püschel, "Distributed ADMM for model predictive control and congestion control," in *IEEE Conference on Decision and Control*, 2012, pp. 5110–5115.

[43] M. K. Ng, P. Weiss, and X. Yuan, "Solving constrained total-variation image restoration and reconstruction problems via alternating direction methods," *SIAM Journal on Scientific Computing*, vol. 32, no. 5, pp. 2710–2736, 2010.

[44] J. F. C. Mota, J. M. F. Xavier, P. M. Q. Aguiar, and M. Püschel, "A proof of convergence for the alternating direction method of multipliers applied to poyhedral-constrained functions," in *arXiv: 1112.2295*, 2012.

[45] M. Bazaraa, H. Sherali, and C. M. Shetty, *Nonlinear Programming: Theory and Algorithms*, 3rd. Wiley-InterScience, 2006.

[46] C. Sloth, G. Pappas, and R. Wisniewski, "Compositional safety analysis using barrier certificates," in *ACM international conference on Hybrid Systems: Computation and Control*, 2012, pp. 15–24.

[47] M. S. Bazaraa, H. D. Sherali, and C. M. Shetty, *Nonlinear Programming: Theory and Algoritms*, 3rd. Wiley-InterScience, 2006.

[48] L. G. Gubin, B. T. Polyak, and E. V. Raik, "The method of projections for finding the common point of convex sets," *USSR Computational Mathematics and Mathematical Physics*, vol. 7, no. 6, pp. 1–24, 1967.

[49] H. Bauschke and J. Borwein, "Dykstra's alternating projection algorithm for two sets," *Journal of Approximation Theory*, vol. 79, no. 3, pp. 418–443, 1994.

[50] H. Khalil, *Nonlinear Systems*, 3rd. Prentice Hall, 2002.

[51] M. Grant and S. Boyd, *CVX: Matlab software for disciplined convex programming, version 2.0 beta*, `http://cvxr.com/cvx`, Sep. 2013.

[52] M. Arcak, "Passivity as a design tool for group coordination," *IEEE Transactions on Automatic Control*, vol. 52, no. 8, pp. 1380–1390, 2007.

[53] ——, "Passivity approach to network stability analysis and distributed control synthesis," in, ser. The Control Handbook. CRC Press, 2010, pp. 1–18.

[54] J. Wen and M. Arcak, "A unifying passivity framework for network flow control," *IEEE Transactions on Automatic Control*, vol. 49, no. 2, pp. 162–174, 2004.

[55] S. Coogan and M. Arcak, "A dissipativity approach to safety verification for interconnected systems," in *IEEE Transactions on Automatic Control, Accepted*, 2015.

[56] F. Permenter and P. Parillo, "Partial facial reduction: Simplified, equivalent SDPs via approximations of the PSD cone," in *arXiv:1408.4685*, 2014.

[57] A. Papachristodoulou and S. Prajna, "Analysis of non-polynomial systems using the sum of squares decomposition," English, in *Positive Polynomials in Control*, ser. Lecture Notes in Control and Information Science, D. Henrion and A. Garulli, Eds., vol. 312, Springer Berlin Heidelberg, 2005, pp. 23–43.

[58] A. S. R. Ferreira and M. Arcak, "A graph partitioning approach to predicting patterns in lateral inhibition systems," *SIAM Journal on Applied Dynamical Systems*, vol. 12, no. 4, pp. 2012–2031, 2013.

[59] B. Goodwine and P. Antsaklis, "Multi-agent compositional stability exploiting system symmetries," *Automatica*, vol. 49, no. 11, pp. 3158–3166, 2013.

[60] K. Gatermann and P. A. Parrilo, "Symmetry groups, semidefinite programs, and sums of squares," *Journal of Pure and Applied Algebra*, vol. 192, no. 1-3, pp. 95–128, 2004, ISSN: 00224049. DOI: 10.1016/j.jpaa.2003.12.011. arXiv: 0211450 [math].

[61] R. Cogill, S. Lall, and P. A. Parrilo, "Structured semidefinite programs for the control of symmetric systems," *Automatica*, vol. 44, no. 5, pp. 1411–1417, 2008, ISSN: 00051098. DOI: 10.1016/j.automatica.2007.10.004.

[62] S. P. Boyd, P. Diaconis, P. A. Parrilo, and L. Xiao, "Symmetry analysis of reversible Markov chains.," *Internet Math.*, vol. 2, no. 1, pp. 31–71, 2005.

[63] A. Rahmani, M. Ji, M. Mesbahi, and M. Egerstedt, "Controllability of multi-agent systems from a graph-theoretic perspective," *SIAM Journal on Control and Optimization*, vol. 48, no. 1, pp. 162–186, 2009. DOI: 10.1137/060674909.

[64] C. Godsil and G. Royle, *Algebraic Graph Theory*. Springer, Apr. 2001, ISBN: 0387952209.

[65] A. Lubiw, "Some NP-complete problems similar to graph isomorphism," *SIAM Journal on Computing*, vol. 10, no. 1, pp. 11–21, 1981. DOI: 10.1137/0210002.

[66] M. Bisgaard, "Modeling, estimation, and control of helicopter slung load system," PhD thesis, Aalborg University, 2008.

[67] D. Mellinger, M. Shomin, N. Michael, and V. Kumar, "Cooperative grasping and transport using multiple quadrotors," in *Distributed Autonomous Robotic Systems: The 10th International Symposium*. Springer Berlin Heidelberg, 2013, pp. 545–558.

[68] M. Bernard, K. Kondak, I. Maza, and A. Ollero, "Autonomous transportation and deployment with aerial robots for search and rescue missions," *Journal of Field Robotics*, vol. 28, no. 6, pp. 914–931, 2011.

[69] N. Michael, J. Fink, and V. Kumar, "Cooperative manipulation and transportation with aerial robots," *Autonomous Robots*, vol. 30, no. 1, pp. 73–86, 2011.

[70] K. Klausen, T. I. Fossen, and T. A. Johansen, "Suspended load motion control using multicopters," in *Mediterranean Conference on Control and Automation*, 2014.

[71] I. Maza, K. Kondak, M. Bernard, and A. Ollero, "Multi-uav cooperation and control for load transportation and deployment," *Journal of Intelligent and Robotic Systems*, vol. 57, no. 1, pp. 417–449, 2009.

[72] M. Bernard and K. Kondak, "Generic slung load transportation system using small size helicopters," *2009 IEEE International Conference on Robotics and Automation*, pp. 3258–3264, May 2009.

[73] M. Arcak, "Passivity as a design tool for group coordination," *IEEE Transactions on Automatic Control*, vol. 52, no. 8, pp. 1380–1390, Aug. 2007, ISSN: 0018-9286. DOI: 10.1109/TAC.2007.902733.

[74] H. Bai, M. Arcak, and J. Wen, *Cooperative Control Design: A Systematic, Passivity-Based Approach*, ser. Communications and Control Eng. New York: Springer, 2011.

[75] R. Mahony, V. Kumar, and P. Corke, "Multirotor aerial vehicles: Modeling, estimation, and control of quadrotor," *IEEE Robotics Automation Magazine*, vol. 19, no. 3, pp. 20–32, Sep. 2012, ISSN: 1070-9932. DOI: 10.1109/MRA.2012.2206474.